Thermal Contact Resistance of Polymer Interfaces

by

Josh Gibbins

A thesis
presented to the University of Waterloo
in fulfilment of the
thesis requirement for the degree of
Master of Applied Science
in
Mechanical Engineering

Waterloo, Ontario, Canada, 2006

©Josh Gibbins 2006

I hereby declare that I am the sole author of this thesis. This is a true copy of the thesis, including any required final versions, as accepted by my examiners.

I understand that my thesis may be made electronically available to the public.

Josh Gibbins

Abstract

In this study an experimental program was carried out to determine the thermal contact resistance at polymer interfaces. Specifically, a polycarbonate to stainless steel interface along with a polycarbonate to polycarbonate interface were investigated. The thermal contact resistance at a stainless steel to stainless steel interface was also investigated for comparison purposes. Experimental data was obtained over a pressure range of approximately 600 - 7000 kPa, in a vacuum environment.

The experimental data was compared to the CMY plastic contact model, the Mikic elastic contact model and the SY elasto-plastic contact model to investigate the ability of such established thermal contact models to predict the thermal contact resistance at polymer interfaces. Based upon predictions made in regards to the mode of deformation of the asperities on the contacting surfaces the appropriate contact model showed good agreement with the experimental data for the stainless steel-stainless steel data set and the polycarbonate-stainless steel data sets. There was poor agreement between the all three contact models and the experimental data for the polycarbonate-polycarbonate data sets. It was determined that uncertainties in the proposed experimental method prevented an accurate measurement of the thermal contact resistance values for the polycarbonate-polycarbonate data sets.

The purpose of this investigation was to extend the use of established thermal contact models to polymer interfaces and to provide a comparison between the thermal contact resistance values of metal and polymer interfaces.

Thermal contact resistance for the polymer to metal interface was shown to be predicted by the Mikic elastic contact model in comparison to the metal to metal interface which was shown to be predicted by the CMY plastic contact model. The thermal contact resistance for a polymer interface was found to be on the same order as a metal interface.

Acknowledgements

I would like to thank Professor J. R. Culham for the supervision he provided to me during this study. His guidance and support was appreciated. Also, I wish to thank Professor Emeritus M. M. Yovanovich for his enthusiasm and guidance he afforded to me. My sincere thanks also extend to Dr. Pete Teertstra for his valuable assistance with the experimental program.

There are many others who have assisted me in my research including Dr. Majid Bahrami and Paul Karayacoubian Esq. for their thoughtful comments and discussions.

I would also like to thank the many students and staff at Conrad Grebel University College for their support. Finally, I am forever indebted to my beautiful wife Rebecca for her patience, support and love.

When people asked me, "How could you give up this great job/life and go sailing?" I said, "The truth is I don't have long to live." After a pregnant pause, I'd say, "In ten, twenty or thirty years, I'll be dead and I won't be able to do this!"

John Gambill, St. Petersburg, FL

Contents

List of Tables

List of Figures

Nomenclature

A	contact area, $[m^2]$
a_i	radius associated with each contact spot, $[m]$
a	mean contact spot radius, $[m]$
	radius of source area, $[m]$
B	intermediate term
b_i	flux tube radius, $[m]$
C	fitting parameter
C_c	dimensionless contact conductance
c_1	Vickers microhardness correlation coefficient, $[Pa]$
c_2	Vickers microhardness correlation coefficient
CMY	Cooper, Mikic and Yovanovich (1969)
d_V	Vickers indentation diagonal, $[m]$
d_0	reference diagonal, $[m]$
E	elastic modulus, $[Pa]$
E'	equivalent elastic modulus, $[Pa]$
f	blending parameter
f_{ep}	elasto-plastic parameter
H	microhardness, $[Pa]$
h	thermal conductance, $[W/m^2 \cdot K]$
K	fitting parameter
k	thermal conductivity, $[W/m \cdot K]$
k_s	harmonic mean thermal conductivity, $[W/m \cdot K]$
L	length of profilometer trace, $[m]$
m	absolute mean asperity slope

N	number of contact spots
	number of data points
n	contact spot density, $[1/m^2]$
P	apparent contact pressure, $[Pa]$
Q	heat transfer rate, $[W]$
q	heat flux, $[W/m^2]$
R	thermal resistance, $[K/W]$
R_q	surface RMS roughness, $[m]$
r	radial axis
RMS	root mean square
S_f	material yield/flow stress, $[Pa]$
SY	Sridhar and Yovanovich (1996)
T	temperature, [°C]
$\overline{T}$	average temperature, [°C]
T_g	glass transition temperature, [°C]
T_m	mean interface temperature, [°C]
t_0	initial thickness, $[m]$
TIM	thermal interface material
u	dimensionless position
Y	mean plane seperation, $[m]$
	material yield stress, $[Pa]$
$y(x)$	seperation of surface and the mean plane, $[m]$
x	horizontal axis
x_i	percent difference, [%]
Z^*	normalized seperation of surface and the mean plane
z	height axis

Greek Symbols:

Γ	arbitrary distance in z axis, $[m]$
δ_n	eigenvalues of $J_n(x)$
ΔT	temperature drop, [°C]
ϵ	radius ratio
ϵ_c^*	contact strain
λ	relative mean plane seperation
	intermediate term
μ	parameter to account for shape of flux distribution
	intermediate term
ν	Poisson's ratio
σ	surface RMS roughness, $[m]$
ψ	spreading resistance parameter
ω	uncertainty

Subscripts:

$1, 2$	contacting surfaces
a	apparent
avg	average
$bulk$	bulk
c	contact
e	elastic
ep	elasto-plastic
$elastic$	elastic deformation
$expt$	experiment

$graphite$	graphite
i	single asperity
$interface$	interface
$joint$	joint
$Marsh$	Marsh
$material$	material
$model$	model
p	plastic
$plastic$	plastic deformation
$poly$	polymer-elastic
PC	polycarbonate
r	real
s	spreading
$sink$	sink
$SS304$	304 Stainless Steel
$total$	total
$tube$	flux tube
V	Vickers
max	maximum
min	minimum
$elec.iron$	electrolytic iron

Chapter 1

Introduction

Understanding and predicting heat transfer through surfaces in contact is an important aspect of thermal network designs with applications including microelectronics cooling, heat exchangers and satellite components. In each of these applications the contacting surfaces are not perfectly smooth but exhibit roughness on the microscopic scale. As shown in Fig. 1.1 discrete contact spots are created where the surface asperities make contact with each other. Therefore, in a vacuum the flow of heat from one surface to another must pass through the discrete contact spots creating a constriction and spreading resistance to the heat flow. The result of this resistance is a localized temperature drop at the interface. Overall only a small portion, (approximately 2%) [41] of the apparent area (A_a) makes up the real area of contact (A_r). The remaining area is covered by a thin void which may be empty if the interface is in a vacuum or may be filled with a gas. Heat transfer due to radiation in the voids can be considered negligible if the temperatures are less than 700 K [10].

1.1 Thermal Contact Resistance

The thermal resistance to heat flow at an interface is known as thermal contact resistance and is defined as:

$$R_c = \frac{\Delta T_{interface}}{Q} \quad (K/W) \tag{1.1}$$

where Q is the heat transferred through the interface and $\Delta T_{interface}$ is the localized temperature drop at the interface. Considering the temperature profile shown in Fig. 1.1 the difference in temperature of the contacting surfaces is $\Delta T_{interface}$. The temperature of each surface is obtained by extrapolating a steady-state temperature profile of each contacting surface to the interface. Both Q and $\Delta T_{interface}$ are determined experimentally in order to calculate the thermal contact resistance of a particular interface.

Thermal contact conductance and thermal contact resistance are related by the following:

$$h_c = \frac{1}{R_c\ A_a} \quad (W/m^2 \cdot K) \tag{1.2}$$

where A_a is the apparent (or total) area of the contacting surfaces.

1.2 Polymer Interfaces

Polymers have traditionally not been used for heat transfer applications because of their poor thermal conductivity in comparison to metals but through the use of polymer additives significant increases in thermal conductivity can be achieved. For comparison Table 1.1 presents the thermal conductivity of selected materials.

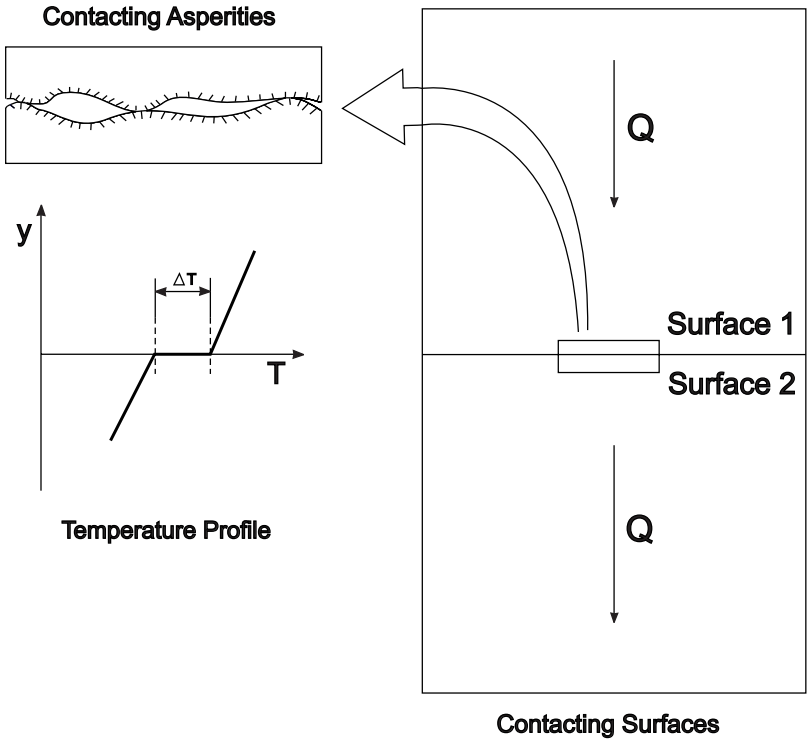

Figure 1.1: Flow of heat between contacting surfaces in a vacuum

Possible applications for thermally conductive polymers include thermal interface materials (TIM), heat sinks, and heat exchangers. Benefits for each of these applications include the ability to easily form complex shapes using molding techniques, polymers parts can be made up to 50% lighter than aluminum parts and the ability to form electrically isolative - thermally conductive interfaces [19]. Cool Polymers, Inc. a company which specializes in thermal conductive polymers performed an experiment to measure the thermal performance of identical heat sinks made of two seperate materials. One of the materials evaluated was aluminum and the other was a thermally conductive polymer. Under typical operating conditions they found equivalent performance from both heat sinks [19].

Considering the vast possibilities for the use of polymers in thermal designs an understanding and characterization of the thermal contact resistance at polymer interfaces is necessary. There are two types of polymer interfaces that require investi-

Table 1.1: Material thermal conductivity, $(W/m \cdot K)$ [19]

Conventional Polymers	0.2-0.3
Stainless Steel	16
CoolPoly® Thermally Conductive Polymers	1-20
Steel	50
Aluminum	200

gation. The first is the contact of a polymer against a metal and the second is the contact of a polymer against a polymer.

1.2.1 Polymer Background

To aid in the understanding of a solid polymers' response to heat and select a suitable polymer for evaluation it is necessary to first investigate the structural arrangement of the polymer chains which when combined form a solid polymer. The two basic arrangements of the polymer chains is an ordered crystalline structure or an irregular amorphous structure with most polymers possessing at least a portion of each type of arrangement.

According to Hall [15] crystallinity is the normal condition of solid substances, while in the liquid state chains are free to move around in an random manner. Polymers with a high viscosity at the melting point are reluctant to reorganize themselves from a random orientated liquid into a fully crystalline solid. This allows the random nature of the liquid to persist into the solid state. These materials do not exhibit a change in phase at a specific temperature during solidification rather they gradually change from a liquid to a solid.

The lower limit of this transition range is noticed by plotting the density of the polymer during cooling which follows a linear profile. There is a temperature at

which the slope of this linear profile changes, this temperature is referred to as the glass transition temperature (T_g). T_g signals a change in the availability of free space between the polymer chains. Such space (free volume) must exist for large-scale motion of the polymer chains to occur. It is these large-scale movements which give rise to large deformations characteristic of the viscoelastic state. Below T_g the free volume reduces to a critical value below which large-scale motion is impossible (or extremely slow). For this reason only limited chain motion is allowed below T_g. Hall [15] states that the limited motion of polymer chains below the glass transition temperature allows polymers to exhibit a mechanical response much the same as metals. Above T_g the mechanical behavior begins to exhibit a mechanical response similar to viscous liquids and can be considered a viscoelastic material which shows a time dependent response to an applied stress.

For evaluations of thermal contact resistance it is necessary to avoid temperatures which bring a polymer into this viscoelastic region. Therefore only polymers which have a relatively high glassy temperature would be suitable for thermal contact resistance evaluation. For comparison the glass transition temperature of various polymers is given in Table 1.2. Based upon these requirements, polycarbonate was selected as suitable for thermal contact resistance experiments.

Table 1.2: Glass transition temperature of various polymers (T_g) [4].

Polysulphone (PSul)	195 $^\circ C$
Polycarbonate (PC)	150 $^\circ C$
Polystyrene (PS)	100 $^\circ C$
Polyvinylchloride (PVC)	65 $^\circ C$
Nylon 6 (PA6)	50 $^\circ C$

1.3 Problem Statement

The vast majority of researchers who have looked into the problem of thermal contact resistance of joints that incorporate polymers have focused primarily on the total resistance of the joint, that is they included both the bulk resistance of the polymer and the resistance due to the interface in reported results. For researchers looking into the thermal isolation of a particular gasket material the reported results were suitable for their application.

More recent work in this area has investigated the thermal contact conductance of a rigid polymer-metal interface but still have included the bulk conductance of the polymer layer in reported experimental results. To predict these experimental results adaptions to both the Mikic elastic conductance model [29] and to the CMY plastic conductance model [8] have been completed with both adaptions showing reasonable agreement to experimental results. To support their theoretical work, arguments have been presented for both elastic and plastic asperity deformation while little has been completed to validate these predictions. Based on previous research the objectives of this project are:

1. To make predictions in regards to the mode of deformation of asperities at polymer-metal, polymer-polymer and metal-metal interfaces. A metal-metal interface will be investigated to provide validity to the experimental results as this type of interface has been thoroughly studied [17].

2. To investigate experimentally the thermal contact resistance of polymer-metal, polymer-polymer and metal-metal interfaces. Experimental results will then be compared to established thermal contact resistance models in order to validate the mode of deformation predictions and show the ability of established thermal contact models to predict the thermal contact resistance of polymer interfaces.

1.4 Outline

In Chapter 2, a literature review is presented which discusses the following areas:

1. Existing models of thermal contact resistance which include the CMY plastic contact model, the Mikic elastic contact model and the SY elasto-plastic contact model.
2. Two methods to determine the mode of deformation of contacting surfaces.
3. A review of relevant experimental and analytical work which have investigated the thermal resistance of polymer joints.

Chapter 3 describes the experimental setup and the procedure necessary to obtain thermal contact resistance data of polymer interfaces. In Chapter 4, preliminary experiments necessary for thermal contact resistance modelling are discussed. In Chapter 5, experimentally obtained data is presented and compared with models of thermal contact resistance. Chapter 6 presents conclusions drawn from this study and recommendations are made.

Chapter 2

Literature Review

2.1 Review of Conforming Rough Surface Models

There have been a number of models presented to predict the flow of heat between conforming rough surfaces in contact. Greenwood and Williamson [14] define conforming rough surfaces as:

... those in which the area of apparent contact is large so that the individual contacts are dispersed and the forces acting through neighbouring spots do not influence each other

The deformation mode of the asperities is what sets these models apart and defines them as either a elastic, plastic or elasto-plastic model. For small contact strains the contact is elastic and the model is based on the Hertz model [21]. If the contact strain is very large, plastic deformation of the asperities in contact occurs and the area of contact is based on the microhardness of the softer material [8]. The elasto-plastic model is a combination of both these models.

In his development of a thermal contact conductance correlation for conforming rough surfaces Yovanovich [43] proposed a list of assumptions as a basis for model de-

velopment. The assumptions are proposed for conforming rough surfaces in a vacuum regardless of the mode of deformation.

1. The surfaces are microscopically rough and macroscopically conforming.
2. The surface asperities of each contacting surface have a Gaussion height distribution about a mean plane passing through each surface and the asperities are randomly distributed over the apparent area.
3. As a result of asperity deformation, there are N circular contact spots of radius a_i within the apparent area A_a.
4. The contact spots are isothermal.
5. An equivalent circular flux tube of radius b_i is associated with each contact spot.
6. The total heat flow through each flux tube moves through the contact spots.
7. The surfaces are clean, and free of oxides, films.
8. Radiative heat transfer in the voids between the contact spots is negligible.

The implication of these assumptions is that the contact of two conforming, (nominally flat) surfaces can be simplified into a system that can be modelled in order to predict the thermal contact resistance of the interface.

2.1.1 Effective Surface Geometry

To proceed with an evaluation of thermal contact conductance of an interface it is first necessary to determine the geometry of each contacting surface. Two important parameters which are used for thermal contact conductance modelling are: RMS roughness (σ) and absolute mean asperity slope (m) as shown in Fig. 2.1. These

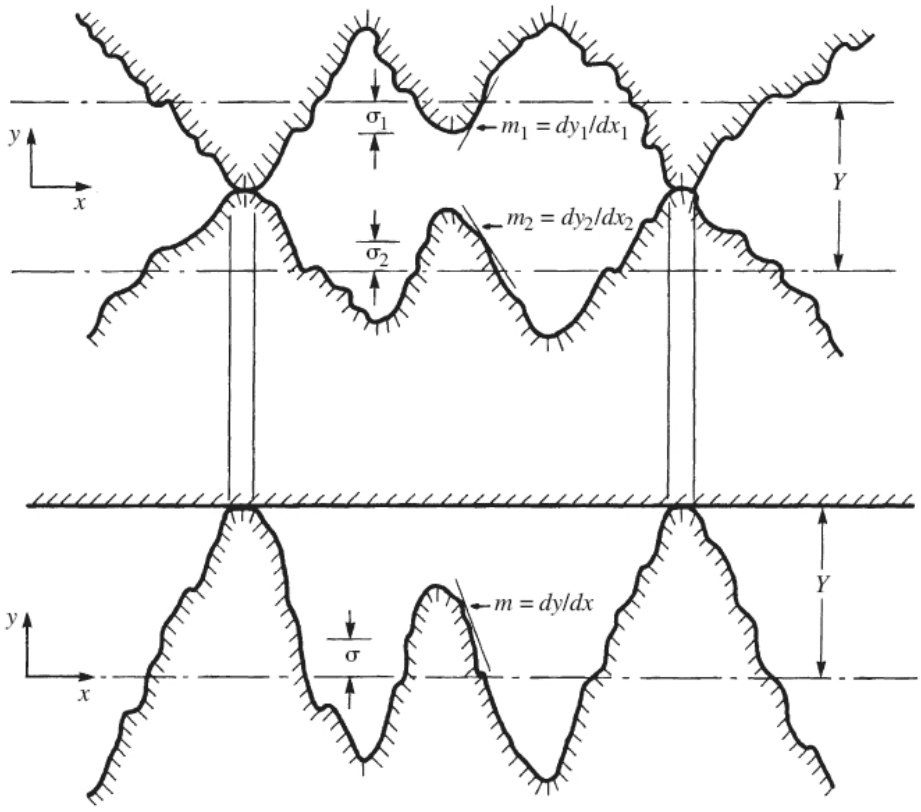

Figure 2.1: Contact between conforming rough surfaces are modeled by the contact between a single rough surface and a smooth surface (from Hegazy [17]).

parameters are required regardless of the mode of deformation. The RMS roughness of a surface is given by Yovanovich and Marotta [41] as:

$$\sigma = R_q = \sqrt{\frac{1}{L}\int_0^L y^2(x)\,dx} \tag{2.1}$$

where L is the length of the trace and $y(x)$ is the distance between the surface and the mean plane. The mean asperity slope is given Yovanovich and Marotta [41] as:

$$m = \frac{1}{L}\int_0^L \left|\frac{dy(x)}{dx}\right| dx \tag{2.2}$$

Greenwood and Williamson [14] have shown that two Gaussian rough surfaces

in contact can be approximated by a single rough surface in contact with a smooth surface as shown in Fig. 2.1. The result of this is an effective surface geometry that can be used in thermal contact conductance models. The effective RMS roughness and the effective absolute mean asperity slope are calculated by the following equations [41]:

$$\sigma = \sqrt{\sigma_1^2 + \sigma_2^2} \quad \text{and} \quad m = \sqrt{m_1^2 + m_2^2} \tag{2.3}$$

2.1.2 Thermal Analysis

Regardless of the asperities mode of deformation the general thermal model is the same. The model requires knowledge of thermal constriction/spreading resistance in a half-space and a flux tube. Each of these components will be examined in detail in the following sections. Also, the general thermal model will be presented.

Thermal Constriction/Spreading Resistance: Half-Space

A half space is defined as a region whose outer dimensions are significantly larger than the heat source/sink area as shown in Fig. 2.2. Outside of the source/sink at $z = 0$ is an adiabatic surface. If heat is entering the half-space moving towards the sink the flux lines diverge causing a thermal resistance referred to as spreading resistance. If heat is leaving the half-space the flux lines converge causing a thermal resistance referred to as constriction resistance. Under conditions of geometric similarity spreading resistance is equal to constriction resistance. Yovanovich and Marotta [41] defined spreading resistance as the difference between the average temperature of the contact area ($\overline{T}_{contact}$) and the average temperature of the heat sink ($\overline{T}_{sink}$) divided by the heat transfer rate Q through the contact area:

$$R_s = \frac{\overline{T}_{contact} - \overline{T}_{sink}}{Q} \quad (K/W) \tag{2.4}$$

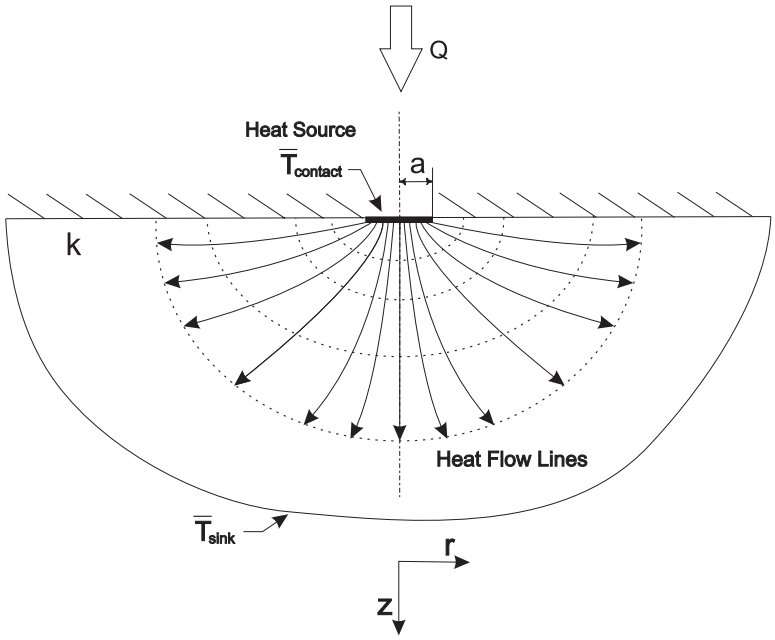

Figure 2.2: Circular heat source on a half-space.

Analytical solutions for thermal spreading resistance for both *isoflux* and *isothermal* heat source boundary conditions have been developed by Carslaw and Jaeger [7]. They solved this problem for a circular heat source area of radius a on the surface of a isotropic halfspace of thermal conductivity k. Their solution for the spreading resistance for the isoflux boundary condition:

$$R_s = \frac{8}{3\pi^2}\frac{1}{ka} \quad (K/W) \tag{2.5}$$

Their solution for the spreading resistance for the isothermal boundary condition:

$$R_s = \frac{1}{4ka} \quad (K/W) \tag{2.6}$$

A dimensionless spreading resistance for a half space is defined as:

$$\psi = 1 = 4kaR_s \tag{2.7}$$

Yovanovich [44] also determined that the majority of the spreading resistance occurs in a small volume near the contact area. It was determined that over 98% of the spreading resistance occurs in an area defined by $r/a \leq 40$. This means that for asperities with micron-sized contact areas the spreading resistance occurs in a layer with thickness on the order of microns.

Thermal Spreading Resistance: Flux Tube Solution

For the system consisting of a long isotropic heat flux tube of cross-sectional area A_{tube}, the heat enters through a circular source area. As the heat moves into the flux tube it "spreads" out causing spreading resistance. An illustration of this system is shown in Fig. 2.3. Yovanovich [45] defines spreading resistance for a flux tube as:

$$R_s = R_{tube} - R_{material} \quad (K/W) \tag{2.8}$$

where R_{tube} is the thermal resistance between the contact area and some arbitrary plane in the flux tube, $z = \Gamma$. Γ is located at a distance that is *much* greater than the dimension of the source area. The material resistance ($R_{material}$) is the resistance due to conduction in the material. This leads to the definition of spreading resistance in the system:

$$R_s = \frac{\overline{T}_c - \overline{T}_{z=\Gamma}}{Q} - \frac{\Gamma}{kA_{tube}} \quad (K/W) \tag{2.9}$$

From the steady-state conduction problem in cylindrical coordinates:

$$\frac{\partial^2 T}{\partial r^2} + \frac{1}{r}\frac{\partial T}{\partial r} + \frac{\partial^2 T}{\partial z^2} = 0 \tag{2.10}$$

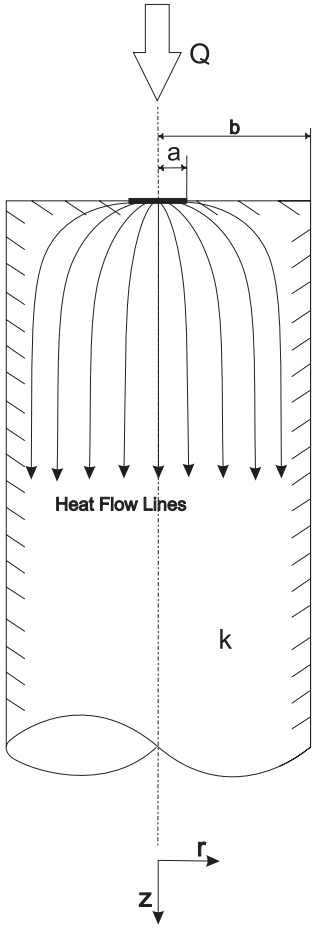

Figure 2.3: Circular heat source on a circular flux tube.

Yovanovich [42] considered the system as shown in Fig. 2.3 and determined an analytic solution for the spreading resistance in a flux tube. A heat flux distribution over the circular heat source was specified as:

$$q(u) = \frac{Q}{\pi a^2}(1+\mu)(1-u^2) \quad 0 \leq u \leq 1 \tag{2.11}$$

where $u = r/a$ and Q is the total heat flow rate through the tube. Yovanovich [45] made note of three heat flux distrubutions over the contact area, illustrated in Fig. 2.4.

Yovanovich [42] obtained the solution for the dimensionless spreading resistance using the conditions: μ=-1/2, circular source area, and a circular flux tube as:

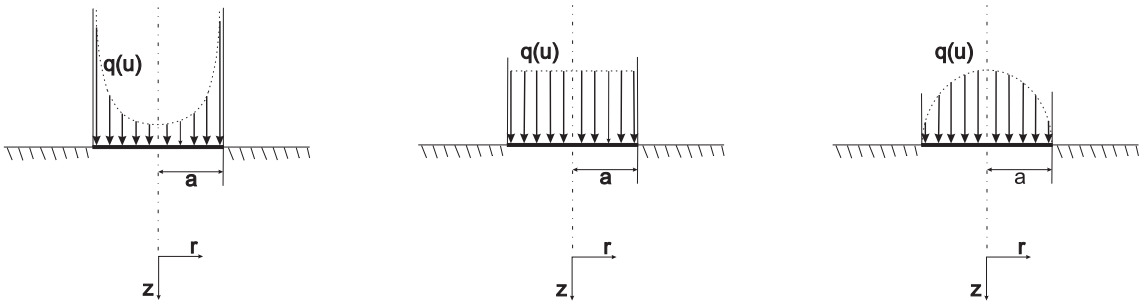

(i) (ii) (iii)

Figure 2.4: (i) μ= -1/2, the equivalent isothermal flux distribution, (ii) $\mu = 0$, the isoflux distribution, and (iii) $\mu = 1/2$, the parabolic flux distribution.

$$\psi = 4kaR_s = \frac{8}{\pi\epsilon}\sum_{n=1}^{\infty}\frac{J_1(\delta_n\epsilon)\sin\delta_n\epsilon}{\delta_n^3 J_0^2(\delta_n)} \tag{2.12}$$

where the geometric parameter ϵ is defined as a/b. The eigenvalues δ_n are the positive roots of $J_1(\delta_n) = 0$ where $J_1()$ is the Bessel function of the first kind of order one. Yovanovich [42] proposed the following approximation for Eq. 2.12 for values of $\epsilon < 0.3$:

$$\psi = 4kaR_s = (1-\epsilon)^{1.5} \tag{2.13}$$

This result can also be expressed in a way that allows easy comparison to the half space solution:

$$R_s = \frac{\psi(\epsilon)}{4ka} \tag{2.14}$$

A comparsion of Eq. 2.14 to the half space spreading resistance solution given in Eq. 2.6 allows one to see that when ψ approaches one the flux tube solution approaches the half space solution.

General Thermal Model

Based upon the flux tube solution (Eq. 2.14) Yovanovich [43] proposed a general thermal model to extend this work to conforming rough surfaces. He describes the constriction and spreading resistance of a single asperity in contact and extends this to the full surface which includes N contact spots. For a single contact spot (i) in contact there is both constriction and spreading resistance from surface 1 and surface 2:

$$R_{si} = \frac{\psi_{i.1}}{4k_1 a_i} + \frac{\psi_{i.2}}{4k_2 a_i} \tag{2.15}$$

Due to symmetry about the contact plane and letting $k_s = 2k_1k_2/(k_1 + k_2)$, Eq. 2.15 becomes:

$$R_{si} = \frac{\psi_i}{2k_s a_i} \tag{2.16}$$

Yovanovich [43] let the value of ψ_i for each contact spot be replaced by the average value of this parameter ψ. Extending Eq. 2.16 to the full surface results in the following thermal contact conductance model as given by Cooper et al. [8] and Yovanovich [43]:

$$h_c = \frac{2nak_s}{\psi(\epsilon)} \quad (W/m^2 \cdot K) \tag{2.17}$$

where n is the contact spot density (N/A_a) with the parameter ψ approximated by:

$$\psi(\epsilon) = (1 - \epsilon)^{1.5} \tag{2.18}$$

with $\epsilon = a/b = \sqrt{A_r/A_a}$. To make predictions of the conductance of conforming rough surfaces (h_c), the terms $(n, a, A_r/A_a)$ must be determined based on the mode of deformation.

2.1.3 Plastic Contact Model: CMY

A relationship is required for the ratio A_r/A_a in order to predict thermal contact conductance using Eq. 2.17. To solve for this ratio Yovanovich [43] assumed the following:

1. The strain of the contacting asperities is significantly large such that plastic deformation of the asperities occurs during the first loading of the contacting surfaces.

2. The contacting asperities of the softer surface undergoes plastic deformation.

Using a force balance on the real and apparent areas, Yovanovich [43] gives the following relationship:

$$\frac{A_r}{A_a} = \frac{P}{H_p} \tag{2.19}$$

where P is the apparent contact pressure and H_p is the plastic microhardness of the softer contacting surface. The plastic microhardness (H_p) is a material property which must be determined from experiment.

The other geometric parameters necessary to predict the thermal contact conductance using Eq. 2.17 have been determined by Cooper et al. [8] and Yovanovich [43]:

$$n = \frac{1}{16}\left(\frac{m}{\sigma}\right)^2 \frac{\exp(-\lambda^2)}{\operatorname{erfc}(\lambda/\sqrt{2})} \tag{2.20}$$

$$a = \sqrt{\frac{8}{\pi}}\frac{\sigma}{m}\exp\left(\frac{\lambda^2}{2}\right)\operatorname{erfc}\left(\frac{\lambda}{\sqrt{2}}\right) \tag{2.21}$$

$$\lambda = \sqrt{2}\,\operatorname{erfc}^{-1}\left(\frac{2A_r}{A_a}\right) \tag{2.22}$$

The term $\lambda = Y/\sigma$ is called the relative mean plane seperation. Using the above relations together with Eq. 2.17 yields the following dimensionless thermal contact conductance parameter:

$$C_c = \frac{h_c \sigma}{k_s m} = \frac{1}{2\sqrt{2\pi}} \frac{\exp(-\lambda^2/2)}{\left[1 - \sqrt{\frac{1}{2}\text{erfc}(\lambda/\sqrt{2})}\right]^{1.5}} \tag{2.23}$$

A correlation for the dimensionless thermal contact conductance based on the relative contact pressure P/H_p has been proposed by Yovanovich [43].

$$C_c = \frac{h_c \sigma}{k_s m} = 1.25 \left(\frac{P}{H_p}\right)^{0.95} \tag{2.24}$$

This correlation agrees with the theoretical values to within $\pm 1.5\%$ in the range $2 \leq \lambda \leq 4.75$.

In their study of contact resistance of worked metals Yovanovich et al. [40] introduced the idea of a microhardness surface layer. From experimental results it was shown that Vickers microhardness measurements with indentation depths of less than 10 μm resulted in significantly higher hardness values than observed for the bulk of the material. They found that in this surface layer microhardness is dependent on indentation depth (or indentation diagonal) by the function:

$$H_V = c_1 \left(\frac{d_V}{d_0}\right)^{c_2} \tag{2.25}$$

where c_1 and c_2 are correlation coefficients which must be determined from experimental results, d_V is the indentation diagonal and d_0 is a reference diagonal set to 1 μm. Using Eq. 2.25 Yovanovich et al. [40] found the appropriate plastic microhardness value from an iterative procedure for a given σ and m that could be used in the CMY contact model. Song and Yovanovich [34] later developed an explicit relationship for the relative contact pressure as:

$$\frac{P}{H_p} = \left[\frac{P}{c_1(1.62 \cdot (\sigma/m))^{c_2}}\right]^{1/(1+0.071c_2)} \tag{2.26}$$

The value of P/H_p determined from Eq. 2.26 is used in Eq. 2.24 to determine the dimensionless thermal contact conductance of an interface.

2.1.4 Elastic Contact Model: Mikic

A relationship for A_r/A_a is again required for Eq. 2.17 to determine the thermal contact conductance for an interface where the mode of deformation is elastic. Mikic [29] considered this problem using the work of Mikic and Roca [28]. They determined that the area of contact under elastic deformation is exactly proportional to the applied pressure by the following:

$$\frac{A_r}{A_a} = \frac{P}{E'\ m/\sqrt{2}} \tag{2.27}$$

where E', an equivalent elastic modulus of the two contacting surfaces is determined by:

$$\frac{1}{E'} = \left(\frac{1-\nu_1^2}{E_1} + \frac{1-\nu_2^2}{E_2}\right) \tag{2.28}$$

where E and ν are the elastic modulus and Poisson's ratio of the individual surfaces respectively. From Eq. 2.27 Yovanovich [41] described an "elastic microhardness" term which is analagous to the microhardness for the plastic mode of deformation:

$$H_e = \frac{E'\ m}{\sqrt{2}} \tag{2.29}$$

Mikic [29] considered an asperity in contact with a rigid flat surface where the asperity deformed elastically to determine the remaining geometric parameters in Eq. 2.17. He compared the elastic contact area to that found if the deformation were

purely plastic. At the same seperation (λ being equal), Mikic found that the contact area for any specific asperity in plastic deformation would be twice the contact area in elastic deformation. This would hold true for the entire surface. For the same λ:

$$\frac{A_{elastic}}{A_{plastic}} = \frac{1}{2} \tag{2.30}$$

The other geometric parameters necessary to predict the thermal contact conductance using Eq. 2.17 have been determined by Mikic [29]:

$$n = \frac{1}{16}\left(\frac{m}{\sigma}\right)^2 \frac{\exp(-\lambda^2)}{\text{erfc}(\lambda/\sqrt{2})} \tag{2.31}$$

$$a = \frac{2}{\sqrt{\pi}}\frac{\sigma}{m}\exp\left(\frac{\lambda^2}{2}\right)\text{erfc}\left(\frac{\lambda}{\sqrt{2}}\right) \tag{2.32}$$

$$\lambda = \sqrt{2}\,\text{erfc}^{-1}\left(\frac{4A_r}{A_a}\right) \tag{2.33}$$

Using the above relations together with Eq. 2.17 yields the following dimensionless thermal contact conductance parameter [29], [35]:

$$C_c = \frac{h_c\sigma}{k_s m} = \frac{1}{4\sqrt{\pi}}\frac{\exp(-\lambda^2/2)}{\left[1 - \sqrt{\frac{1}{4}\text{erfc}(\lambda/\sqrt{2})}\right]^{1.5}} \tag{2.34}$$

A correlation for the dimensionless thermal contact conductance based on calculated values from the theoretical relationship and using Eq. 2.29 has been proposed by Sridhar and Yovanovich [35]:

$$C_c = \frac{h_c\sigma}{k_s m} = 1.54\left(\frac{P}{H_e}\right)^{0.94} \tag{2.35}$$

where H_e is determined by Eq. 2.29. This correlation agrees with the theoretical values to within $\pm 2\%$ for the relative pressure range $10^{-5} \leq P/H_e \leq 0.2$. In the original correlation proposed by Mikic [29] the factor 1.54 in Eq. 2.35 was 1.55.

2.1.5 SY Elasto-Plastic Contact Model

Based upon the thermal model developed by Yovanovich [43] a model was proposed by Sridhar and Yovanovich [36] to describe the entire range of material behavior (elastic $\rightarrow$ plastic) which contains the deformation analysis of the plastic contact model of Cooper et al. [8] and Yovanovich [43] along with the deformation analysis of the elastic contact model of Mikic [29]. Sridhar and Yovanovich present a relationship for A_r/A_a similar to both the plastic and elastic contact models as:

$$\frac{A_r}{A_a} = \frac{P}{H_{ep}} \tag{2.36}$$

where H_{ep} is the elasto-plastic hardness, given by Sridhar and Yovanovich as:

$$H_{ep} = \frac{2.76 \cdot S_f}{\left[1 + \left(\frac{6.5}{\epsilon_c^*}\right)^2\right]^{\frac{1}{2}}} \tag{2.37}$$

where the non-dimensional contact strain is defined as:

$$\epsilon_c^* = 1.67 \cdot \frac{E'}{S_f} \cdot m \tag{2.38}$$

S_f is defined by Sridhar and Yovanovich [36] as a material yield/flow stress. A value for S_f must be determined to calculate Eqs. 2.37 and 2.38. Sridhar and Yovanovich [36] developed an iterative procedure to calculate the appropriate value of S_f and thus the elasto-plastic hardness (H_{ep}) for a conforming rough surface pair. This procedure includes solving Eqs. 2.39 to 2.45 sequentially until convergence.

$$S_f = \frac{1}{2.76\sqrt{\frac{1}{(H_{ep})^2} - \frac{1}{(H_e)^2}}} \tag{2.39}$$

$$\epsilon_c^* = 1.67 \cdot \frac{E'}{S_f} \cdot m \tag{2.40}$$

$$f_{ep} = \frac{\left[1 + \left(\frac{6.5}{\epsilon_c^*}\right)^2\right]^{\frac{1}{2}}}{\left[1 + \left(\frac{13.0}{\epsilon_c^*}\right)^{1.2}\right]^{\frac{1}{1.2}}} \tag{2.41}$$

$$\lambda = \sqrt{2}\ \mathrm{erfc}^{-1}\left(\frac{1}{f_{ep}(\epsilon_c^*)} \cdot \frac{2P}{H_{ep}}\right) \tag{2.42}$$

$$a = \sqrt{\frac{8}{\pi}}\sqrt{f_{ep}(\epsilon_c^*)}\frac{\sigma}{m}\ \exp\left(\frac{\lambda^2}{2}\right)\mathrm{erfc}\left(\frac{\lambda}{\sqrt{2}}\right) \tag{2.43}$$

$$d_V = \sqrt{2\pi} \cdot a \tag{2.44}$$

$$H_{ep} = \frac{H_V}{0.9272} = \frac{c_1}{0.9272} \cdot (d_V)^{c_2} \tag{2.45}$$

In Eq. 2.45 the Vickers microhardness H_V was divided by 0.9272 to convert the Vickers microhardness which is based on the total surface area of indentation to a hardness which is based on the projected area. The initial guess for H_{ep} was calculated as $\sqrt{H_p \cdot H_e}$. Similar to the CMY plastic contact model and the Mikic elastic contact model n is defined as:

$$n = \frac{1}{16}\left(\frac{m}{\sigma}\right)^2 \frac{\exp(-\lambda^2)}{\mathrm{erfc}(\lambda/\sqrt{2})} \tag{2.46}$$

Using the described relations together with Eq. 2.17 yields the following dimensionless thermal contact conductance parameter [36]:

$$C_c = \frac{h_c\sigma}{k_s m} = \frac{1}{2\sqrt{2\pi}} \frac{\sqrt{f_{ep}(\epsilon_c^*)}\ \exp(-\lambda^2/2)}{\left[1 - \sqrt{\frac{f_{ep}(\epsilon_c^*)}{2}}\ \mathrm{erfc}(\lambda/\sqrt{2})\right]^{1.5}} \tag{2.47}$$

An approximate correlation equation for the dimensionless thermal contact conductance relation for $\epsilon_c^* < 5$ is as follows [41]:

$$C_c = \frac{h_c \sigma}{k_s m} = 1.54 \left(\frac{P}{H_{ep}} \right)^{0.94} \tag{2.48}$$

2.2 Mode of Deformation Review

The mode of deformation must be known in order to accurately predict the thermal contact conductance of conforming rough surfaces. This is only the case if it is required to choose between the CMY plastic contact model or the Mikic elastic contact model. In contrast the SY elasto-plastic model does not require the mode of deformation to be known. While it is known that most "engineering" surfaces deform plastically [14], there are some cases where elastic deformation of the contacting surfaces could possibly be expected.

Two methods are presented here which give insight into the mode of deformation that could be expected with contacting surfaces. The first is based on the work completed by Sridhar and Yovanovich [36] for their SY elasto-plastic contact conductance model. It can be used to directly evaluate the mode of deformation of the surfaces in contact using properties from both surfaces. The second method is based on the work completed by Marsh [27]. This method uses results from a compression test along with indentation hardness to estimate the mode of deformation of the material below an "indenter".

2.2.1 Non-Dimensional Contact Strain : ϵ_c^*

The parameter ϵ_c^* developed by Sridhar and Yovanovich [36] for their SY elasto-plastic contact model is used to determine which mode of deformation is appropriate for surfaces in contact. Since ϵ_c^* is defined as dependent only on material and surface

properties and independent of load, it can be used to evaluate the mode of deformation of conforming rough surfaces. As a comparison between the elastic and plastic modes of deformation Sridhar and Yovanovich [36] plotted H/S_f as a function of ϵ_c^* using the SY elasto-plastic model for H_{ep}/S_f (Eq. 2.37) as a way to "blend" the two modes of deformation.

Sridhar and Yovanovich [36] non-dimensionlised the elastic hardness given in Eq. 2.29 with S_f which lead to the following *elastic* relationship:

$$\frac{H_e}{S_f} = \frac{4}{3\pi} \cdot \epsilon_c^* \tag{2.49}$$

For fully work hardened materials undergoing *plastic* deformation Tabor [37] gives the relationship between hardness (based on the projected area of indentation) and yield stress as:

$$\frac{H_p}{S_f} = 2.8 \tag{2.50}$$

Tabor [37] developed this relationship based on experimental analysis but by doing so he was confirming his theoretical analysis of a rigid-die indenting a rigid plastic material which gave approximately the same value.

The result of their comparison is given in Fig. 2.5. From Fig. 2.5 the following behaviour for surfaces in contact is determined:

1. As $\epsilon_c^* \to 0$, $H_{ep} \to H_e$ which indicates that the SY elasto-plastic contact model has reduced to the Mikic elastic contact model. In this situation the strain of the contacting asperities is at a level such that only elastic deformation of the contacting asperities occurs. For practical purposes the mode of deformation becomes predominantly elastic when ϵ_c^* is less than 4.

2. As $\epsilon_c^* \to \infty$, $H_{ep} \to H_p$ which indicates that the SY elasto-plastic contact model has reduced to the CMY plastic contact model. In this situation the strain of

the contacting asperities is at a level such that only plastic deformation of the contacting asperities occurs. For practical purposes the mode of deformation becomes predominantly plastic when ϵ_c^* is greater than 11.

3. For intermediate values of ϵ_c^* which for practical purposes is when ϵ_c^* is between 4 and 11 the strain of the contacting asperities is at a level such that a combination of elastic and plastic deformation of the contacting asperities occurs.

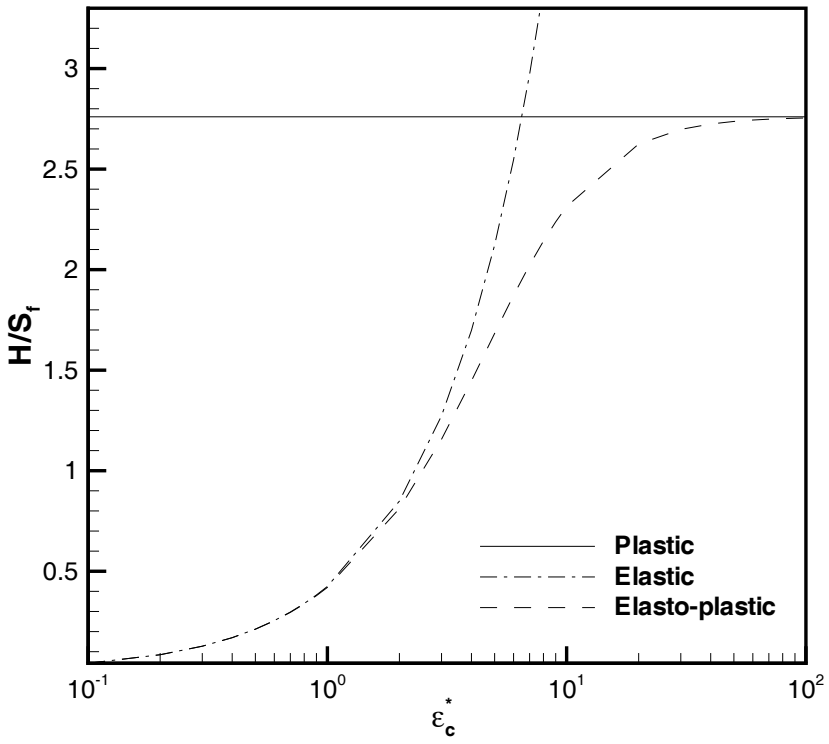

Figure 2.5: H/Y as a function of ϵ_c^* for the plastic, elastic and SY elasto-plastic contact models [36].

2.2.2 Indentation Hardness

The mode of deformation of an individual polymer surface in contact with a rigid indenter can be determined from the analysis of Marsh [27]. While this analysis was not directly developed for the situation of two surfaces in contact, it can provide insight into the situation where a rigid material (ie. metal) is making contact with a significantly less rigid material (ie. polymer).

Marsh [27] looked at the relationship between hardness and yield stress in glasses and noticed that they did not follow the rigid-die indentation hardness theory proposed by Tabor [37], given in Eq. 2.50. Marsh found that glasses and other highly elastic materials gave values of H/Y significantly lower than the value of 2.8 suggested by Tabor. Since Tabor's relation had been firmly established both experimentally and analytically Marsh [27] stated:

.. the solution must lie in the introduction of some alternative mode of deformation energetically more favourable than the flat rigid die system for highly elastic materials.

Marsh [27] proposed the following indentation hardness model for these *elastic* materials that is based on the premise that elastic materials (or materials with low E/Y values) allow displaced material to move radially away from the indentation due to material elasticity:

$$\frac{H}{Y} = C + K \cdot \frac{3}{3-\lambda} \ln\frac{3}{\lambda + 3\mu - \lambda\mu} \tag{2.51}$$

where

$$\lambda = (1-2\nu)\cdot Y/E \quad \text{and} \quad \mu = (1+\nu)\cdot Y/E$$

Marsh [27] suggested the following expression based on Eq. 2.51:

$$\frac{H}{Y} = C + K \cdot B \ln Z \tag{2.52}$$

The contstants C and K were fitted from experimental results and found to be: $C = 0.28$, $K = 0.60$ [27]. To verify his model Marsh performed microhardness and compression tests on a wide range of materials of varying E/Y values and found remarkable agreement.

Assuming a Poisson's ratio of 0.35 the model proposed by Marsh [27] is shown in Fig. 2.6 as H/Y versus E/Y along with the rigid-die model given by Tabor [37]. Since there is nothing in Marsh's model to indicate that H/Y has an upper limit at 2.8 the rigid-die model must become energetically more favourable for materials with large E/Y values [38].

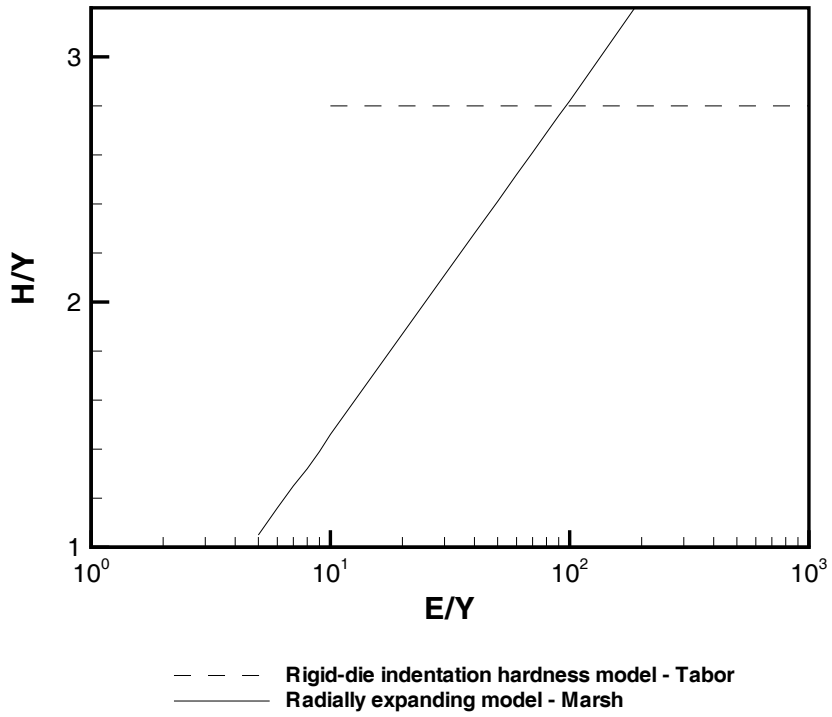

Figure 2.6: Marsh indentation hardness model [27] along with the rigid-die model given by Tabor [37].

From Fig. 2.6 the mode of deformation of an individual surface in contact with a rigid indenter can be found. Materials with E/Y values less than 100 (such as polymers) should follow an *elastic* mode of deformation while materials with E/Y values greater than 100 (such as most work hardened metals) should follow a *plastic* mode of deformation.

2.3 Thermal Resistance of Polymer Joints

Early research that was conducted to investigate the thermal contact conductance of a joint involving a polymer focused primarily on gasket materials. They were interested in experimentally determining the thermal isolation characteristics of materials suitable for spacecraft applications. Recent work has been completed to both model and experimentally determine the thermal contact resistance of a joint involving a more rigid polymer layer.

2.3.1 Gasket Materials

At a time when few investigators had measured the thermal conductance of a joint involving an interstitial material Fletcher and Miller [12] conducted experiments involving elastomer gasket materials located between aluminum flux-meters. Their results were reported as a total joint conductance which included both the bulk conductance of the polymer along with the contact conductance at both interfaces. They made no direct measurements of the thermal contact conductance of the gasket - aluminum interface. Operating in a vacuum environment they evaluated the joint conductance of 13 elastomer gasket materials over an interfacial pressure range that varied from 345 kPa - 2068 kPa. Experimental data were obtained for sample mean temperatures of 38 $^{\circ}C$ and 66 $^{\circ}C$.

Their results are presented in graphical form as joint conductance versus pressure.

They showed that all elastomers gave lower joint conductance values than that of the bare aluminum-aluminum joint. The majority of the elastomers tested proved useful for thermal isolation. Thermal isolation is necessary in applications requiring insulation between systems of different temperature. They did not propose any models for predicting the results of their data.

Fletcher et al. [11] investigated the insulation characteristics of polyethlene materials with and without carbon black added. They also measured the total conductance of the joint rather than determining the thermal contact conductance of the polyethylene-aluminum interface. Their tests were conducted in a vacuum environment for apparent contact pressures that ranged from 414 kPa - 2758 kPa. Experimental data were obtained for sample mean temperatures of 29 $^{\circ}C$ and 57 $^{\circ}C$. They evaluated two different sample thicknesses (1.9 mm and 3.2 mm) for six different polyethylene types. They presented their results in graphical format as joint conductance versus pressure. They found that polyethylenes with carbon black as an additive displayed conductance values approximately 20 % higher than those without. Also, all polyethlyene types tested showed excellent thermal insulation properties.

Parihar and Wright [33] completed an experimental study by looking at the thermal contact resistance and total joint resistance of a SS304/silicone rubber/SS304 joint in air over an interfacial pressure range that varied from 20 kPa - 250 kPa. The silicone rubber was cut from a 4.76 mm thick sheet and instrumented with T-type thermocouples. The SS304 surfaces in contact with the silicone were prepared by bead blasting. Surface parameters for both materials were determined from the use of an optical profilometer. Their experimental results include thermal contact resistance because they used thermocouples in the silicone which allowed them to determine the actual temperature drop at the SS304-silicone interfaces. This procedure had not been completed by previous researchers who only determined the full joint resistance which included the contact and bulk resistance. They found that the bulk resistance accounted for 65%-70% of the total resistance but do not state what value

for the thermal conductivity of silicone was used. The thermal contact resistance at the "hot" interface was found to be 1.3-1.6 times greater than the thermal contact resistance at the "cold" interface. They suggest that this may be due to large differences in temperature at the interfaces as well as a large difference in the ratio of the thermal conductivities of the contacting materials in the direction of heat flow.

Parihar and Wright [33] claim that existing thermal contact resistance models such as the CMY plastic contact model [8] and the Mikic elastic contact model [29] which were developed for the interfaces of hard materials are not applicable to contacts which involve elastomeric materials because of the intrinsic properties of elastomers. They make note of three properties to support this premise:

1. Elastomers lack a single modulus of elasticity.
2. Elastomers are subjected to thermo-mechanical softening.
3. Elastomers have a strongly temperature dependent thermal conductivity.

They do not provide any comparison of their data to the described contact models. Parihar and Wright [33] also state that because elastomers can readily deform to fill the cavities of the metal surface that the real area of contact becomes greater than the apparent contact area. To argue this premise Bahrami et al. [5] state that since the real area of contact is a projection of the contacting surfaces on a plane normal to the direction of the applied load the real area of contact is always less than or at most equal to the apparent area. Also, the heat flow direction through the contact plane must be perpendicular.

2.3.2 Rigid Polymer Layer

Fletcher and Marotta [26] completed an experimental study investigating the thermal conductivity and thermal contact conductance of several polymer/aluminum joints

in a vacuum. The polymers tested include: ABS, Delrin, teflon, nylon, phenolic, polycarbonate, polyethlyene, polypropelyene, and PVC. They performed steady state thermal conductivity tests for three different polymer thicknesses (12.70 mm, 6.35 mm, 3.17 mm) at specimen mean temperatures that varied from 10 $^{\circ}C$ to 100 $^{\circ}C$. Using this method they found little variation in thermal conductivity values over the temperature range [26].

Fletcher and Marotta [26] used polymer samples of thickness 1.524 mm with surfaces prepared by machining for their determination of thermal contact conductance. They used a stylus profilometer to determine relevant surface properties. Fig. 2.7 shows a typical joint used in the determination of contact conductance. They performed contact conductance tests over an interfacial pressure range that varied from 510 kPa - 2760 kPa. The experimental results collected include both the bulk conductance of the polymer along with the contact conductance at one interface. Dow Corning 340 heat sink compound was used at one interface as indicated in Fig. 2.7. Thermal resistance at this interface was assumed to be negligible. They compared their collected results to the Mikic elastic contact model (Eq. 2.35) and to the CMY plastic contact model (Eq. 2.24). Both models were unable to predict the trends of the data. Bahrami et al. [5] note that this comparison between experimental data and the conductance models was "not appropriate" because the experimental data of Fletcher and Marotta mistakenly contained both bulk and contact conductance while the models only describe contact conductance. Fletcher and Marotta did not propose any additional thermal contact conductance models.

Fuller and Marotta [13] investigated the thermal contact conductance between conforming rough surfaces at a polymer-metal interface. They developed a new thermal contact conductance correlation based on the Mikic elastic model which they modified to incorporate the surface properties of a polymer. Their full joint model described in Eq. 2.55 includes their new contact conductance correlation and the bulk conductance of the polymer layer. To verify their model an experimental program

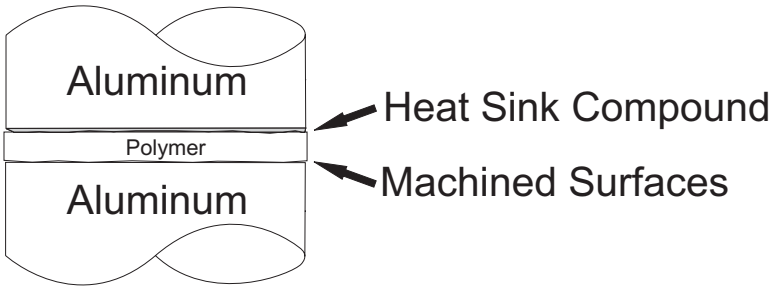

Figure 2.7: Typical joint used by Fletcher and Marotta [26] to determine contact conductance of joint.

was completed in which they measured the combined conductance of a polymer layer along with the contact conductance at the polymer-metal interface.

The basis for their development of a new thermal contact conductance correlation was the assumption that because the elastic modulus of a polymer is significantly lower than that of metals the real area of contact can actually become greater than the apparent contact area at high loads. Therefore, contact conductance models previously developed for metal-metal interfaces would require modifications to make them applicable to polymer-metal interfaces. Bahrami et al. [5] again state that this premise that A_r could be greater than A_a is incorrect since the real area of contact is a projection of the contacting asperities onto a plane normal to the applied load. This would only allow the real area to at most be equal to the apparent area.

Fuller and Marotta [13] chose to establish their new thermal contact conductance model as an elastic model based on the experimental study completed by Parihar and Wright [33], which measured the RMS roughness of stainless steel fluxmeters and a silicone specimen before and after loading. The roughness values were almost identical before and after loading which led to Parihar and Wright making the conclusion of elastic deformation. This conclusion is not correct because with two surfaces in contact only a small portion of asperities support the load and there would be little chance of detecting the deformed asperities.

Along with the study conducted by Parihar and Wright [33], Fuller and Marotta [13] supported their assumption of elastic deformation by performing a contact mechanics analysis of a rigid indenter making contact with an elastic layer. They found that unless the load was greater than approximately $5{\times}10^5\ N$, which for most applications is extremely large the contact radius of the single indenter could be modelled by the Hertzian solution. They used this analysis to support the assumption of using a thermal contact conductance model based on a Hertzian analysis (ie. an elastic model). A problem with this assumption is that for conforming rough surfaces there are only a few asperities that support the load and the pressure at the contacting asperities can reach extremely high values and show plastic deformation. Also, assuming elastic deformation may lead to the problem of calculating elastic microhardness values higher than material microhardness values which is physically impossible [5].

Based upon the elastic thermal contact model developed by Mikic [29], a thermal contact conductance model was proposed which incorporated surface properties of polymers [13]. They suggested to change the elastic contact hardness (H_e) in the Mikic model [29] to a polymer elastic contact hardness (H_{poly}), which they defined as:

$$H_{poly} = \frac{E_{poly}\ m}{2.3} \tag{2.53}$$

The basis for this change was that the Mikic elastic model [29] assumes deformation of the contacting asperities onto a rigid flat surface while for polymer-metal interfaces the new Fuller and Marotta model assumes rigid metal asperities in contact with a deforming polymer surface. Using H_{poly} together with the Mikic model allowed Fuller and Marotta to develop a new dimensionless contact conductance correlation:

$$C_c = \frac{h_c \sigma}{k_s m} = 1.49 \left(\frac{P}{H_{poly}} \right)^{0.935} \tag{2.54}$$

The full joint conductance model proposed by Fuller and Marotta [13] includes both

contact conductance due to the interface and the bulk conductance of the polymer layer:

$$\frac{1}{h_{joint}} = \frac{1}{h_c} + \frac{1}{h_{bulk}} \tag{2.55}$$

Fuller and Marotta [13] conducted experiments to measure the joint conductance of several metal/aluminum joints under vacuum over an interfacial pressure range that varied from 138 kPa - 2758 kPa. The polymers they tested include: PC, Delrin and PVC. Their prepared polymer surfaces were ground and surface parameters were measured using an optical profilometer. Figure 2.8 shows a typical joint used in the determination of contact conductance. The thermal conductivity of the polymers tested were taken from Marotta and Fletcher [26]. The experimental results collected include both the bulk conductance of the polymer along with the thermal contact conductance at one interface. Dow Corning 340 heat sink compound was used at one interface as indicated in Fig. 2.8. Thermal resistance at this interface was assumed to be negligible.

They compared their measured data to their full joint model. They showed dimensionless joint conductance plotted as a function of dimensionless pressure. The proposed model and their data show good agreement. They did not compare their collected experimental data to any other elastic or plastic conductance models.

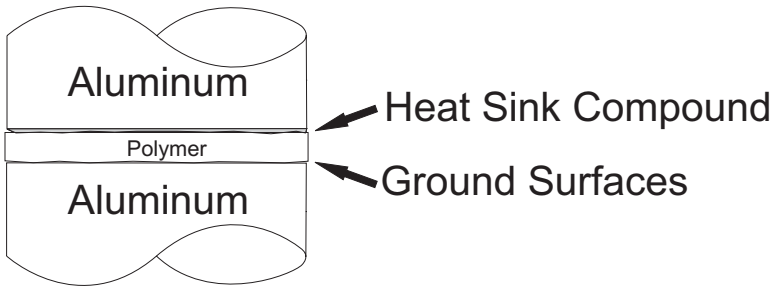

Figure 2.8: Typical joint used by Fuller and Marotta [13] to determine joint conductance.

Bahrami et al. [5] completed a review of the current works in the area of thermal contact resistance of polymer-metal joints. It was shown through a mode of deformation analysis based on the plasticity index given by Mikic [29] that the asperities in a polymer-metal joint deform plastically [5]. Also, they reiterated the point given by Greenwood and Williamson [14] that the mode of deformation of contacting asperities is not arbitrary and must be determined. Based on the assumption of plastic contact, Bahrami et al. [5] developed a compact model based on the CMY plastic contact model to predict the thermal joint resistance of a polymer-metal joint in a vacuum. The model includes both the bulk resistance of the polymer and contact resistance of the interface. Using the experimental data collected by Fletcher and Marotta [26] and Fuller and Marotta [13]; Bahrami et al. [5] found that the proposed model predicted the data trends quite well.

Narh and Sridar [32] performed thermal contact resistance experiments and proposed an interface resistance model to predict the thermal contact resistance of a polymer-metal interface. The motivation behind their study was to improve the modelling analysis for polymer molding applications. The method they used to determine the contact resistance was given by Hall et al. [16] where steady state thermal tests are performed on samples of varying thickness. With results plotted as joint resistance versus thickness thermal conductivity and thermal contact resistance can be extracted from the plot. To use this method the contact resistances from each sample must be the same. Narh and Sridar [32] were able to do this by first preheating the polymer samples above their glassy temperature in the apparatus and then completing the thermal tests at temperatures below their glassy temperatures. This step effectively removed any surface roughness and therefore they did not investigate the effects of surface roughness. Polystyrene was selected for their experimental work and tests were conducted in air. They completed two sets of tests, one at 65 $^{\circ}C$ and the second at 75 $^{\circ}C$ over an pressure range that varied from 300 kPa - 2100 kPa. They presented their results in graphical form for both thermal contact resistance

versus pressure and thermal conductivity versus pressure. Their data shows a trend of decreasing thermal contact resistance with increased pressure. They also present the following model to predict their thermal contact resistance data.

$$h = \frac{c_2\ k_1}{1 + e^{\ c_1(T-T_g)}} \left[1.25\ \frac{m}{\sigma}\ P_{hc}^{0.9}\right] + \left[A_1 v + A_2^{(T-T_g)}\ \ln(1+P)\right] \frac{k_2}{t} \qquad (W/m^2 \cdot K) \tag{2.56}$$

where A_1, A_2, c_1, c_2 are material constants, k_1, k_2 are the harmonic mean of the plastic and metal conductivities and plastic conductivity respectively, t is the thickness of the polymer, v is the specific volume of the polymer, P_{hc} is a dimensionless contact pressure, P is the contact pressure, T is the temperature of the polymer and T_g is the glass transition temperature of the polymer. They do not present the development of the model and make use of many undefined material constants. The model also bears a resemblence to the CMY plastic contact model [8].

Chapter 3

Experimental Study

The experimental configuration and procedure which allows for the measurement of thermal contact resistance of various interfaces under vacuum conditions is presented in this chapter. Three different interfaces were evaluated in this program:

1. The first experiment conducted involved a stainless steel interface. This type of interface involving similar metals had been previously studied by Hegazy [17] where the experimental results closely matched the theoretical predictions. The procedure/setup suggested by Hegazy [17] was followed for this experiment. This includes forming the interface with a rough, bead blasted surface and a lapped surface illustrated in Fig. 3.1a.

2. The next experiments involved metal to polymer contacting surfaces. This interface consisted of a bead blasted polycarbonate surface in contact with a lapped stainless steel surface illustrated in Fig. 3.1b. A stainless steel flux-meter was used as the contacting lapped surface for both experiments.

3. The final experiments involved polymer to polymer contacting surfaces. This interface consisted of a bead blasted polycarbonate surface in contact with a lapped polycarbonate surface illustrated in Fig. 3.1c.

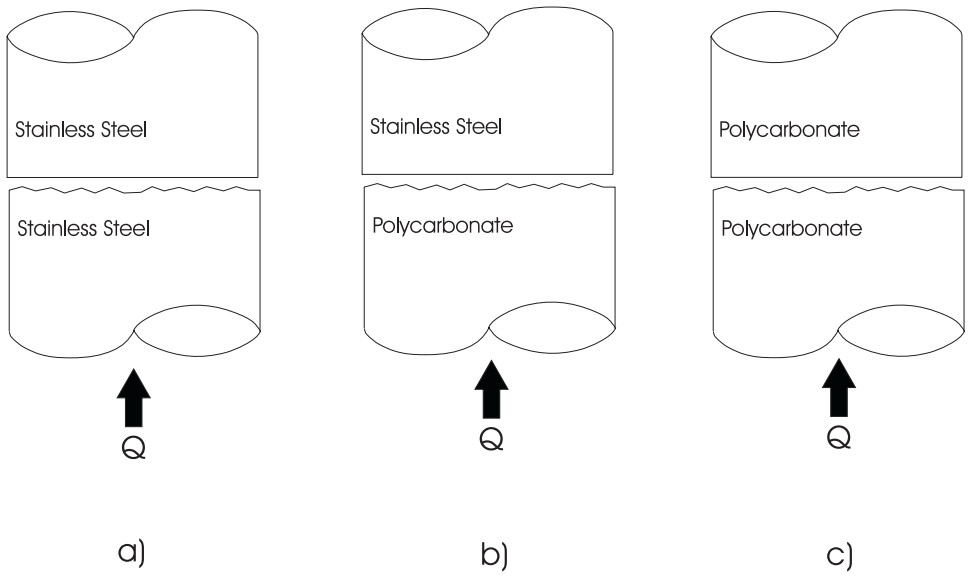

Figure 3.1: Overview of contacting surfaces: a) Stainless Steel to Stainless Steel, b) Polycarbonate to Stainless Steel, c) Polycarbonate to Polycarbonate

3.1 Apparatus

All thermal experiments were carried out in a vacuum system as shown in Fig. 3.2. The system is composed of a test column contained under a Labglass vacuum bell jar, a personal computer running a LabVIEW^{TM} program written by Dr. P. Teertstra to fully automate the thermal experiments, a Keithley Model 2700 data acquisition system, and a mechanical and diffusion pump which operate in series to create a vacuum of approximately 10^{-5} torr.

3.1.1 Test Column: Base Configuration

The base configuration of the vertically aligned test column used to determine the thermal contact resistance of a metal to metal interface is shown in Fig. 3.3. From top to bottom, the test column consisted of: load cell, heat sink, flux-meters, and heater block. The test column was placed inside a vacuum chamber, connected to a

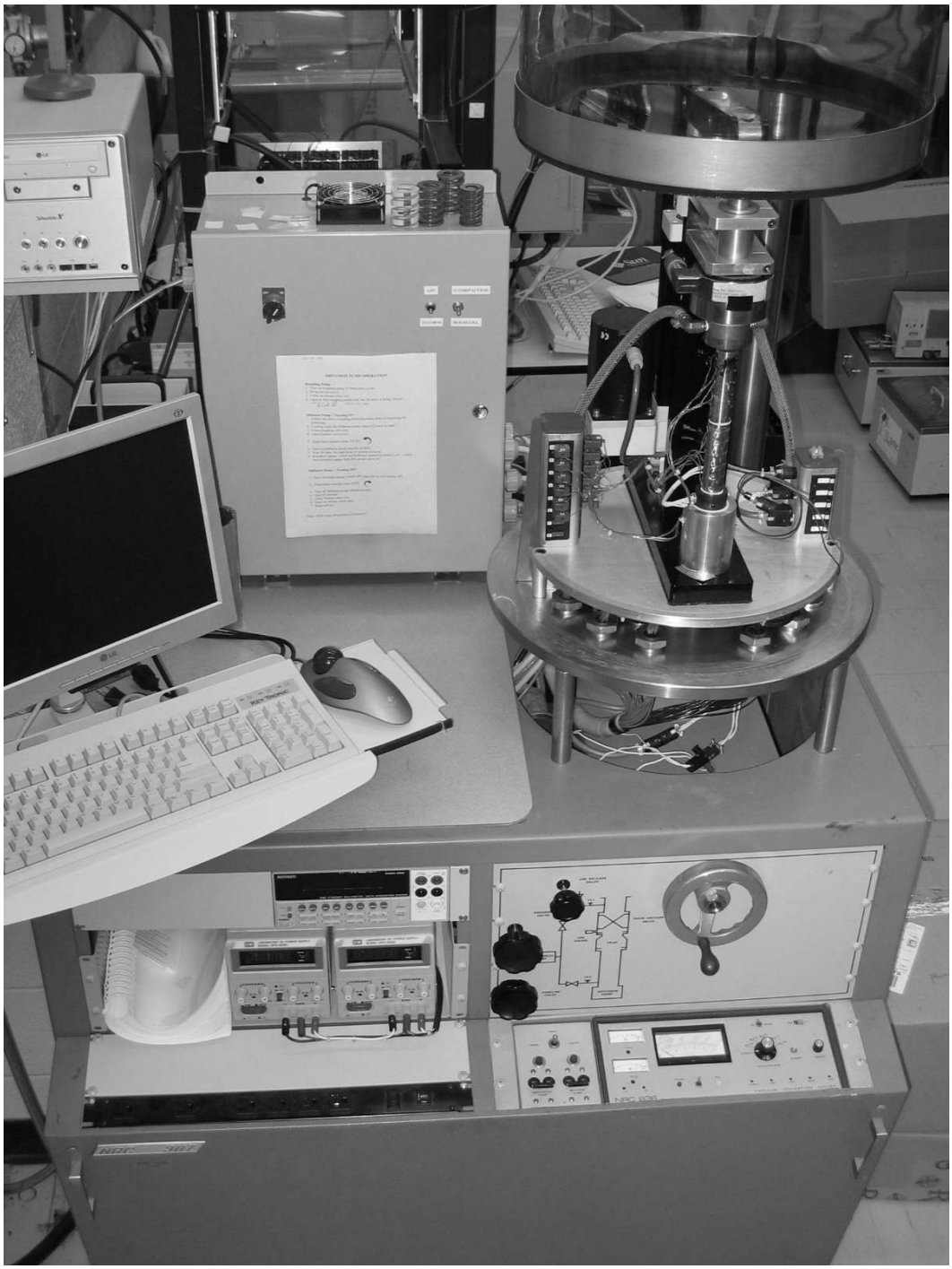

Figure 3.2: Experimental Apparatus

mechanical pump and a diffusion pump in series.

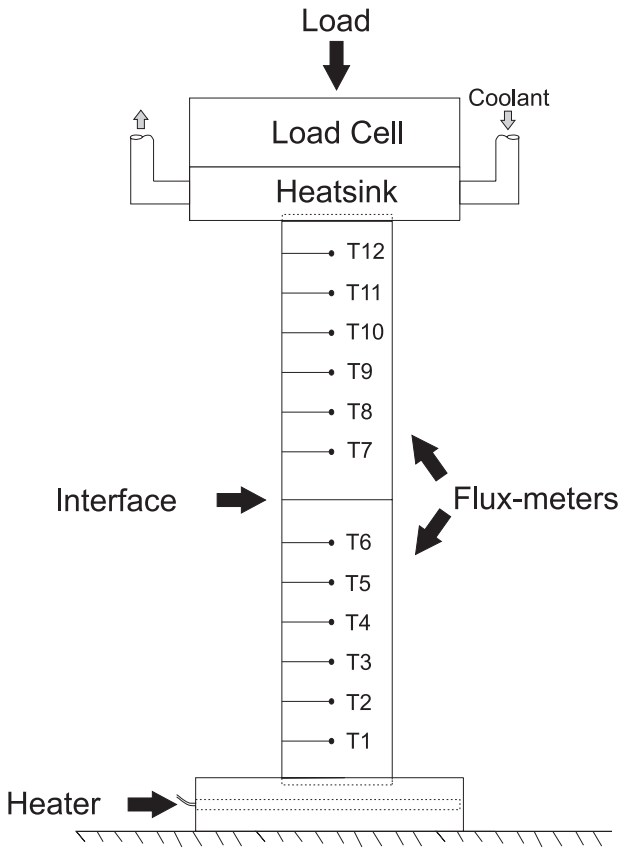

Figure 3.3: Base configuration of test column.

The load was applied to the test column by means of a IDC electric linear actuator. The operation of the linear actuator was controlled by LabVIEW^{TM}. LabVIEW^{TM} only adjusted the load prior to the start of a thermal test. During testing thermal expansion would cause an increase in load on the test column. The load was read by means of a calibrated Sensotec-2000 lbf load cell which was connected to the data acquisition system.

A copper heat sink was used to remove heat from the test column. The contacting surface of the heat sink was maintained at approximately 8 $^{\circ}C$ during each of the experiments by means of a Haake F3 thermal bath containing glycol. Flexible hoses were used to connect the heat sink to the thermal bath. A slight recess was machined

into the heat sink to allow proper placement of the upper flux-meter.

A copper heater block containing Omegalux cartridge heaters was used to supply heat to the system. A slight recess was also machined into this block to ensure proper placement of the lower fluxmeter. The Omegalux cartridge heaters were connected to a GW GPS-3030D DC power supply that was under LabVIEW^{TM} control during the duration of an experiment.

Two flux-meters were required in order to determine the average value of the heat conducted through the interface and the temperature drop across the interface. Details required to calculate these values are fully discussed in Section 5.1. The contact of the flux-meters formed the metal to metal interface under investigation. The circular flux-meters were constructed from a 25.4 mm diameter 304 stainless steel rod. Temperature readings in the flux-meters were accomplished using six T-type thermocouples imbedded into each flux-meter using Devcon® aluminum putty. A calibration of an equivalent thermocouple setup was completed by Milanez [31]. It was found in a comparison between thermocouples that the uncertainty of temperature difference readings could be assumed to be $\pm$ 0.1 $^{\circ}C$.

It was necessary to use relatively low heat flux values to perform thermal testing with polymers. This was necessary because polymers possess a thermal conductivity of approximately $0.2 - 0.3$ $(W/m \cdot K)$ and a high heat flux would raise the polymer above the glassy temperature whereby it would deform and/or melt effectively ending the experiment. To maximize the temperature drop along the flux-meters when a relatively low heat flux passed through them a material with a low thermal conductivity was necessary. Maximizing the temperature drop along the flux-meters minimized the effect of the error in the thermocouple readings. Another way to maximimize the temperature drop along the flux-meters was to increase the spacing between the thermocouples. This was accomplished by using a flux meter of 90 mm in length which was twice the length than that used by previous researchers [17, 30]. Thermocouples were positioned 15 mm apart from each other and spread along the longitudinal di-

rection as opposed to a 6 mm spacing which was used with 45 mm flux-meters. Also, the first and last thermocouples were positioned 7.5 mm from each end.

The metal typically used for flux-meters in thermal testing is calibrated electrolytic iron which has a thermal conductivity on the order of 70 $(W/m \cdot K)$. In comparison 304 stainless steel has a thermal conductivity on the order of 16 $(W/m \cdot K)$. Table 3.1 presents a comparison of the thermal performance of these two materials.

Table 3.1: Thermal performance of electrolytic iron and 304 stainless steel flux-meters, $Q = 3.5\ W$

	Electrolytic Iron		304 Stainless Steel	
Flux-meter Length (mm)	90	45	90	45
Thermocouple Spacing (mm)	15	6	15	6
Flux-meter ΔT ($^\circ C$)	8.9	4.4	38.8	19.4
Spacing ΔT ($^\circ C$)	1.5	0.6	6.5	2.6

Using the 90 mm stainless steel flux-meters as compared to the 45 mm electrolytic iron flux-meters resulted in a increase in ΔT between the flux-meters by a factor of 11. This decreases the uncertainty of temperature difference readings between the thermocouples in this example from 17% for the 45 mm electrolytic iron flux-meters to 1.5% for the 90 mm stainless steel flux-meters. For this reason the 90 mm stainless steel flux-meters were selected for thermal testing with polymers.

Thermal Conductivity of 304 Stainless Steel

Since the thermal conductivity of a material can show significant variation between manufacturers, this property was experimentally determined for the 304 stainless steel flux-meters. The thermal conductivity of stainless steel was obtained through thermal testing with calibrated electrolytic iron flux-meters. Electrolytic iron was

supplied with known thermal conductivity values given in Table A.1 in Appendix A. To calculate the thermal conductivity of stainless steel using electrolytic iron, a series of thermal experiments were conducted to calibrate the stainless steel flux-meters. For each experiment the thermal conductivity of stainless steel was calculated at the average temperature of the six thermocouples using the following modified Fourier's equation:

$$k_{SS304} = \frac{Q_{avg}}{A_a \cdot \Delta T/\Delta z} \quad (W/m \cdot K) \tag{3.1}$$

where Q_{avg} is the average value of Q calculated from each of the calibrated electrolytic iron flux-meters, A_a is the apparent area, $\Delta T/\Delta z$ is the slope of a linear fit of the stainless steel temperature measurements. Details required to calculate these values are fully discussed in Section 5.1. Based on the experimental data presented in Table A.2 in Appendix A the thermal conductivity correlation for 304 stainless steel was determined to be:

$$k_{SS304} = 0.0237 \cdot T(^\circ C) + 13.467 \quad (W/m \cdot K) \tag{3.2}$$

which is accurate to less than $\pm 1\%$ in the temperaure range 50 $^\circ C$ to 90 $^\circ C$. It was assumed that the linear trend of the stainless steel thermal conductivity described by Eq. 3.2 can be extrapolated to include 120 $^\circ C$.

3.1.2 Test Column: Polymer Interfaces

The column configurations used to measure the thermal contact resistance of both a polymer-metal interface and a polymer-polymer interface were similar to the base configuration shown in Fig. 3.3. Modifications were required at the metal-metal interface and are shown in Fig. 3.4 for a polymer-metal interface and Fig. 3.5 for a polymer-polymer interface.

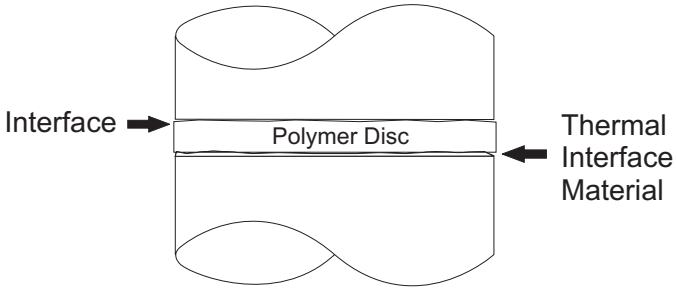

Figure 3.4: Modification of base configuration - polymer-metal interface

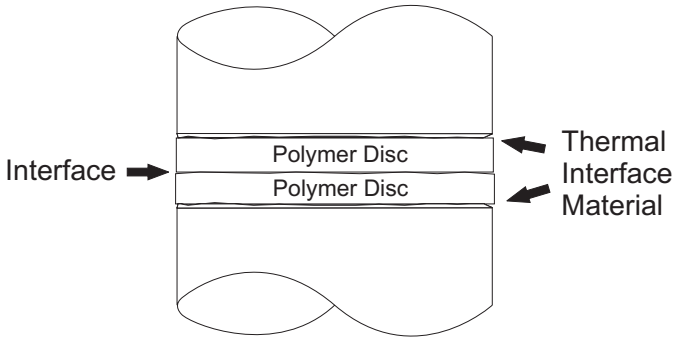

Figure 3.5: Modification of base configuration - polymer-polymer interface

It was necessary to use polycarbonate discs of thickness 0.79 mm (1/32 inch) for thermal testing because they created a minimal temperature drop across the disc. A minimal temperature drop was required in order to maintain the polycarbonate discs at a temperature well below the glass transition temperature of polycarbonate.

Initially polycarbonate discs of thickness 5 mm were used for polymer interface evaluation. These discs were each instrumented with thermocouples to allow a direct evaluation of the thermal contact resistance at a polycarbonate to polycarbonate interface. Several difficulties with this experimental method include: the heat which flowed through the interface, Q was typically half of the value which flowed through the thin (0.79 mm (1/32 inch)) polycarbonate discs. Decreasing the value of Q emphasizes the effect of the error in the flux-meter thermocouple readings. Another difficulty was that the thermocouples imbedded in the polycarbonate provided an additional path for heat to leave the polycarbonate and resulted in a non-linear tem-

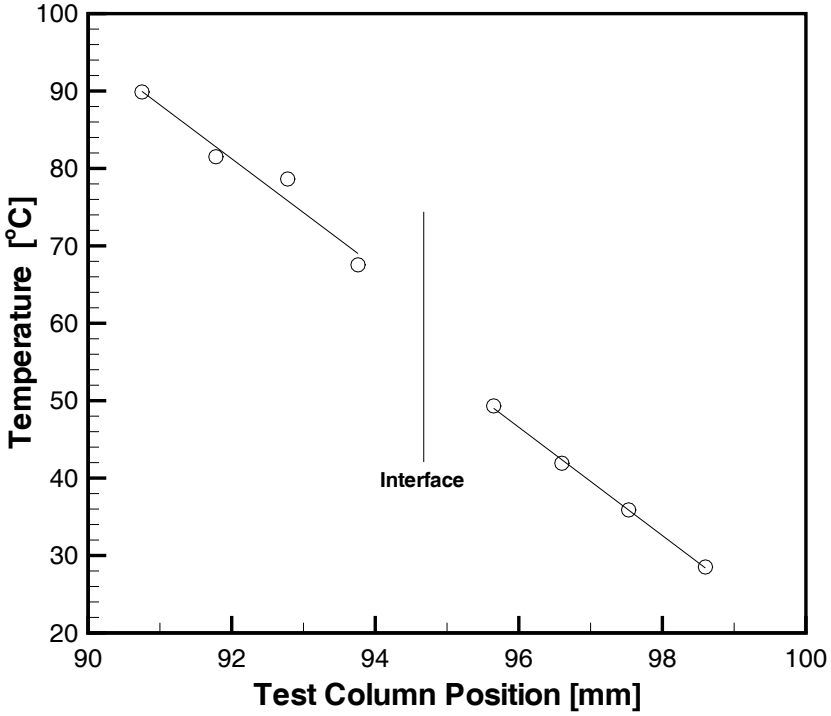

Figure 3.6: Temperature profile of two 5 mm polycarbonate discs in contact with each other. Polycarbonate discs are outfitted with thermocouples.

perature profile. Figure 3.6 presents a typical steady-state temperature profile of two 5 mm discs in contact with each other where this problem is illustrated. A linear fit of the temperature data in each disc is also shown for comparison.

Thermal interface materials were required at interfaces where the thermal contact resistance was not being investigated to ensure a minimal temperature drop in the joint. Dow Corning 340 heat sink compound was initially used but was found to be drawn into the interface under investigation effectively ending the experiment. To evaluate alternative thermal interface materials thermal tests were conducted with a setup similar to the base configuration with modifications to the interface as shown in Fig. 3.7. Alternative materials tested include Powerstrate^{TM}, a phase-change

thermal interface material, eGraf® 1220, a thin graphite thermal interface material and a bare interface as a baseline. To compare these materials the calculated thermal resistance of a joint using the described thermal interface materials is shown in Table 3.2. Calculation details are discussed in Section 5.1.2.

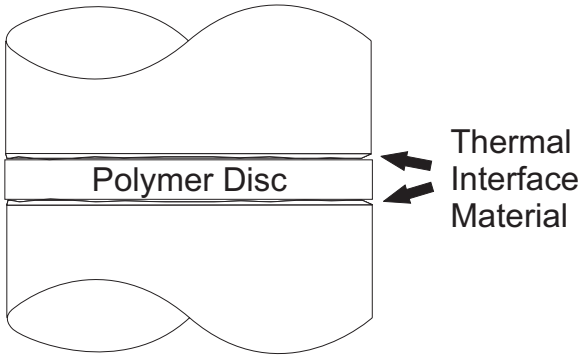

Figure 3.7: Modification of base configuration - thermal interface materials

Table 3.2: Thermal joint resistance using various thermal interface materials evaluated at approximately 700 kPa (100 psi)

Thermal Interface Material	R_{joint} $[K/W]$
Dow Corning 340	7.21
Powerstrate™	7.88
eGraf® 1220	8.02
Bare Interface	41.22

The alternative interface materials tested showed to be comparable to the Dow Corning 340 heat sink compound in regards to minimizing joint resistance in comparison to the bare interface. During thermal testing the Powerstrate™ moved out of the joint when heated to the liquid phase which could lead to the same problem encountered when testing with the Dow Corning 340 heat sink compound. For this reason eGraf® 1220 which maintained its shape during testing was selected for use in

thermal contact resistance tests involving polymers. A new piece of eGraf® 1220 was used for each thermal test. Specifications for eGraf® are presented in Appendix B.

3.2 Specimen Preparation

Thin polymer discs were cut to a diameter of 25.4 *mm* from a polycarbonate sheet of thickness 0.79 *mm* (1/32 inch). The following is a description of the surface preparation carried out for each of the three types of interfaces under investigation:

1. For the metal to metal test, both contacting faces were prepared on a lathe then hand lapped. Additionally, the face of the lower stainless steel flux meter was then prepared by glass bead blasting. One interface was evaluated and is referred to as SS-SS.

2. For polymer to metal tests, the contacting face of the polycarbonate disc was prepared by glass bead blasting. The other face of that disc was hand lapped. The stainless steel heat flux-meter with a lapped surface was also used as the metal contacting surface for this type of interface. Two seperate polymer-metal interfaces were evaluated and are referred to as PC-SS-1 and PC-SS-2.

3. For polymer to polymer tests, two polycarbonate discs were required for each experiment. The contacting face of the lower polycarbonate disc was prepared by glass bead blasting. The other face of that disc was hand lapped. Both faces of the upper polycarbonate disc were hand lapped. Two seperate polymer-polymer interfaces were evaluated and are referred to as PC-PC-1 and PC-PC-2.

Flex-O-Lite BT-5 industrial glass beads were used for the bead blast surface treatment. The diameter of the glass beads were approximately 0.35 *mm*. The surfaces were bead blasted for 30 seconds at 60 *psi*. One of the effects of bead blasting thin polycarbonate discs was that it caused the surface of the disc that underwent the

bead blast treatment to develop a concave geometry. The cause of this effect was the compressive stresses imparted to the surface by the bead blast treatment. The concave surface profile was noticed by completing a full trace of the surface using a Mitutoyo SJ-401 Profilometer. It was found that the concave surface was out of flat by approximately 80 μm. A solution to this problem was to initially bead blast both surfaces of the polycarbonate disc followed by hand lapping one of the surfaces.

Prior to thermal testing polycarbonate discs were first cleaned in an ultrasonic bath, rinsed in water and finally dried in a stream of air. Contacting stainless steel faces were thoroughly cleaned with acetone prior to each thermal experiment.

A closer inspection of both bead blasted and lapped polycarbonate surfaces were completed using a Scanning Electron Microscope (SEM) and is shown in Fig. 3.8 for a bead blasted surface and Fig. 3.9 for a lapped surface.

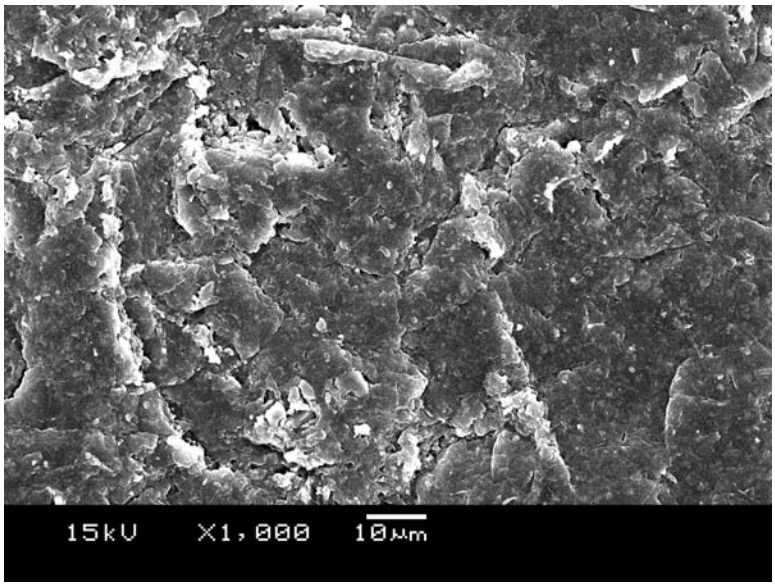

Figure 3.8: SEM micrograph of a bead-blasted polycarbonate surface, 1000X

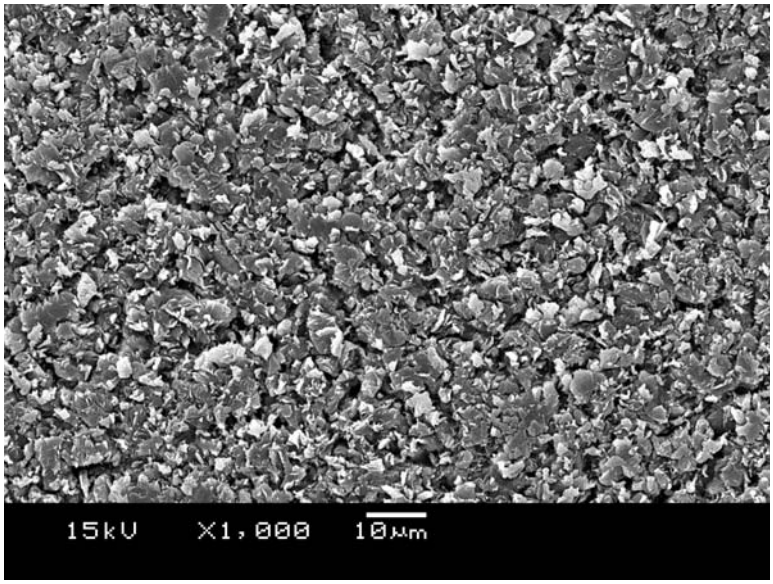

Figure 3.9: SEM micrograph of a lapped polycarbonate surface, 1000X

3.3 Test Procedure

For each of the three types of interfaces (metal-metal, polymer-metal, and polymer-polymer) the thermal contact resistance was determined from the following procedure:

1. The test column configuration was assembled and aligned with a relatively small load manually applied to the column to maintain its position. Between the heat sink/source and the flux-meters a thin layer of Dow Corning 340 heat sink compound was applied. Thermocouples from the flux-meters were connected to the Keithley Model 2700 data acquisition unit.

2. A guard heater was positioned around the lower flux-meter and adjusted so that the inner temperature of the guard heater approximately matched the temperature of the column. The guard heater consisted of a polycarbonate tube with dimensions: 32 mm (1.25 inch) inner diameter by 90 mm (3.5 inch) with reflective aluminum tape on the inside surface and a 5 watt adhesive resistance heater attached to the outside surface.

3. LabVIEW^{TM} software designed to measure thermal contact resistance of contacting surfaces was initiated. This program received the following user input: flux-meter configuration, cartridge heater voltage, test column load, and convergence criteria level. Through the Keithley data acquisition system, LabVIEW^{TM} adjusted the cartridge heater voltage and test column load to the user specified settings. Thermocouple and load cell data were subsequently recorded. The thermal contact resistance of the contacting surfaces were calculated and recorded every 10 seconds. A screenshot of the LabVIEW^{TM} software is given in Fig. 3.10.

4. The Labglass vacuum bell jar was lowered to enclose the test column and the mechanical pump and diffusion pump were run in series to create a vacuum of approximately 10^{-5} torr.

5. The system was considered to have reached a steady state when the difference in consecutive thermal contact resistance values were less than the convergence criteria level specified. The convergence criteria level was specified at 10^{-6} and was typically reached within 6-8 hours.

3.4 Uncertainty Error Analysis

An uncertainty error analysis was carried out to estimate the uncertainty associated with each thermal contact resistance measurement. This analysis is based on the procedure described by Wheeler and Ganji [39]. Analysis details can be found in Appendix C.

For metal-metal tests the uncertainty in the reported thermal contact resistance values was found to be approximately 6%, independent of load. For polymer-metal tests the uncertainty in the reported thermal contact resistance values was found to

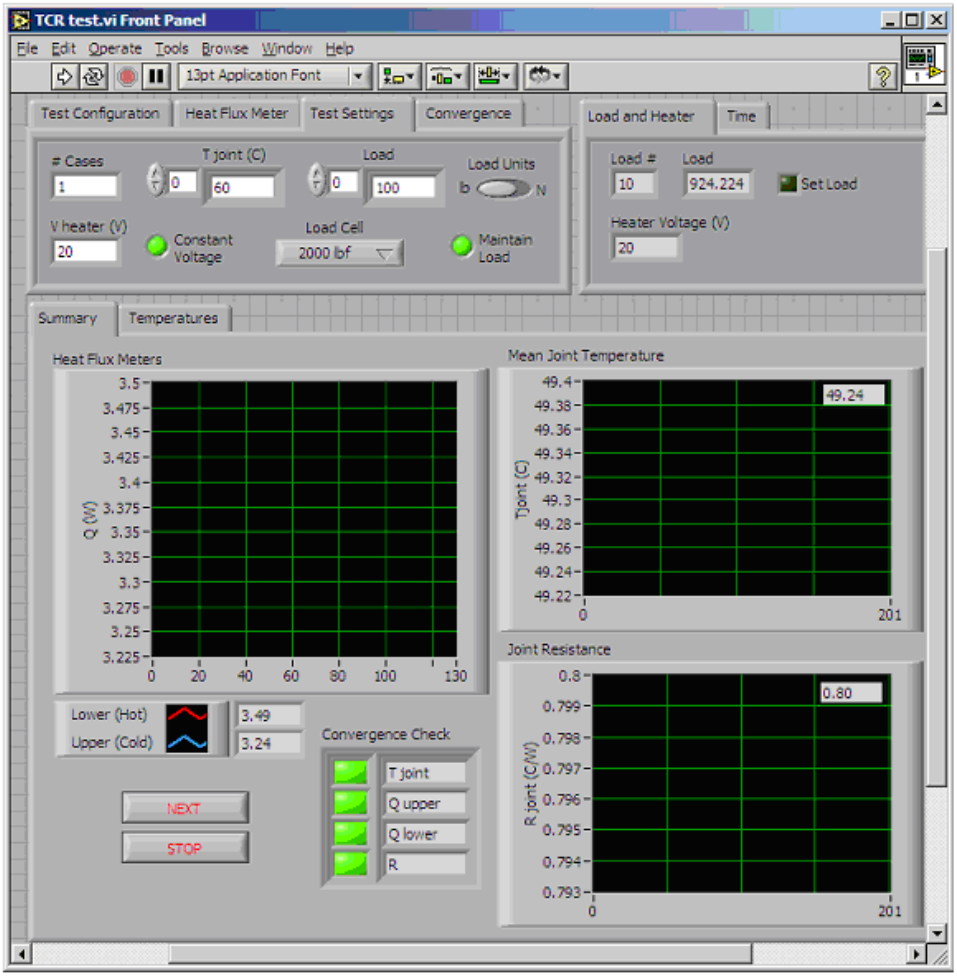

Figure 3.10: LabVIEW^{TM}screenshot

range from 18% at the lightest load to greater than 100% at the highest applied load. For polymer-polymer tests the uncertainty in reported thermal contact resistance values was found to range from 39% at the lightest load to greater than 250% at the highest applied load. The high uncertainty percentage estimates occur in part because the measured thermal contact resistance values decrease in value with load and approach the uncertainty estimates which remain relatively constant for each thermal test regardless of load.

Chapter 4

Surface Roughness, Microhardness and Compression Experiments

Preliminary tests were required to provide necessary information for thermal contact resistance modelling. Necessary information includes: surface roughness, surface microhardness, and mechanical properties. Surface microhardness and mechanical properties were also compared to the radially expanding model of Marsh [27].

4.1 Surface Roughness

In order to predict the flow of heat through conforming rough surfaces, roughness parameters which characterize the topography of each surface must be determined. Two important parameters which are used for thermal contact resistance modelling are: RMS roughness (σ) and absolute mean asperity slope (m).

For each thermal test where thermal contact resistance was determined, the surface roughness parameters of each surface in the interface were evaluated prior to loading. This was accomplished using a Mitutoyo SJ-401 Profilometer. Each test followed ASME standard: B46.1 - 2002 [2] as a reference for test procedure. The output of a

profilometer trace included the required parameters: σ and m. Five random traces were made on each surface that underwent thermal testing. The average roughness of the stainless steel surfaces investigated are presented in Table 4.1. The average roughness of the bead blasted polycarbonate surfaces used in the polycarbonate to stainless steel interfaces are also presented in Table 4.1. The average roughness of the polycarbonate surfaces used in the polycarbonate to polycarbonate interfaces are presented in Table 4.2. Full details of this surface roughness study are presented in Appendix D.

Table 4.1: Average roughness of each surface investigated: SS-SS and PC-SS

		SS-SS		PC-SS-1	PC-SS-2
		Bead Blasted	Lapped	Bead Blasted	Bead Blasted
σ	(μm)	1.48	0.31	1.87	1.53
m	(radian)	0.076	0.053	0.078	0.075
σ/m	(μm)	19.54	5.79	23.88	20.46

Table 4.2: Average roughness of each surface investigated: PC-PC

		PC-PC-1		PC-PC-2	
		Bead Blasted	Lapped	Bead Blasted	Lapped
σ	(μm)	2.45	0.39	1.78	0.49
m	(radian)	0.115	0.062	0.084	0.085
σ/m	(μm)	21.35	6.36	21.28	5.7

In his development of the CMY thermal contact conductance model Yovanovich [43] posed an assumption that the surface asperities of each contacting surface have a Gaussion height distribution about a mean plane passing through each surface.

To verify this assumption for polymer materials six different bead blasted polycarbonate surfaces were examined. For each bead blasted surface five random traces were taken using the profilometer. The surface profile output, discrete readings of $y(x)$ taken at regularly spaced intervals were normalized with respect to the RMS roughness of that trace or $Z^* = y(x)/\sigma$. The range of Z^* values for the combined five data sets were divided into fifty bins and the frequency of Z^* values in each of the bins was normalized with respect to the bin size and the total amount of Z^* values. The normalized frequency along with a Gaussian profile is given in Fig. 4.1.

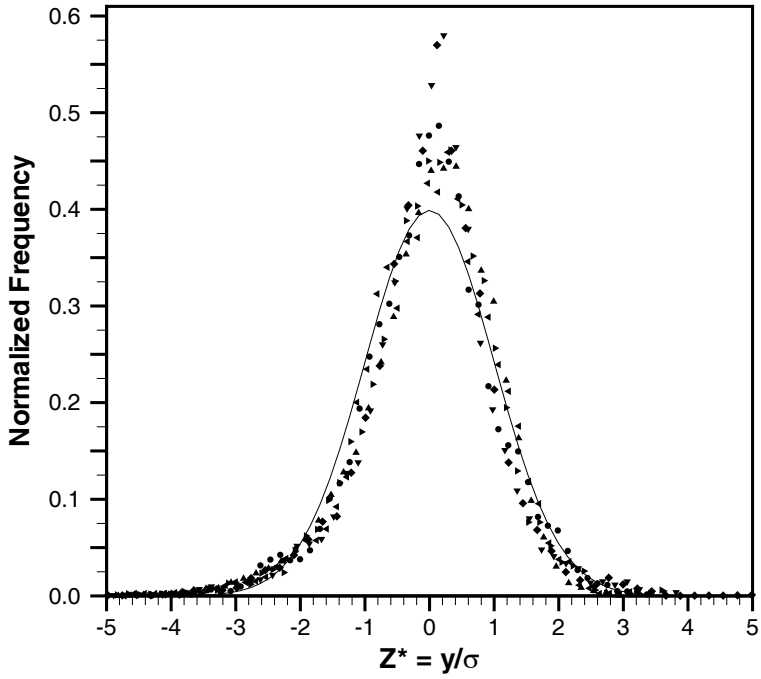

Figure 4.1: Normalized frequency versus Z^* for six bead-blasted polycarbonate surfaces compared to a Gaussian profile.

From this comparison the bead-blasted polycarbonate surfaces were found to exhibit the assumed Gaussion height distribution.

4.2 Surface Microhardness

A required parameter for the prediction of thermal contact resistance using the CMY plastic contact model is the microhardness of the softer material at the interface [41]. For plastic deformation, microhardness is used to determine the ratio of real to apparent contact area. Microhardness testing, (ie. Vickers, Knoop) are indentation methods for measuring the hardness of a material on a micro scale. This technique can detect the hardness profile of a surface at depths on the order of microns. Vickers microhardness is calculated from the following:

$$H_V = \frac{1854.4 \cdot \text{Load}}{\text{d}_V^2} \cdot 9.81 \quad (MPa) \tag{4.1}$$

where *Load* is the applied load in grams and d_V is the average of the two measured indentation diagonals in μm. Bulk hardness testing (ie. Rockwell, Brinell) are indentation methods which measure the hardness of a material on a macro scale. Typical surface treatments can not be detected with bulk hardness testing methods.

4.2.1 Metals

It was necessary to provide the CMY contact model, Eq. 2.24 with an appropriate plastic microhardness value to calculate the predicted thermal contact resistance value for a stainless steel to stainless steel interface. This was completed using the explicit relationship given by Eq. 2.26 which required the surface roughness and the microhardness surface layer to be characterized. The microhardness surface layer is characterized by the correlation coefficients: c_1 and c_2 used in Eq. 2.25.

A Shimadzu HMV-2000 Vickers Indenter was used to make a series of indentations under loads of: 15 g, 25 g, 100 g, 300 g, and 500 g to characterize the microhardness surface layer. Five indentations were made for each load. Details of this study are presented in Table E.1 in Appendix E.

The result of this study is shown in Fig. 4.2 as Vickers microhardness as a function of indentation diagonal on a log-log plot. From Fig. 4.2 the correlation coefficients: c_1 and c_2 were determined from the trendline fit to the data. The correlation coefficients: c_1 and c_2 for the stainless steel sample are 5.893 GPa and -0.249 respectively. Hegazy [17] conducted similar microhardness tests on 304 stainless steel and found values for c_1 and c_2 of 6.27 GPa and -0.229 respectively. Differences can be attributed to variations between the materials tested and different surface preparations.

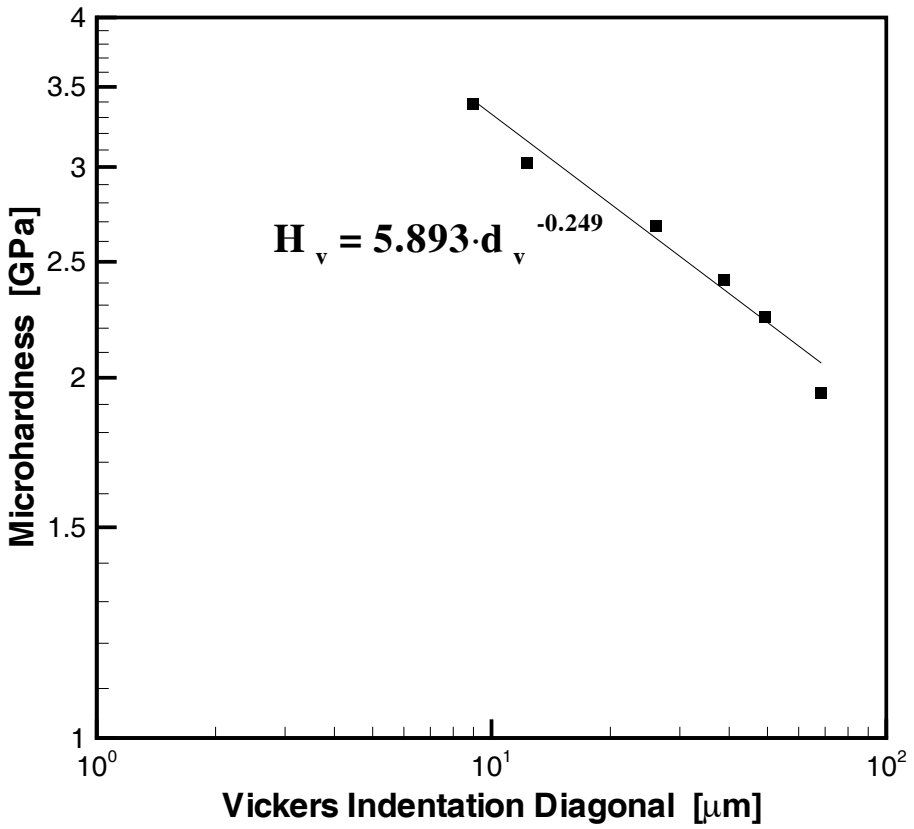

Figure 4.2: Stainless Steel: Vickers microhardness versus indentation diagonal along with correlation

4.2.2 Polymers

In order to predict the thermal contact resistance of a polymer-metal joint or polymer-polymer joint using the CMY plastic contact model a microhardness of the polymer must be determined. Microhardness testing of polymers, while not achieving the same popularity to that of metals has been shown by several researchers [6, 9, 22, 24] to be a useful tool to characterize the mechanical properties of polymers. In their work each researcher proposes an experimental method to determine the microhardness of a polymer. One of the noticable differences in their methods is the holding time for the application of the load. Holding times suggested vary from 6 seconds [6] to 2 minutes [9].

Vickers microhardness tests were conducted at loading times of 15 and 30 seconds to evaluate the effect of holding time on the microhardness of polycarbonate. Polycarbonate samples were cut from a 25.4 mm rod and polished to allow the indentation diagonals to be easily viewed at magification. A indentation typical for a polymer is shown in Fig. 4.3.

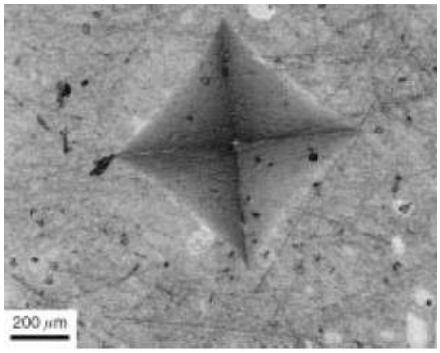

Figure 4.3: Indentation diagonals of an epoxy material [25].

A LECO DM-400LF Vickers Indenter was used to indent polycarbonate under loads of 5 g, 10 g and 20 g and a standard Shimadzu HMV-2000 Vickers Indenter was used for loads of 25 g, 50 g, 100 g, 200 g[1] and 500 g. Four indentations were made for

[1]The 200 g load was only applied for a holding time of 15 seconds.

each load to allow an average hardness for each load to be calculated. Details of this study are presented in Tables E.2 and E.3 in Appendix E. The result of this study is shown in Fig. 4.4 as Vickers microhardness as a function of indentation diagonal on a log-log plot.

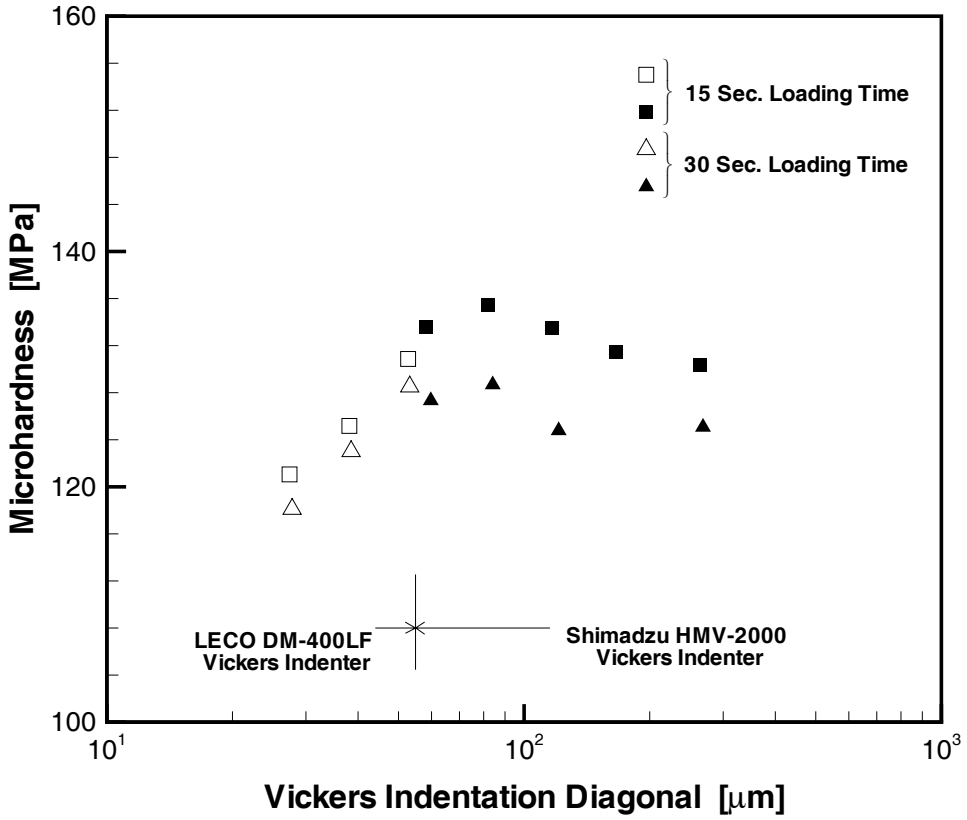

Figure 4.4: Vickers microhardness versus indentation diagonal for polycarbonate.

From Fig. 4.4 the time that the load is applied is shown to have a noticable effect on measured microhardness values. The increase in loading time appears to have decreased the microhardness values by 6 MPa. It is important to note that only a very slight increase in indentation diagonal causes a significant increase in the measured microhardness value. A reason for the difference in hardness with loading time is the possible viscoelastic behavior of the plastic [9]. Also, noticable in Fig. 4.4 is

the lack of the surface microhardness layer shown in the stainless steel microhardness profile. The polycarbonate hardness profile shows a complex profile (with increasing indentation size): increasing, peaking, then decreasing and finally levelling off. The initial low values of microhardness indicates a softening phenomona occuring at the surface of the polymer. From these microhardness measurements a value of 130 MPa was selected to represent an appropriate hardness value for polycarbonate.

Another cause for concern when completing microhardness tests of polymers is that during unloading of the indenter the diagonals may recover an appreciable amount due to the elastic nature of the material. Crawford [9] investigated this concern and found that there was negligible recovery of the diagonals.

Additional polymers were tested in a similar manner using a holding time of 30 seconds to confirm the general trends found in the polycarbonate microhardness study. Additional polymers include Polyvinyl Chloride (PVC) and Acrylonitrile Butadiene Styrene, (ABS). Again, four indentations were made for each load to allow an average hardness for each load to be calculated. Table E.4 in Appendix E contains details for PVC and Table E.5 in Appendix E contains details for ABS. The results from this work are shown in Fig. 4.5 as a comparison to the polycarbonate microhardness results. Similar microhardness trends were observed between the three polymer types.

4.3 Mechanical Properties

The following material properties must be determined to model the thermal contact resistance of a conforming rough interface using the Mikic elastic contact model and the SY elasto-plastic contact model:

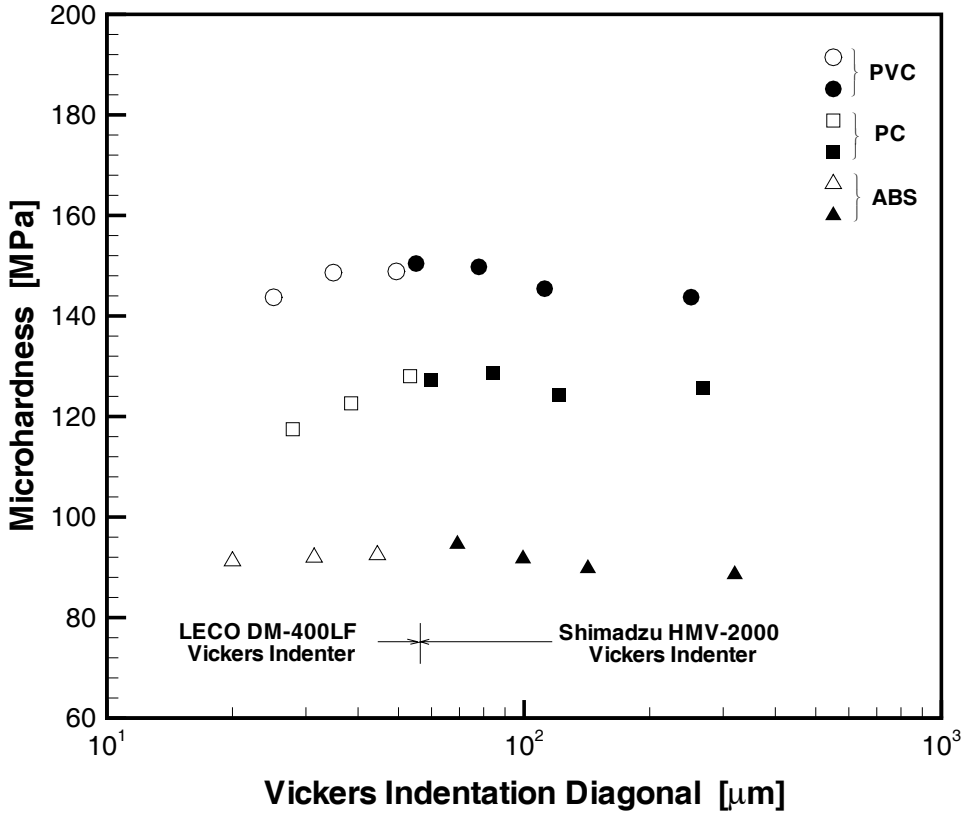

Figure 4.5: Vickers microhardness versus indentation diagonal for PC, ABS and PVC. Holding time = 30 seconds.

$$\text{Elastic Modulus \& Poisson's Ratio} \rightarrow \begin{cases} \text{Mikic contact model} \\ \text{SY elasto-plastic contact model} \end{cases}$$

$$\text{Yield Stress} \rightarrow \begin{cases} \text{SY elasto-plastic contact model} \end{cases}$$

The elastic modulus and Poisson's ratio of both materials at the interface are used in the calculation of the effective elastic modulus (E') of the joint given in Eq. 2.28. The effective elastic modulus is required for the calculation of the elastic microhardness value used in the thermal contact conductance correlation. The mechanical

properties of stainless steel reported in Table 4.3 were taken from Hibbeler [18].

A compression test was conducted to determine the elastic modulus and yield stress of polycarbonate while the Poisson's ratio was taken from Aharoni [1]. The compression test followed ASTM D 695-02a [3] for both test procedure and specimen preperation. Five cylindrical specimens of dimensions: 100 mm long by 25.4 mm were tested and the results plotted as stress versus strain as shown in Fig. 4.6. The elastic modulus for each specimen was calculated from the slope of the curve in the initial elastic region. The average elastic modulus value was used for contact conductance model calculations. The yield stress was determined as the stress in which the stress-strain curve becomes noticably non-linear. A summary of material properties for both stainless steel and polycarbonate are given in Table 4.3.

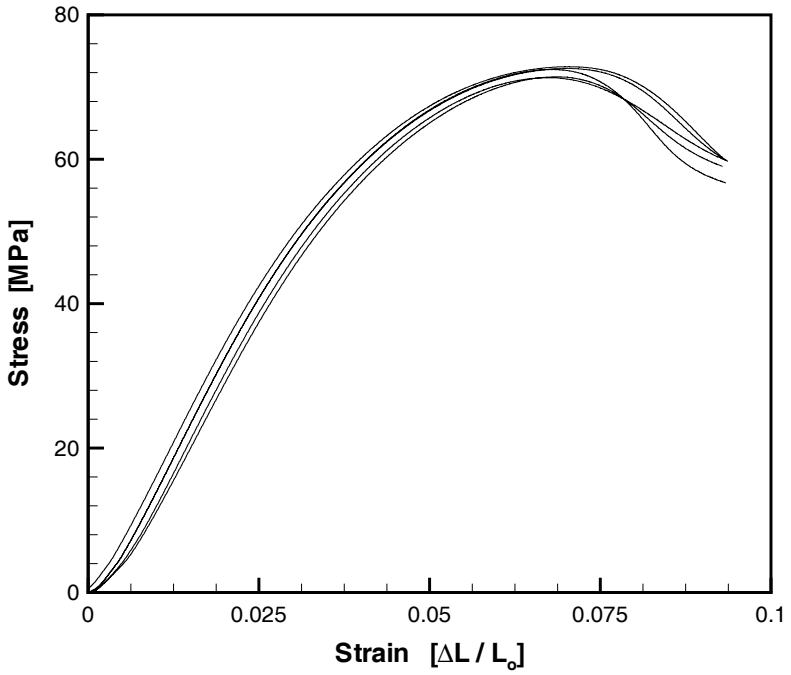

Figure 4.6: Compression test results of polycarbonate samples.

The compressive yield stress of polycarbonate was also reported by Gallina USA LLC as 70 MPa [23]. The elastic modulus of polycarbonate was also reported by

Table 4.3: Material properties required for thermal contact resistance modelling

Material	**E** $[GPa]$	$\boldsymbol{\nu}$	$\boldsymbol{Y}$ $[\boldsymbol{MPa}]$
304 Stainless Steel	193	0.27	-
Polycarbonate	1.79	0.39	65

Plastics International as 2.379 GPa [20].

4.4 Marsh's Work

The results from the polycarbonate compression test can be combined with the polycarbonate microhardness measurements in order to compare the collected data to the radially expanding model of Marsh [27]. The value of E/Y for polycarbonate equals approximately 27.5 and the value of H/Y equals approximately 2.15. These results are presented in Fig. 4.7 compared against both the radially expanding model of Marsh [27] and to the rigid-die indentation hardness model of Tabor [37]. The percent difference for the polycarbonate experimental data point is 5% where percent difference is defined as:

$$\% \text{ Difference} = \left(\frac{H/Y_{PC} - H/Y_{Marsh}}{H/Y_{Marsh}} \right) \cdot 100 \ \% \tag{4.2}$$

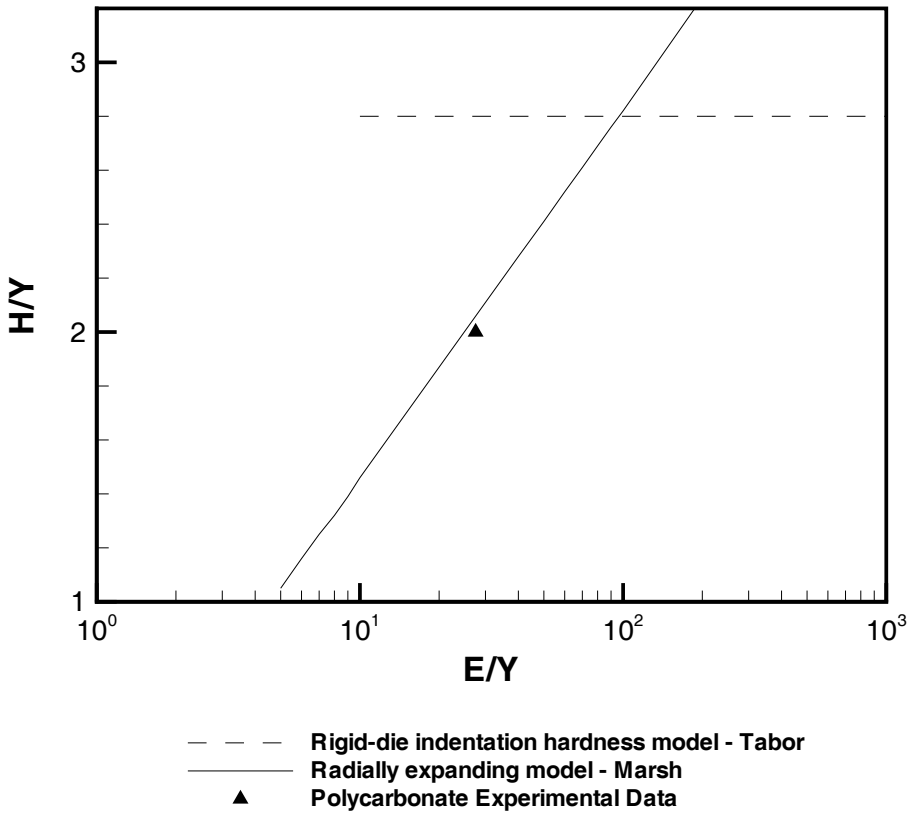

Figure 4.7: Polycarbonate experimental data point compared against both the Marsh indentation hardness model [27] and the rigid-die model given by Tabor [37].

Chapter 5

Comparisons of Test Results and Contact Models

An experimental program was completed to collect thermal contact resistance data between carefully prepared surfaces. The data were then compared to reviewed contact models. Models reviewed include the CMY plastic contact model, the Mikic elastic contact model and the SY elasto-plastic contact model. Experiments which involved polymer-metal contacting surfaces were also compared to the Fuller-Marotta contact model. The purpose of this comparison was to verify the proposed methods used to determine the mode of deformation for that particular interface.

5.1 Experimental Data Reduction

The process of determining the thermal contact resistance of each interface described in Chapter 3 began with the calculation of the total thermal resistance between the stainless steel flux-meters:

$$R_{total} = \frac{\Delta T_{total}}{Q_{avg}} \quad (K/W) \tag{5.1}$$

where Q_{avg} is the average value of the heat conducted through both the upper and lower stainless steel heat flux-meters and ΔT_{total} is the temperature drop between the stainless steel flux-meter surfaces. The surface temperature of each flux-meter was calculated from an extrapolation of a linear fit of the temperature measurements in the flux-meter to the interface as shown graphically in Figs. 5.1 and 5.2.

5.1.1 Heat Transfer: Q_{avg}

For each interface Q_{avg} was calculated based on the following:

$$Q_{avg} = \frac{(Q_1 + Q_2)}{2} \quad (W) \tag{5.2}$$

where Q_1 and Q_2 were the heat conducted through each stainless steel flux-meter. Q_1 and Q_2 were both determined from Fourier's equation:

$$Q_1 = \left(-k_{SS304}\ A_a \cdot \frac{dT}{dz} \right)_1 \quad (W) \tag{5.3}$$

$$Q_2 = \left(-k_{SS304}\ A_a \cdot \frac{dT}{dz} \right)_2 \quad (W) \tag{5.4}$$

where dT/dz is the slope of a linear fit of the temperature measurements in the stainless steel heat-flux meters and k_{SS304} is the thermal conductivity of the stainless steel described in Eq. 3.2 evaluated at the average temperature of each flux-meter.

5.1.2 Thermal Interface Resistance: $R_{interface}$

For each of the three interfaces, $R_{interface}$ was calculated slightly different:

1. For the first experiment involving contacting stainless steel surfaces the heat-flux meters form the interface. In this situation $R_{interface}$ equals R_{total} as described in Eq. 5.1.

2. The next series of experiments which involved metal to polymer contacting surfaces required additional calculations to determine $R_{interface}$. As shown in Fig. 5.1 there is a temperature drop due to the polycarbonate disc and the eGraf® 1220 graphite interface material. Both of these described temperature drops are caused by a thermal resistance which must be removed from R_{total} to calculate $R_{interface}$. Therefore, it is necessary to calculate the thermal resistance of a polycarbonate disc and the eGraf® 1220 graphite interface material.

3. The next series of experiments which involved polymer to polymer contacting surfaces required a slight modification to the procedure described for metal to polymer interfaces to determine $R_{interface}$. As shown in Fig. 5.2 there are two temperature drops due to the polycarbonate discs and two temperature drops due to the eGraf® 1220 graphite interface material. Since each of these temperature drops are caused by thermal resistance it is again necessary to calculate the thermal resistance of a polycarbonate disc and the eGraf® 1220 graphite interface material.

To calculate the bulk resistance due to the polycarbonate disc the expression proposed by Fuller and Marotta [13] was used:

$$R_{bulk} = \frac{t_0 \ (1 - P/E_{PC})}{A_a \ k_{PC}} \quad (K/W) \tag{5.5}$$

Thermal Conductivity of Polycarbonate

The thermal conductivity of polycarbonate (k_{PC}) was determined using three seperate thermal joint resistance experiments each using a different thickness of polycarbonate. The stainless steel flux-meters were used to determine Q_{avg} using Eq. 5.2 and the joint surface temperatures through extrapolation. The first experiment used one

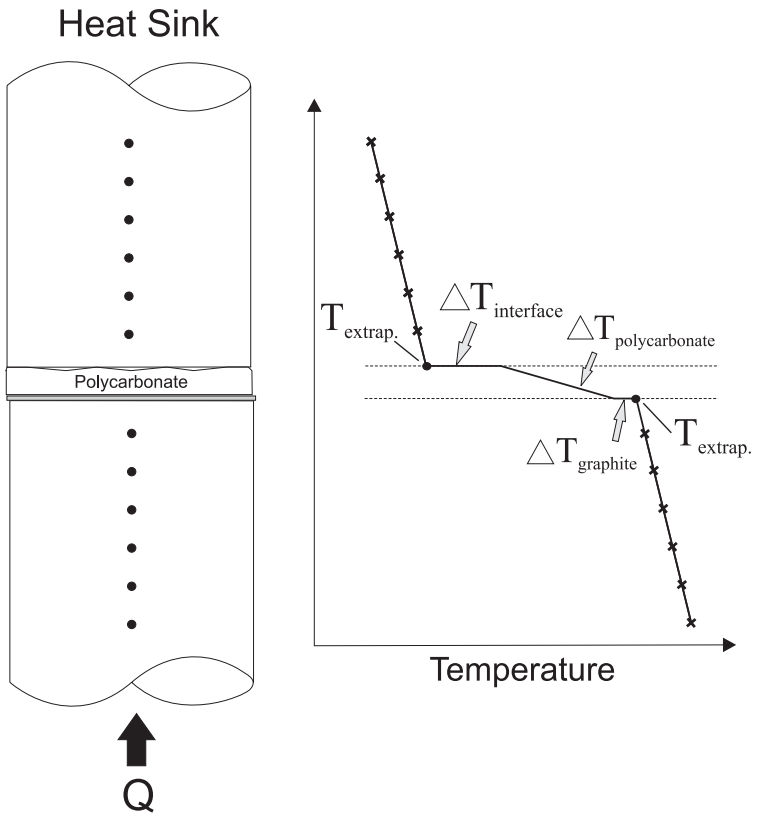

Figure 5.1: Temperature drop across a polymer to metal interface.

polycarbonate disc with Dow Corning 340 heat sink compound between both of the interfaces to minimize contact resistance. The second experiment required two stacked discs while the third experiment used three discs. Again, Dow Corning 340 heat sink compound was used at all interfaces. The average temperature of the polycarbonate was approximately 55 $^{\circ}C$.

Plotting the total joint resistance from each of the experiments against specimen thickness results in a linear relationship as shown in Fig. 5.3. The slope ($\Delta R_{joint}/\Delta t_0$) of a linear fit of these three points is related to the thermal conductivity of the polycarbonate by the following relationship:

$$k_{PC} = \frac{1}{A_a \cdot \Delta R_{joint}/\Delta t_0} \quad (W/m \cdot K) \tag{5.6}$$

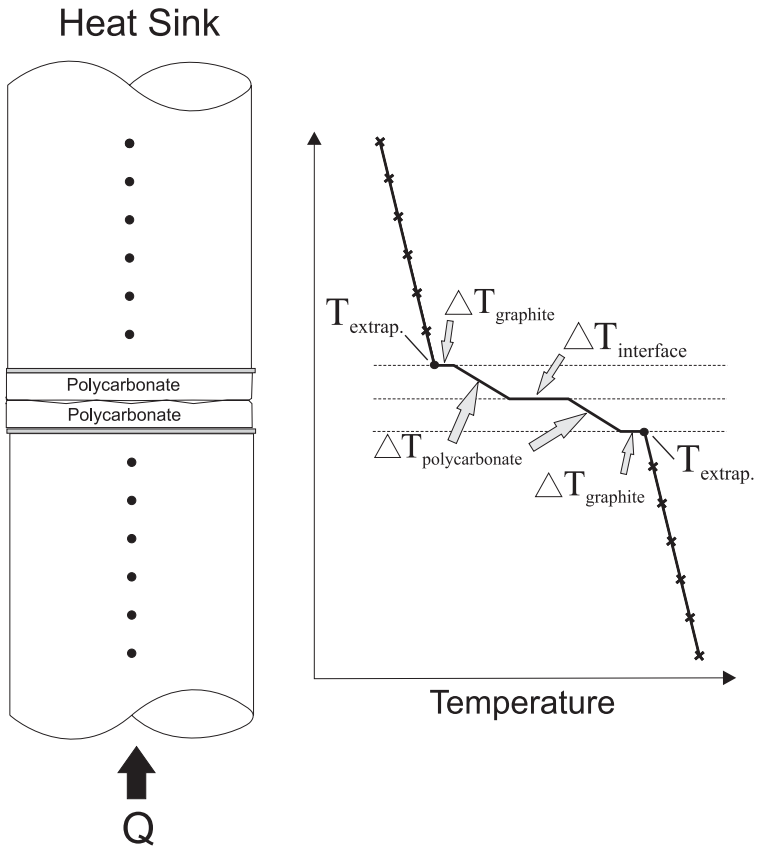

Figure 5.2: Temperature drop across a polymer to polymer interface.

From this procedure the thermal conductivity of polycarbonate was calculated to be 0.24 $W/(m \cdot K)$. This value of thermal conductivity allows the bulk resistance of the polycarbonate to be calculated from Eq. 5.5.

Fletcher and Marotta [26] completed a similar study to measure the thermal conductivity of polycarbonate using single discs placed between aluminum flux-meters with Dow Corning 340 heat sink compound at both disc to flux-meter interfaces. Using Eq. 5.5 without the $(1 - P/E_{PC})$ component they directly attributed the total thermal resistance of the joint to the bulk resistance of the polycarbonate disc to determine k_{PC}. This procedure overestimated the thermal resistance due to the bulk of the polycarbonate disc because the interfaces with the Dow Corning 340 heat sink compound will still contribute to the total resistance of the joint. This procedure did

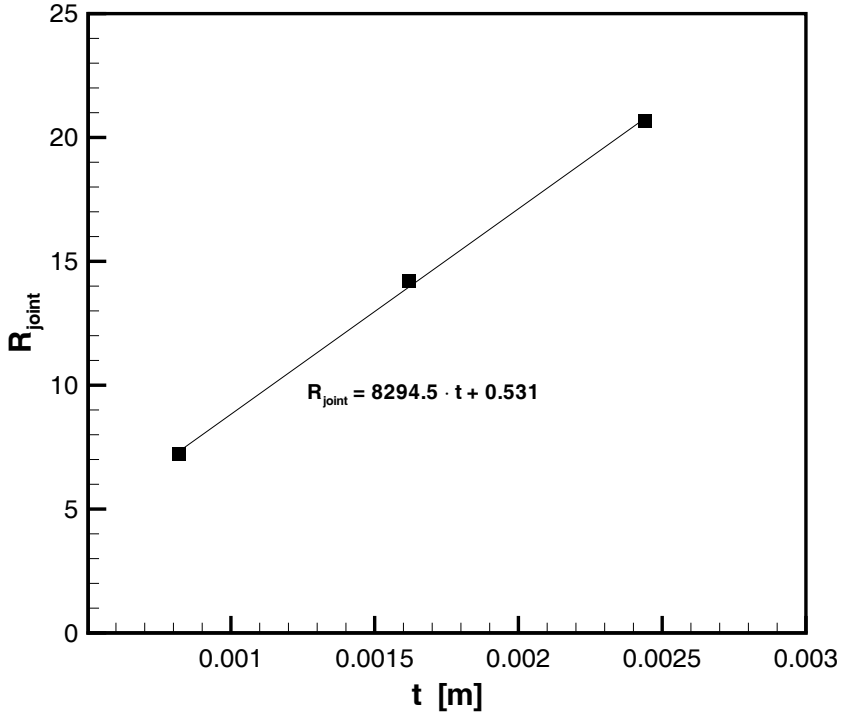

Figure 5.3: Measured joint resistance of polycarbonate versus thickness

allow them to determine the thermal conductivity of polycarbonate over a temperature range. They reported a single thermal conductivity value for polycarbonate of $0.22\ W/(m \cdot K)$ but in a plot of thermal conductivity versus temperature they showed values of thermal conductivity that ranged from approximately 0.23 - 0.31 $W/(m \cdot K)$ at room temperature.

Thermal Resistance of Graphite TIM

It was also necessary to determine the thermal resistance of the eGraf® 1220 graphite interface material in a stainless steel to polycarbonate interface. This was completed in order to calculate the temperature drop due to the graphite as shown in Figs. 5.1-

5.2. An experimental series was conducted and setup as shown in Fig. 3.7. Pressure was varied from 0.659 MPa to 8.148 MPa which approximately matched the pressure range used for thermal contact resistance testing. The thermal resistance from the graphite layer was calculated from the following:

$$R_{graphite} = \frac{R_{joint} - R_{bulk}}{2} \quad (K/W) \tag{5.7}$$

The result of this experimental series is presented in Fig. 5.4.

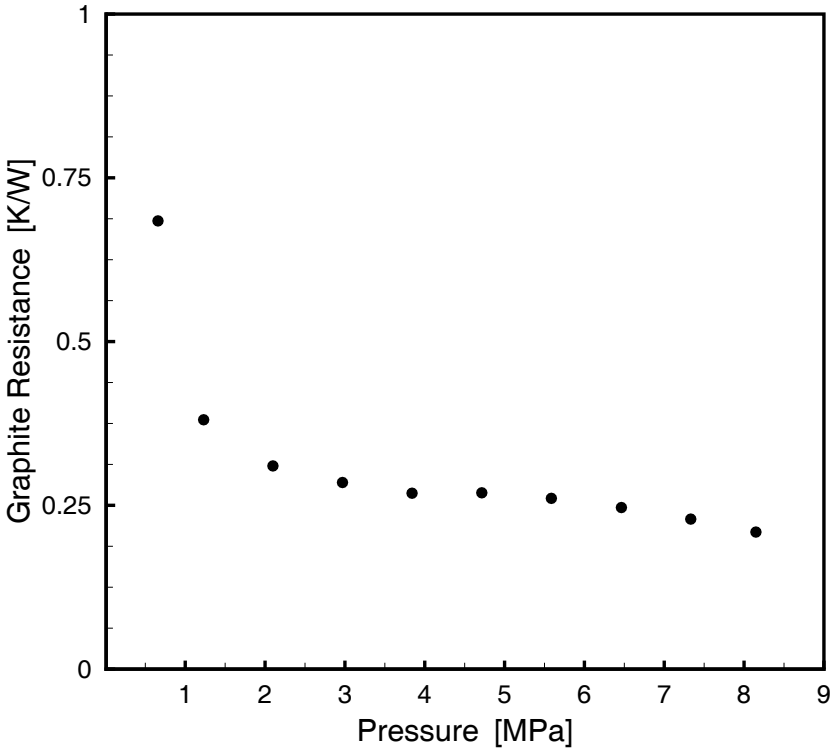

Figure 5.4: Thermal resistance of a eGraf® 1220 layer in a stainless steel to polycarbonate interface.

5.1.3 Summary of Thermal Interface Resistance Equations

The equations necessary to calculate the thermal contact resistance of each interface are as follows:

1. A stainless steel surface in contact with another stainless steel surface:

$$R_{interface} = \frac{\Delta T_{total}}{Q_{avg}} \quad (K/W) \tag{5.8}$$

2. A stainless steel surface in contact with a polycarbonate surface:

$$R_{interface} = \frac{\Delta T_{total}}{Q_{avg}} - R_{bulk} - R_{graphite} \quad (K/W) \tag{5.9}$$

3. A polycarbonate surface in contact with another polycarbonate surface:

$$R_{interface} = \frac{\Delta T_{total}}{Q_{avg}} - 2 \cdot R_{bulk} - 2 \cdot R_{graphite} \quad (K/W) \tag{5.10}$$

5.2 Summary of Experimental Results

The experimental evaluation of thermal contact resistance for the three different types of interfaces resulted in the collection of over forty data points. For each of the experiments completed Table 5.1 presents minimum and maximum results. The pressure range for each experiment was approximately the same and was similar to the pressure range used by Hegazy [17]. Experiments completed involving polycarbonate were all conducted at approximately 72 $^{\circ}C$. This temperature allowed for enough heat to pass through the polycarbonate discs while ensuring that the polycarbonate remained well below its glassy temperature. Detailed test results are presented in Tables F.1 - F.5 in Appendix F.

Table 5.1: Experimental parameter ranges

		SS-SS	PC-SS-1	PC-SS-2	PC-PC-1	PC-PC-2
P_{max}	(MPa)	8.02	7.34	7.34	8.16	5.60
P_{min}	(MPa)	1.18	0.70	0.52	0.72	0.66
$Q_{avg.max}$	(W)	9.83	4.18	3.99	3.50	3.45
$Q_{avg.min}$	(W)	9.18	3.70	3.46	3.24	3.30
$T_{avg.max}$	$(°C)$	128.0	76.9	73.8	77.6	75.0
$T_{avg.min}$	$(°C)$	112.9	70.4	68.3	70.7	71.3
$\Delta T_{overall.max}$	$(°C)$	24.5	54.4	54.2	66.3	60.3
$\Delta T_{overall.min}$	$(°C)$	4.3	31.7	30.8	48.2	49.8
$\Delta T_{graphite.max}$	$(°C)$	-	2.5	2.4	2.2	2.3
$\Delta T_{graphite.min}$	$(°C)$	-	1.0	0.9	0.7	0.9
$\Delta T_{PC.max}$	$(°C)$	-	27.8	26.5	23.3	22.9
$\Delta T_{PC.min}$	$(°C)$	-	24.6	23.0	21.6	21.9
$R_{interface.max}$	(K/W)	2.55	7.36	8.32	5.78	3.61
$R_{interface.min}$	(K/W)	0.46	0.91	0.99	0.75	0.70

5.3 Parameter Summary

Parameters necessary for thermal contact resistance modelling are presented in the following section. This includes geometric, thermal and mechanical parameters.

5.3.1 Geometric Parameters

The diameter of all circular surfaces is 25.4 mm. This creates an apparent contact area (A_a) of 0.000507 m^2.

Following the procedure of Greenwood and Williamson [14] in Section 2.1.1 an effective RMS roughness (σ) and the effective absolute mean asperity slope (m) are calculated using Eq. 2.3 for each interface investigated. Results from these calculations are presented in Table 5.2. Tables 4.1 and 4.2 contain the surface roughness parameters for the individual surfaces that form each interface.

Table 5.2: Effective surface roughness of each interface investigated

		SS-SS	PC-SS-1	PC-SS-2	PC-PC-1	PC-PC-2
σ	(μm)	1.51	1.89	1.57	2.48	1.84
m	(radian)	0.091	0.093	0.090	0.131	0.120
σ/m	(μm)	16.6	20.4	17.3	19.0	15.4

5.3.2 Thermal Parameters

The thermal conductivity of 304 stainless steel is presented in Section 3.1.1. The thermal conductivity of polycarbonate is presented in Section 5.1.2. The harmonic mean thermal conductivity (k_s) described in Section 2.1.2 is presented in Table 5.3 for each interface investigated.

Table 5.3: Harmonic mean thermal conductivity of each interface investigated

		SS-SS	PC-SS-1	PC-SS-2	PC-PC-1	PC-PC-2
k_s	$(W/m \cdot K)$	16.1 - 16.5	0.47	0.47	0.24	0.24

5.3.3 Mechanical Parameters

The mechanical properties of both 304 stainless steel and polycarbonate are presented in Section 4.3. Mechanical parameters of the interfaces investigated along with the necessary equations to calculate the values as shown are presented in Table 5.4.

Table 5.4: Mechanical parameters of each interface investigated

		Eq. #	SS-SS	PC-SS-1	PC-SS-2	PC-PC-1	PC-PC-2
c_1	(GPa)	2.25	5.89	-	-	-	-
c_2	-	2.25	-0.249	-	-	-	-
H_p	(GPa)	2.26	2.88 - 2.98	0.130	0.130	0.130	0.130
E'	(GPa)	2.28	104.1	2.09	2.09	1.06	1.06
H_e	(GPa)	2.29	6.70	0.137	0.133	0.097	0.089
H_{poly}[1]	(GPa)	2.53	-	0.072	0.070	-	-
H_{ep}	(GPa)	2.37	3.30 - 3.45	0.109	0.107	0.086	0.080

The calculation of H_{ep} for the SS-SS interface required the full iterative method described by Eqs. 2.39 to 2.45. An example of this procedure is shown in Appendix G.

[1] H_{poly} was used in the Fuller-Marotta contact conductance correlation, Eq. 2.54

The iterative procedure required for the calculation of H_{ep} for both types of polymer interfaces failed because of the inability to determine S_f in the second iteration using Eq. 2.39. As a first approximation the yield stress of polycarbonate shown in Table 4.3 was used to directly calculate H_{ep} using Eq. 2.37 by setting $S_f = Y_{PC}$.

5.4 Thermal Contact Modelling

To describe the flow of heat across an interface a thermal contact conductance model is required. In this study the models reviewed include the CMY plastic contact model, the Mikic elastic contact model and the SY elasto-plastic contact model. Experiments which involved polymer-metal contacting surfaces were also compared to the Fuller-Marotta contact model.

The output of these models is a dimensionless thermal contact conductance (C_c) which is defined as: $(h\ \sigma)/(k_s\ m)$. It was necessary to solve for the conductance (h) and convert to a thermal resistance (R) in order to compare the experimental results to the theoretical model predictions. This was accomplished using Eq. 1.2.

For all three interface types the dimensionless thermal contact conductance was calculated for the CMY plastic contact model from Eq. 2.24. Also, for all three interface types the dimensionless thermal contact conductance was calculated for the Mikic elastic contact model from Eq. 2.35. For the stainless steel to stainless steel interface the dimensionless thermal contact conductance was calculated for the SY elasto-plastic contact model from Eq. 2.47. For the two polymer joint types the dimensionless thermal contact conductance was calculated for the SY elasto-plastic contact model from Eq. 2.48. For the polymer to metal joint type the dimensionless thermal contact conductance was calculated for the Fuller-Marotta contact model from Eq. 2.54.

5.5 Stainless Steel - Stainless Steel Interface

The first thermal contact resistance experiment was performed using a stainless steel to stainless steel interface. As previously described, the goal of this experiment was to verify the experimental procedure/setup by comparing a measured set of thermal contact resistance data to established theoretical predictions.

The reduced data from this experiment are shown in Fig. 5.5 as thermal contact resistance as a function of pressure. These experimental results are shown along with the theoretical thermal contact resistance values calculated from the dimensionless thermal contact conductance models presented in Section 2.1. Necessary modelling parameters are presented in Section 5.3. Detailed model comparisons are presented in Table H.1 in Appendix H.

To predict the mode of deformation the value of ϵ_c^* for this interface was examined with respect to the assumptions presented in Section 2.2:

$$\epsilon_c^* = 10.84 \rightarrow 11.52 \quad \approx 11 \quad \rightarrow \quad \text{plastic mode of deformation}$$

Since this evaluation method gives an indication that this interface will follow a plastic mode of deformation the following is assumed:

1. The SY elasto-plastic contact model should approach and overlap the CMY plastic contact model.

2. The CMY contact model should show agreement with the experimental data.

As shown in Fig. 5.5 both of these assumptions are validated with excellent agreement between the CMY plastic contact model and the experimental data. To support this conclusion it was also found by Hegazy [17] that stainless steel interfaces

follow the plastic mode of deformation with excellent experimental agreement with the CMY plastic contact model. This results in permanent plastic deformation of the asperities in contact with each other. For each of the models presented in Fig. 5.5, Table 5.5 provides RMS percent difference values. RMS percent difference is defined as:

$$\text{RMS \% Difference} = \sqrt{\frac{1}{N}\sum_{i=1}^{N} x_i^2} \cdot 100 \quad \% \tag{5.11}$$

where

$$x_i = \left(\frac{R_{interface.expt} - R_{interface.model}}{R_{interface.model}} \right) \tag{5.12}$$

Table 5.5: RMS percent difference between experimental values and model predictions for stainless steel interface

	CMY	Mikic	SY elasto-plastic
RMS % Difference	6	64	9

The experimental results and theoretical predictions both follow the same trend given by Hegazy [17] where the thermal contact resistance of an interface decreases as the pressure increases. From the results of this thermal investigation, as the pressure was increased by a factor of 6.8 from 1180 kPa to 8016 kPa, the contact resistance calculated from the CMY elastic contact model decreased by a factor of 5.5 from 2.55 K/W to 0.46 K/W. To investigate the cause in the reduction of thermal contact resistance with increased loading the parameters calculated from the CMY plastic contact model are presented in Table 5.6 for comparison. It is noticed in Table 5.6 that the radius of the contact area a increased by a factor of 1.2 while the number

of contacts increased by a factor of 5.1. The combination of these factors caused the real area of contact to increase by a factor of 7.0. The increase in real contact area subsequently decreased the resistance to the heat flow through the interface.

Table 5.6: Parameters calculated with the CMY plastic contact model: stainless steel interface ($\sigma/m = 16.6$ μm).

Parameter	P = 1180 kPa	P = 8016 kPa
A_r/A_a	0.000396	0.00278
λ (Y/σ)	3.36	2.77
a (μm)	5.8	6.9
N	1870	9481
R_c (K/W)	2.71	0.435

The outcome of this carefully conducted thermal experiment was that the experimental procedure/setup used to determine thermal contact resistance at a metal-metal interface produced results that were in excellent agreement with the appropriate theoretical models. With confidence thermal contact resistance experiments could then be extended to interfaces that involve polymer surfaces.

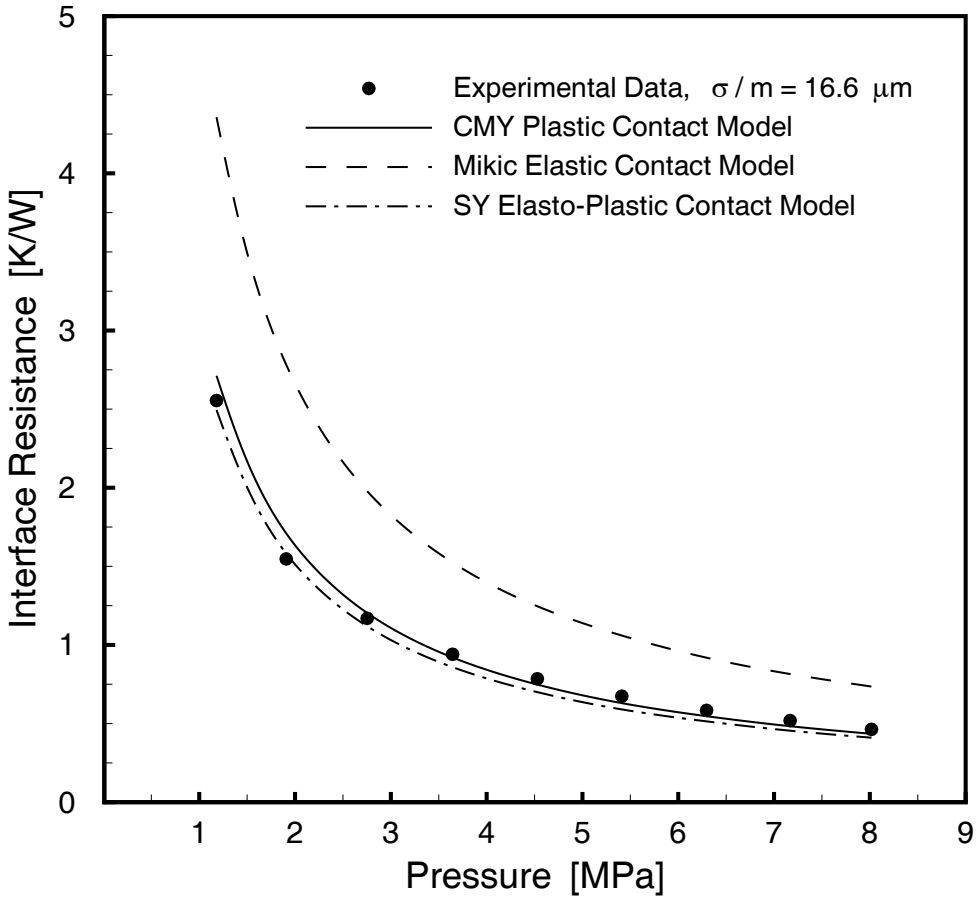

Figure 5.5: Interface resistance for both experimental results and contact conductance models - stainless steel to stainless steel

5.6 Stainless Steel - Polycarbonate Interface

Two experiments were conducted to measure the thermal contact resistance of a stainless steel to polycarbonate interface. The reduced data from these experiments are shown in Figs. 5.6 - 5.7 as thermal contact resistance as a function of pressure. For both experiments the theoretical thermal contact resistance values calculated from dimensionless thermal contact conductance models are shown along with the experimental results in Figs. 5.6 - 5.7. Necessary modelling parameters are presented in Section 5.3. Detailed model comparisons are presented in Tables H.2 and H.3 in Appendix H.

To predict the mode of deformation for these interfaces the values of ϵ_c^* and E'/Y are examined with respect to the assumptions presented in Section 2.2.

$$\begin{cases} \epsilon_c^* = 4.98 \ \& \ 4.85 & \geq 4 & \rightarrow & \text{transition} \\ E'/Y = 32 & \leq 100 & \rightarrow & \text{elastic mode of deformation} \end{cases}$$

The first evaluation method indicates that both interfaces examined will exhibit transitional elasto-plastic behavior while the second method indicates that they will exhibit elastic behavior. Considering this evaluation, it is assumed that experimental data should lie close to both the SY elasto-plastic contact model and the Mikic elastic contact model. From Figs. 5.6 - 5.7 this assumption is shown to hold. Table 5.7 provides RMS percent difference values for each of the metal to polycarbonate experiments. From this comparison the proposed Fuller and Marotta contact model is shown to underpredict the experimental thermal interface resistance data.

As indicated in Figs. 5.6 - 5.7 the mode of deformation for the PC-SS interfaces is approximately elastic. Therefore there should be agreement with the elastic microhardness given by Mikic in Eq. 2.29 and the microhardness relation in Eq. 2.52 developed by Marsh for highly elastic material.

Table 5.7: RMS percent difference between experimental values and model predictions for PC-SS interfaces

	CMY	Mikic	SY elasto-plastic	Fuller-Marotta
PC-SS-1	26	11	14	64
PC-SS-2	17	18	40	102

Using the Marsh model presented in Eq. 2.52 and the results of the polycarbonate compression test presented in Section 4.3 the value of H_{Marsh}/Y can be developed:

$$E_{PC}/Y = 32 \rightarrow \quad H_{Marsh}/Y = 2.14 \rightarrow H_{Marsh} = 139\ MPa$$

The calculated value of H_{Marsh} is in close agreement with the Mikic microhardness values (H_e) given in Table 5.4.

From the results of PC-SS-1, as the pressure was increased by a factor of 10.5 from 697 kPa to 7340 kPa, the contact resistance calculated from the Mikic elastic contact model decreased by a factor of 9.1 from 7.92 K/W to 0.866 K/W. To investigate the cause in the reduction of thermal contact resistance with increased loading the parameters calculated with the Mikic elastic contact model are presented in Table 5.8 for comparison. It is shown in Table 5.6 that the radius of the contact area a increased by by a factor of 1.6 while the number of contacts increased by a factor of 4.5. The combination of these factors caused the real area of contact to increase by a factor of 10.8. The increase in real contact area as the pressure was increased subsequently decreased the resistance to the heat flow through the interface.

In comparison to the results found for the stainless steel interface, there are several notable differences created by the use of a polymer in the interface. The number of contacts for PC-SS-1 is considerably larger than for the stainless steel interface.

Table 5.8: Parameters calculated with the Mikic elastic contact model: PC-SS-1 (σ/m = 20.4 μm).

Parameter	P = 697 kPa	P = 7340 kPa
A_r/A_a	0.005	0.054
λ (Y/σ)	2.33	1.24
a (μ)	6.9	10.7
N	16985	76253
R_c (K/W)	7.92	0.866

This creates a real area of contact for the PC-SS-1 that is consistently larger than that of the stainless steel interface. Thermal contact resistance also depends on the thermal conductivity of the materials that form the interface. The relatively low thermal conductivity of polycarbonate in comparison to stainless steel creates a much larger constriction and spreading resistance for the flow of heat through each contact spot (Eq. 2.16). Through a combination of these effects the thermal contact resistance for polymer to metal interfaces is on the same order as found for the stainless steel interface.

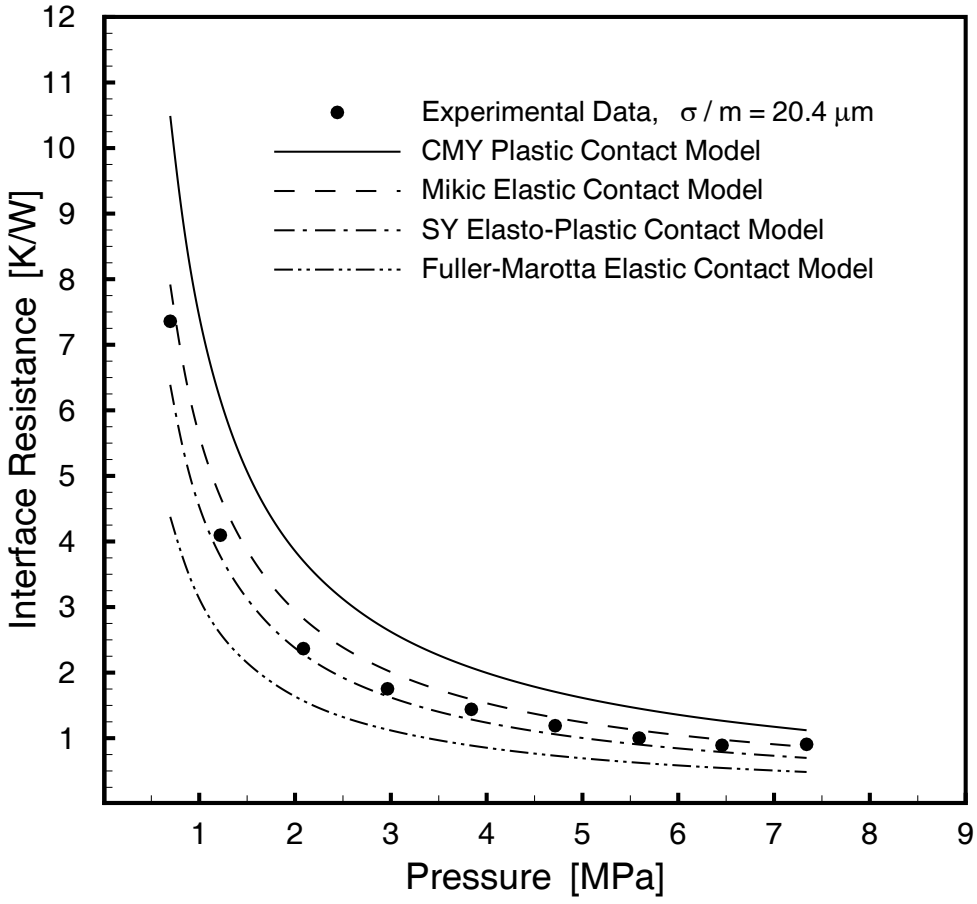

Figure 5.6: Interface resistance for both experimental results and contact conductance model - stainless steel to polycarbonate: PC-SS-1

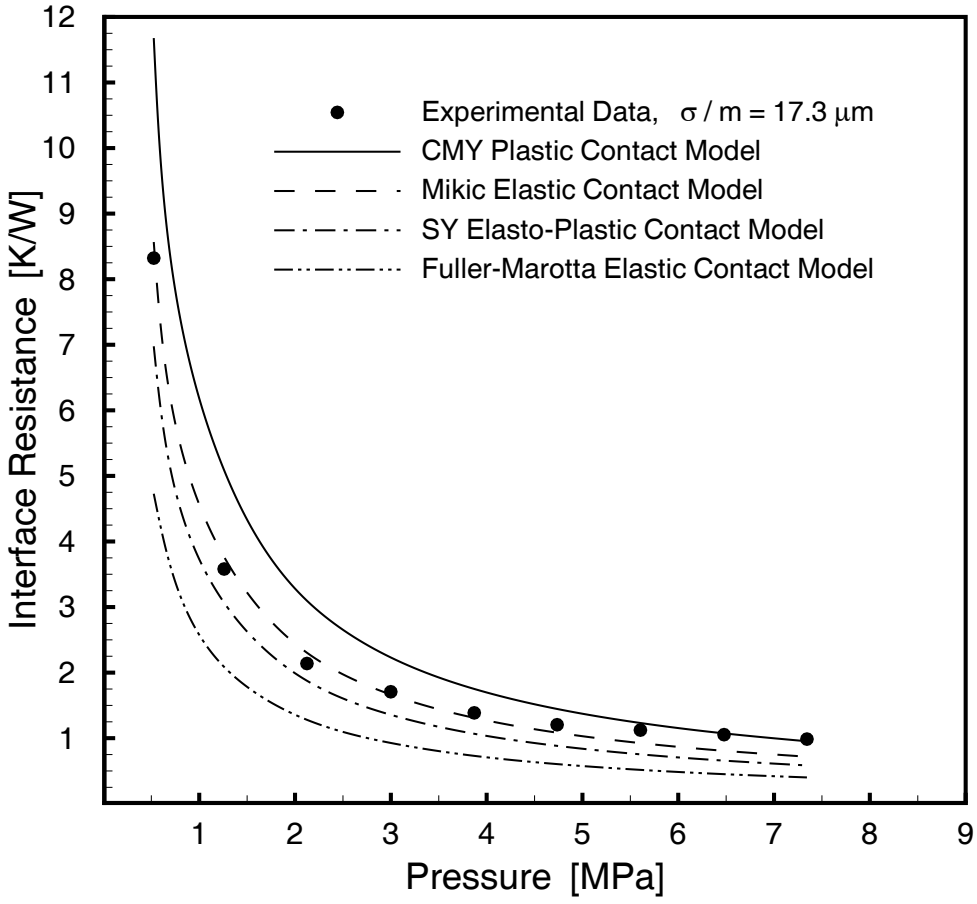

Figure 5.7: Interface resistance for both experimental results and contact conductance model - stainless steel to polycarbonate: PC-SS-2

5.7 Polycarbonate - Polycarbonate Interface

To further expand the investigation of thermal contact resistance of polymer interfaces; two experiments were conducted each measuring the thermal contact resistance of a polycarbonate to polycarbonate interface. The reduced data from these experiments are shown in Figs. 5.8 - 5.9 as thermal contact resistance as a function of pressure.

These experimental results follow the trend of decreasing thermal contact resistance with increasing load as shown in both the stainless-stainless and polycarbonate-stainless experimental results. For both experiments the theoretical thermal contact resistance values calculated from dimensionless thermal contact conductance models are shown along with the experimental results in Figs. 5.8 - 5.9. Necessary modelling parameters are presented in Section 5.3. Detailed model comparisons are presented in Tables H.4 and H.5 in Appendix H.

To predict the mode of deformation the values of ϵ_c^* and E'/Y for both interfaces are examined with respect to the assumptions presented in Section 2.2.

$$\begin{cases} \epsilon_c^* = 3.54 \text{ \& } 3.24 & \leq 4 \quad \rightarrow \quad \text{elastic mode of deformation} \\ E'/Y = 60 & \leq 100 \quad \rightarrow \quad \text{elastic mode of deformation} \end{cases}$$

Since both evaluation methods give an indication that this interface will follow an elastic mode of deformation the following is assumed:

1. The SY elasto-plastic contact model should approach and overlap the Mikic elastic contact model.

2. The Mikic contact model should show agreement with the experimental data.

From Figs. 5.8 - 5.9 the first assumption is shown to be valid while it is clearly shown that the second assumption is not valid as there is a noticable difference between the Mikic model and the experimental data. Table 5.9 provides RMS percent difference values for each of the polycarbonate to polycarbonate interface experiments.

Table 5.9: RMS percent difference between experimental values and model predictions for PC-PC interfaces

	CMY	Mikic	SY elasto-plastic
PC-PC-1	67	41	34
PC-PC-2	236	80	65

As shown in Table 5.9 there is poor agreement between all three models and the experimental data. As noted in Section C.2.3 the uncertainties associated with the experimental procedure to determine the thermal contact resistance of a polymer to polymer interface become extremely large (exceeding 200%). These large uncertainties prevent further work to determine why the experimental thermal contact resistance values are much smaller than the values calculated from the thermal contact models.

The reason for the large uncertainty in the experimental thermal contact resistance values lies with the procedure carried out to determine such values. By removing the bulk resistance of the polycarbonate and the resistance due to the graphite layers from the total resistance the remaining resistance ie. the interface resistance would remain. The problem is that the bulk and the graphite resistance form approximately 90 % of the joint resistance and the uncertainty in the calculation of these two values overshadow the calculated interface resistance value.

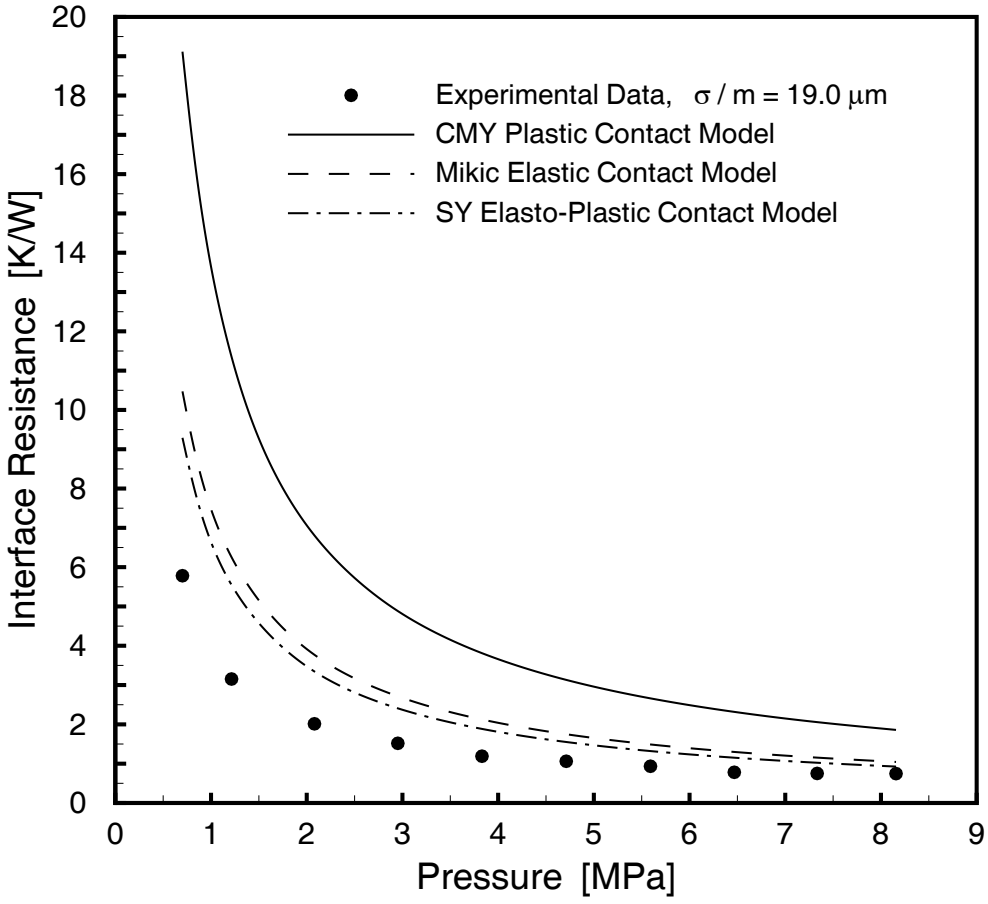

Figure 5.8: Interface resistance for both experimental results and contact conductance models - polycarbonate to polycarbonate: PC-PC-1

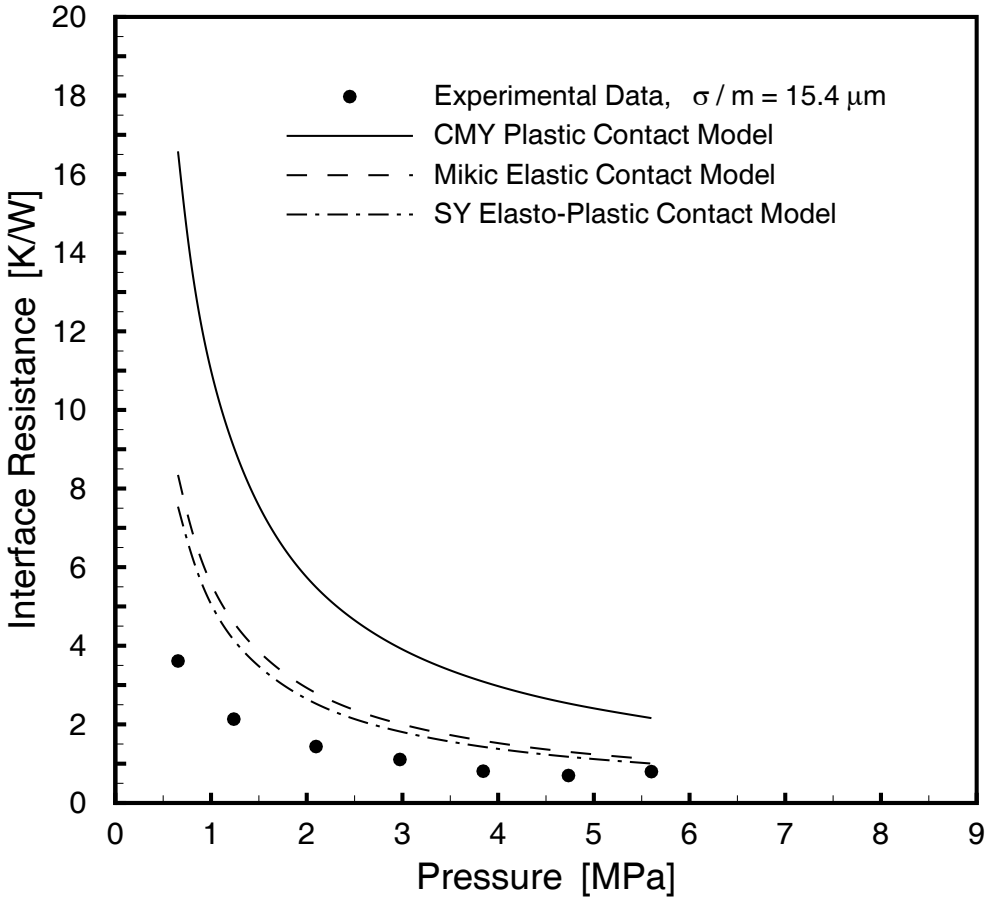

Figure 5.9: Interface resistance for both experimental results and contact conductance models - polycarbonate to polycarbonate: PC-PC-2

Chapter 6

Conclusions and Recommendations

6.1 Conclusions

Currently, there are few experimental investigations into the thermal contact resistance of polymer joints in reported literature. Most of the reported studies have looked at the joint as a whole, which includes the bulk resistance of a polymer layer along with the contact resistance of the polymer to metal interface. With limited success, a number of these studies have investigated the validity of established thermal contact models to predict the thermal contact resistance at polymer interfaces. There have been no investigations into the thermal contact resistance at a polymer to polymer interface.

Considering the works previously completed, an experimental investigation was carried out to look specifically at the thermal contact resistance at polymer interfaces which includes both polymer to metal and polymer to polymer. To maintain a rigid polymer surface during thermal testing polycarbonate was selected because it has a glass transition temperature greater than that which the polymer would reach during the experimental program. A metal to metal interface was also examined to prove the validity of the experimental program as well as to provide experimental data which

the polymer data could be compared to.

The experimental investigation was used to draw conclusions in regards to the following questions:

1. How is the thermal contact resistance of a polymer interface different than that of a metal interface?

2. Can the mode of deformation of the asperities on the contacting surfaces be predicted?

3. Can established thermal contact models be used to predict the thermal contact resistance of polymer and metal interfaces?

It was predicted that asperities in the stainless steel interface would deform plastically. Good agreement between the CMY plastic contact model and the experimental data was shown to verify that the asperities deform plastically. With confidence in the experimental procedure thermal contact resistance experiments were then extended to polymer interfaces.

It was predicted that asperities in the polymer to metal interface would deform either elastically or would be in the elasto-plastic transition zone. There was good agreement between the Mikic elastic contact model and the experimental data to verify the prediction of elastic deformation. It was also found that the number of contact spots for this type of interface was considerably larger than the stainless steel interface. This effect was was counteracted by the decreased thermal conductivity of the polycarbonate to result in a thermal contact resistance on the same order as the stainless steel interface.

It was initially predicted that asperities in the polymer to polymer interface would deform elastically but a noticable difference was found between the Mikic elastic contact model and the experimental data. It was determined that uncertainties in

the proposed experimental method prevented an accurate measurement of the thermal contact resistance values for the polycarbonate-polycarbonate data sets.

6.2 Recommendations

One of the major limitations of this study was that only one polymer was investigated. A confirmation of the conclusions found for polycarbonate with different polymers is therefore necesary. Also, because of the use of thermally conductive polymers for thermal solutions, an experimental investigation using these materials would be advantageous. The use of thermally conductive polymers may also permit the use of thermocouples to be imbedded in the polymer itself.

To further extend the work completed in this study various experimental conditions could be altered. Conditions to consider include the effects of a gaseous atmosphere, the effects of various surface treatments and roughness levels, the effects of relatively light loads on the contact mechanics of the surface and the effects of increasing the temperature of the polymer closer to or at the glassy temperature of the polymer.

It would also be advantageous to investigate the properties of polymers at elevated temperature. This includes both the elastic modulus and the microhardness of the polymer.

References

[1] S.M. Aharoni. Lenses formed under impact loading: shape and Poisson's ratio relationship. *Journal of Materials Science*, 9(7):1153–1158, 1974.

[2] The American Society of Mechanical Engineers, New York, NY. *ASME B46.1 - 2002: Surface Texture, Surface Roughness, Waviness and Lay.*

[3] ASTM International, West Conshohocken, PA. *D 695-02a: Standard Test Method for Compressive Properties of Rigid Plastics.*

[4] AZoM.com. (Available online) http://www.azom.com/details.asp?ArticleID=83. Accessed August 14, 2006.

[5] M. Bahrami, M.M. Yovanovich, and E.E. Marotta. Modeling of thermal joint resistance of polymer-metal rough interfaces. In *Paper No. IMECE2004-60131, ASME International Mechanical Engineering Congress, Anaheim, California, November 13-19*, 2004.

[6] F.J. Baltá-Calleja and S. Fakirov. *Microhardness of Polymers.* Cambridge University Press, Cambridge, 2000.

[7] H.S. Carslaw and J.C. Jaeger. *Conduction of Heat in Solids.* Oxford University Press, London, 2nd edition, 1959.

[8] M.G. Cooper, B.B. Mikic, and M.M. Yovanovich. Thermal contact conductance. *International Journal of Heat and Mass Transfer*, 12:279–300, 1969.

[9] R.J. Crawford. Microhardness testing of plastics. *Polymer Testing*, 3:37–54, 1982.

[10] H. Fenech and W.M. Rohsenow. Prediction of thermal conductance of metallic surfaces in contact. *ASME J. Heat Transfer*, 85:15–24, 1963.

[11] L.S. Fletcher, M.R. Cerza, and R.L. Boysen. Thermal conductance and thermal conductivity of selected polyethylene materials. In *Paper No. 75-187, AIAA 13th Aerospace Sciences Meeting, California, January 20-22*, 1975.

[12] L.S. Fletcher and R.G Miller. Thermal conductance of gasket materials for spacecraft joints. In *Paper No. 73-119, AIAA 11th Aerospace Sciences Meeting, Washington, D.C., January 10-12*, 1973.

[13] J.J. Fuller and E.E. Marotta. Thermal contact conductance of metal/polymer joints: An analytical and experimental investigation. *Journal of Thermophysics and Heat Transfer*, 15(2):228–238, 2001.

[14] J.A. Greenwood and J.B.P. Williamson. Contact of nominally flat surfaces. *Proceedings of the Royal Society of London. Series A, Mathematical and Physical Sciences*, 295(1442):300–319, 1966.

[15] C. Hall. *Polymer Materials*. The Macmillan Press Ltd., London, 1981.

[16] J.A Hall, W.H. Ceckler, and E.V. Thompson. Thermal properties of rigid polymers. i. measurement of thermal conductivity and questions concerning contact resistance. *Journal of Applied Polymer Science*, 33:2029–2039, 1987.

[17] A.A. Hegazy. *Thermal Joint Conductance of Conforming Rough Surfaces: Effect of Surface Micro-Hardness Variation*. PhD thesis, University of Waterloo, 1985.

[18] R.C. Hibbeler. *Mechanics of Materials*. Prentice Hall, Inc., Upper Saddle River, NJ, 4th edition, 2000.

[19] Cool Polymers Inc. (Available online) http://www.coolpolymers.com/heattrans.html. Accessed August 14, 2006.

[20] Plastics International. (Available online) http://www.plasticsintl.com/datasheets/Polycarbonate. Accessed September 10, 2006.

[21] K.L. Johnson. *Contact Mechanics*. Cambridge University Press, 1985.

[22] R. Katare, R. Bajpai, and S.C. Datt. Microhardness of blends of polystyrene and poly (methyl methacrylate). *Polymer Testing*, 10.

[23] Gallina USA LLC. (Available online) http://www.gallinausa.com/polycarbonate.tech.html. Accessed September 10, 2006.

[24] V. Lorenzo, J.M. Perena, and J.M.G. Fatou. Relationships between mechanical properties and microhardness of polyethylenes. *Die Angewandte Makromolekulare Chemie*, 172:25–35, 1989.

[25] I.M. Low, G. Paglia, and C. Shi. Indentation Responses of Viscoelastic Materials. *Journal of Applied Polymer Science*, 70:2349–2352, 1998.

[26] E.E. Marotta and L.S. Fletcher. Thermal contact conductance of selected polymeric materials. *Journal of Thermophysics and Heat Transfer*, 10(2):334–342, 1996.

[27] D.M. Marsh. Plastic flow in glass. *Proceedings of the Royal Society of London. Series A, Mathematical and Physical Sciences*, 279(1378):420–435, 1964.

[28] B.B. Mikic and R.T. Roca. On elastic deformation of rough surfaces in contact. *unpublished paper*, 1971.

[29] B.B. Mikic. Thermal contact conductance; theoretical considerations. *International Journal of Heat and Mass Transfer*, 17:205–214, 1974.

[30] F.H. Milanez, M.M. Yovanovich, and M.B.H. Mantelli. Thermal contact conductance at low contact pressures. *Journal of Thermophysics and Heat Transfer*, 18(1):37–44, 2004.

[31] F.H. Milanez. *Thermal Contact Conductance at Low Contact Pressures*. PhD thesis, Universidade Federal De Santa Catarina, 2003.

[32] K.A. Narh and L. Sridar. Measurement and modeling of thermal contact resistance at a plastic metal interface. *ANTEC 97, Society of Plastics Engineers, 55th Annual Technical Conference, Toronto, Canada, April 27-May 2*, 2:2273–2277, 1997.

[33] S. Parihar and N.T. Wright. Thermal contact resistance at elastomer to metal interfaces. *International Communication Heat and Mass Transfer*, 24(8):1083–1092, 1997.

[34] S. Song and M.M. Yovanovich. Relative contact pressure: Dependence on surface roughness and vickers microhardness. *Journal of Thermophysics and Heat Transfer*, 2(1):43–47, 1988.

[35] M.R. Sridhar and M.M. Yovanovich. Review of elastic and plastic contact conductance models: Comparision with experiment. *Journal of Thermophysics and Heat Transfer*, 8(4):633–640, 1994.

[36] M.R. Sridhar and M.M. Yovanovich. Elastoplastic contact conductance model for isotropic, conforming rough surfaces and comparison with experiments. *Journal of Heat Transfer*, 118(1):3–9, 1996.

[37] D. Tabor. *The Hardness of Metals*. Oxford University Press, 1951.

[38] D. Tabor. Indentation hardness and its measurements: Some cautionary comments. In P.J. Blau and B.R. Lawn, editors, *Microindentation Techniques in Materials Science and Engineering*. ASTM, 1986.

[39] A.J. Wheeler and A.R. Ganji. *Introduction to engineering experimentation*. Prentice Hall Englewood Cliffs, NJ, 1996.

[40] M.M. Yovanovich, A.A. Hegazy, and J. DeVaal. Surface hardness distribution effects upon contact, gap and joint conductances. In *AIAA-82-0887, AIAA/ASME 3rd Joint Thermophysics, Fluids, Plasma and Heat Transfer Conference, St. Louis, MO, June 7-11*, 1982.

[41] M.M. Yovanovich and E.E. Marotta. Thermal spreading and contact resistances. In A. Bejan and A.D. Kraus, editors, *Heat Transfer Handbook*. John Wiley and Sons, Inc., 2003.

[42] M.M. Yovanovich. General thermal constriction parameter for annular contacts on circular flux tubes. *AIAA Journal*, 14:822–824, 1976.

[43] M.M. Yovanovich. Thermal contact correlations. *Progress in Aeronautics and Aerodynamics: Spacecraft Radiative Transfer and Temperature Control*, 83:83–95, 1982.

[44] M.M. Yovanovich. Chapter 6. University of Waterloo - ME 758: Course Notes, 2005.

[45] M.M. Yovanovich. Chapter 7. University of Waterloo - ME 758: Course Notes, 2005.

Appendix A

Thermal Conductivity

A.1 Electrolytic Iron

Table A.1: Electrolytic Iron: thermal conductivity reference data

Temperature	Thermal Conductivity
$°C$	$W/m \cdot K$
0	72.3
50	69.4
100	66.5
150	63.3

A linear correlation was developed to describe the relationship between supplied thermal conductivity reference data and temperature:

$$k_{Elec.Iron} = 72.36 - 0.0598 \cdot T(°C) \quad (W/m \cdot K) \tag{A.1}$$

A.2 304 Stainless Steel

Table A.2: 304 Stainless Steel: experimental thermal conductivity data

Temperature	Thermal Conductivity
$^{\circ}C$	$W/m \cdot K$
50.02	14.56
66.92	15.13
71.79	15.26
90.37	15.52

Appendix B

Properties of eGraf® 1200

Typical Properties eGraf® 1200 Materials

Technical Bulletin: 268

eGraf® 1200 Thermal Interface Materials (TIM) are designed for use in applications requiring low contact resistance and high thermal conductivity. Manufactured entirely from natural graphite with no fillers or binders, eGraf® 1200 TIM will not dry out and will not outgas under vacuum conditions. eGraf® 1200 materials can be used at temperatures up to 400 °C, and its comformable nature optimizes thermal properties, and excellent contact is maintained for the life of the assembly.
Typical applications include chip burn-in and chip testing fixtures, DC-to-DC converters, CPU modules, and hot and cold plates. All eGraf® 1200 materials are available in sheet, roll or die cut form , with or without a pressure sensitive adhesive (PSA), a plastic dielectric layer or both. eGraf® 1200 TIM can be easily cut to any size or shape. The graph below shows the thermal resistance of eGraf® 1200 materials as a function of temperature.

Property	eGraf® 1205	eGraf® 1210	eGraf® 1220	Test Method
Physical				
Color	Dark Grey	Dark Grey	Dark Grey	
Thickness	0.005 in (0.13 mm)	0.010 in (0.25 mm)	0.020 in (0.51 mm)	
Thickness Variation	10%	5%	5%	
Maximum Roll Width	24.0 in (61.0 cm)	24.0 in (61.0 cm)	24.0 in (61.0 cm)	
Flammability Rating	UL 94 V-0	UL 94 V-0	UL 94 V-0	UL 94
Tensile Strength	270 psi (1800 kPa)	470 psi (3200 kPa)	470 psi (3200 kPa)	ASTM F-152
Thermal				
Operating Temperature	-40 to 400 °C	-40 to 400 °C	-40 to 400 °C	
Thermal Impedance @15 psi	0.32 cm^2 °C/W	0.54 cm^2 °C/W	0.98 cm^2 °C/W	ASTM D 5470 Modified
Thermal Resistance @100 psi	0.10 cm^2 °C/W	0.27 cm^2 °C/W	0.56 cm^2 °C/W	ASTM D 5470 Modified
Thermal Conductivity @100 psi				
Thru-thickness	10 W/mK	10 W/mK	10 W/mK	ASTM D 5470 Modified
In-plane	150 W/mK	150 W/mK	150 W/mK	Angstom's
Coefficient of Thermal Expansion				
Thru-thickness	27.0 x 10^{-6} m/m °C	27.0 x 10^{-6} m/m °C	27.0 x 10^{-6} m/m °C	
In-plane	-0.4 x 10^{-6} m/m °C	-0.4 x 10^{-6} m/m °C	-0.4 x 10^{-6} m/m °C	
Specific heat	711 J/kg °C	711 J/kg °C	711 J/kg °C	
Electrical				
Electrical Resistivity Thru-thickness @ 100 psi	15,000 µΩm	15,000 µΩm	15,000 µΩm	ASTM C611
In-plane	10 µΩm	10 µΩm	10 µΩm	ASTM C611

Notes: 1) Thermal Impedance is measured with test blocks that are less than 0.0005 in (13 micron) out of flat
2) These are typical properties and should not be used for specifications
3) Dielectric coatings can be applied to eGraf® materials to increase thru-thickness electrical resistance

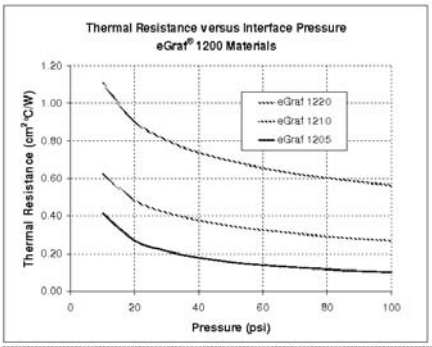

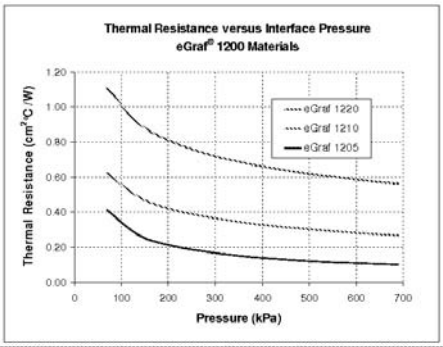

This information is not to be taken as a warranty of representation for which we will assume legal responsibility nor permission or recommendation to practice any patented invention without license. It is offered solely for your consideration, investigation and verification.

eGraf is a trademark of Advanced Energy Technology Inc.
Phone 1-800-253-8003, In Ohio, 1-216-529-3777, Fax 1-216-529-3888
Issued January 2005, Rl.1

GRAFTech
GrafTech International Ltd.
www.egraf.com

Copyright 2005 GrafTech International Ltd.

Appendix C

Uncertainty Analysis

The following is a discussion of the analysis made to estimate the maximum uncertainty in the experimental measurements.

C.1 Differential Error Analysis Method

An estimate of the uncertainty, w of a result, R which is a function of n measured independent variables, $x_1, x_2, .., x_n$ can be calculated from the following differential analysis:

$$w_R = \left(\sum_{i=1}^{n} \left[w_{x_i} \frac{\partial R}{\partial x_i} \right]^2 \right)^{1/2} \tag{C.1}$$

where w_{x_i} are estimates of the uncertainties in the independent variables.

C.2 Uncertainty in the Measured Thermal Contact Resistance

Three different types of interfaces were evaluated for this experimental program. Each type of interface required a different equation to calculate the thermal contact resistance. Interfaces examined include:

1. A stainless steel surface in contact with another stainless steel surface: Eq. 5.8.

$$R_{interface} = \frac{\Delta T_{total}}{Q_{avg}} \quad (K/W)$$

2. A stainless steel surface in contact with a polycarbonate surface: Eq. 5.9.

$$R_{interface} = \frac{\Delta T_{total}}{Q_{avg}} - R_{bulk} - R_{graphite} \quad (K/W)$$

3. A polycarbonate surface in contact with another polycarbonate surface: Eq. 5.10

$$R_{interface} = \frac{\Delta T_{total}}{Q_{avg}} - 2 \cdot R_{bulk} - 2 \cdot R_{graphite} \quad (K/W)$$

C.2.1 Stainless Steel - Stainless Steel Interface

The thermal contact resistance was determined from the total temperature drop between the flux-meters and the value of heat conducted through the interface. The value of heat conducted through the interface (Q_{avg}) was calculated as the average value of heat conducted through each flux-meter. The heat loss in vacuum conditions for this series of experiments was less than 11%. Therefore, the estimated uncertainty in the value of Q_{avg} is $\pm 5.5\%$ or approximately 0.5 W.

The uncertainty in the total temperature drop between the flux-meters was the result of the uncertainties associated with the thermocouple readings. The uncertainty of temperature difference readings were estimated to be accurate to $\pm 0.1^{\circ}C$ based on a calibration completed by Milanez [31] with an equivalent thermocouple setup. The uncertainty in the total temperature drop between the extrapolated temperatures was, therefore, 0.2 $^{\circ}C$. Using the differential error analysis, Eq. C.1 the uncertainty in the measured thermal contact resistance values are approximately 6%. The uncertainty associated with each thermal contact resistance measurement for the stainless steel - stainless steel interface are given in Table C.1.

Table C.1: Uncertainties associated with thermal contact resistance measurements of the stainless steel interface.

Q_{avg}	ΔT_{total}	$R_{interface}$	w_R	$w_R/R_{interface}$
W	$^{\circ}C$	K/W	K/W	%
9.59	24.5	2.55	0.14	5.6
9.83	15.2	1.55	0.09	5.7
9.77	11.4	1.17	0.07	5.8
9.70	9.1	0.94	0.06	5.9
9.65	7.6	0.78	0.05	6.1
9.50	6.4	0.67	0.04	6.3
9.41	5.5	0.58	0.04	6.6
9.31	4.8	0.52	0.04	6.9
9.18	4.3	0.46	0.03	7.2

C.2.2 Stainless Steel - Polycarbonate Interface

The thermal contact resistance was determined from the total temperature drop between the flux-meters, the value of heat being conducted through the interface, the thermal bulk resistance of the polycarbonate disc and the thermal resistance of the graphite sheet. The value of heat being conducted through the interface, Q_{avg} was calculated as the average value of heat being conducted through each flux-meter. The heat loss in vacuum conditions for this series of experiments was less than 16%. Therefore, the estimated uncertainty in the value of Q_{avg} is $\pm 8.0\%$. The uncertainty in the total temperature drop between the flux-meters was 0.2 $^{\circ}C$ as discussed in Section C.2.1.

From the differential error analysis, Eq. C.1 the uncertainty of the bulk resistance, $(\omega_{R.bulk})$ of a typical polycarbonate disc was calculated from the uncertainty of the thermal conductivity of polycarbonate, $(\omega_{k.PC})$. A similar process was used to calculate the uncertainty of the thermal conductivity of polycarbonate. The calculation to determine the thermal conductivity of polycarbonate was based on multiple thermal experiments with polycarbonate layers of varying thickness. The outcome of each of these thermal experiments: thermal joint resistance has an uncertainty, $(\omega_{R.total})$ associated with it. The uncertainty associated with each step in this series of calculations is as follows:

$$\omega_{R.total} \approx 5\% \rightarrow \omega_{k.PC} \approx 8\% \rightarrow \omega_{R.bulk} \approx 9\%$$

Considering that the value of the bulk resistance of the polymer disc was 6.53 K/W, the uncertainty in the thermal bulk resistance of a typical polycarbonate disc is approximately 0.6 K/W. A similar procedure was completed to calculate the uncertainty of the thermal resistance of the graphite sheet as approximately 0.4 K/W. This uncertainty is on the same order as the calculated thermal resistance values for the graphite sheet and reveals how uncertainties can accumulate in calculated values.

Using the differential error analysis, Eq. C.1 the uncertainty in the measured thermal contact resistance values ranged from 17% at the lightest load to greater than 100% at the highest load. The uncertainty associated with each thermal contact resistance measurement for the stainless steel - polycarbonate interface are given in Table C.2 for PC-SS-1 and Table C.3 for PC-SS-2.

C.2.3 Polycarbonate - Polycarbonate Interface

The thermal contact resistance was determined from the total temperature drop between the flux-meters, the value of heat being conducted through the interface, the thermal bulk resistance of the polycarbonate discs and the thermal resistance of the graphite sheets. The value of heat being conducted through the interface, Q_{avg} was calculated as the average value of heat being conducted through each flux-meter. The heat loss in vacuum conditions for this series of experiments was less than 17%. Therefore, the estimated uncertainty in the value of Q_{avg} is $\pm 8.5\%$. The uncertainty in the total temperature drop between the flux-meters was 0.2 $^{\circ}C$ as discussed in Section C.2.1.

The uncertainty in the thermal bulk resistance of a typical polycarbonate disc is approximately 0.6 K/W. The uncertainty in the thermal resistance of the graphite sheet is approximately 0.4 K/W. These uncertainty values were calculated in the same manner as discussed in Section C.2.2.

Using the differential error analysis, Eq. C.1 the uncertainty in the measured thermal contact resistance values ranged from 39% at the lightest load to greater than 250% at the highest load. The uncertainty associated with each thermal contact resistance measurement for the polycarbonate - polycarbonate interface are given in Table C.4 for PC-PC-1 and Table C.5 for PC-PC-2.

Table C.2: Uncertainties associated with thermal contact resistance measurements, PC-SS-1.

Q_{avg}	ΔT_{total}	R_{bulk}	$R_{graphite}$	$R_{interface}$	w_R	$w_R/R_{interface}$
W	$^\circ C$	K/W	K/W	K/W	K/W	%
3.70	54.4	6.7	0.68	7.36	1.38	19
4.00	44.5	6.7	0.38	4.10	1.15	28
4.13	38.5	6.6	0.31	2.37	1.04	44
4.17	36.2	6.6	0.29	1.75	1.00	57
4.18	34.9	6.6	0.27	1.44	0.98	68
4.18	33.8	6.6	0.27	1.19	0.97	82
4.15	32.8	6.6	0.27	1.00	0.96	96
4.13	32.1	6.6	0.25	0.89	0.95	107
4.08	31.7	6.6	0.24	0.91	0.95	105

Table C.3: Uncertainties associated with thermal contact resistance measurements, PC-SS-2.

Q_{avg}	ΔT_{total}	R_{bulk}	$R_{graphite}$	$R_{interface}$	w_R	$w_R/R_{interface}$
W	$^\circ C$	K/W	K/W	K/W	K/W	%
3.46	54.2	6.7	0.68	8.32	1.45	17
3.86	40.9	6.7	0.38	3.58	1.08	30
3.96	36.0	6.6	0.31	2.14	0.99	46
3.96	34.2	6.6	0.29	1.71	0.97	57
3.99	33.1	6.6	0.27	1.39	0.95	69
3.99	32.4	6.6	0.27	1.21	0.95	78
3.97	31.9	6.6	0.27	1.12	0.94	84
3.96	31.4	6.6	0.25	1.05	0.94	89
3.92	30.8	6.6	0.24	0.99	0.93	95

Table C.4: Uncertainties associated with thermal contact resistance measurements, PC-PC-1.

Q_{avg}	ΔT_{total}	R_{bulk}	$R_{graphite}$	$R_{interface}$	w_R	$w_R/R_{interface}$
W	$°C$	K/W	K/W	K/W	K/W	%
3.24	66.3	6.7	0.68	5.78	2.26	39
3.45	59.3	6.7	0.38	3.15	2.06	65
3.50	55.8	6.6	0.31	2.01	1.98	98
3.50	53.8	6.6	0.29	1.52	1.95	128
3.49	52.4	6.6	0.27	1.19	1.93	162
3.47	51.7	6.6	0.27	1.06	1.92	181
3.47	51.1	6.6	0.27	0.93	1.91	205
3.46	50.4	6.6	0.25	0.78	1.90	243
3.42	49.5	6.6	0.24	0.75	1.90	253
3.34	48.2	6.6	0.22	0.75	1.89	254

Table C.5: Uncertainties associated with thermal contact resistance measurements, PC-PC-2.

Q_{avg}	ΔT_{total}	R_{bulk}	$R_{graphite}$	$R_{interface}$	w_R	$w_R/R_{interface}$
W	$^\circ C$	K/W	K/W	K/W	K/W	%
3.30	60.3	6.7	0.68	3.61	2.12	59
3.43	55.5	6.7	0.38	2.13	1.99	94
3.45	52.9	6.6	0.31	1.44	1.95	136
3.43	51.4	6.6	0.29	1.11	1.92	174
3.43	50.2	6.6	0.27	0.81	1.91	236
3.43	49.8	6.6	0.27	0.70	1.90	272
3.42	49.9	6.6	0.27	0.80	1.90	239

Appendix D

Surface Roughness Details

Table D.1: Roughness details for SS-SS interface: Bead Blasted surface

	σ	m	σ / m
	μm	radian	μm
1	1.61	0.078	20.63
2	1.38	0.073	18.93
3	1.21	0.064	18.97
4	1.56	0.084	18.51
5	1.65	0.080	20.58
Avg	1.48	0.076	19.54

Table D.2: Roughness details for SS-SS interface: Lapped surface

	σ	m	σ / m
	μm	radian	μm
1	0.26	0.056	4.66
2	0.37	0.054	6.83
3	0.32	0.052	6.06
4	0.26	0.052	4.98
5	0.33	0.051	6.49
Avg	0.31	0.053	5.79

Table D.3: Roughness details for PC-SS-1 interface: Bead Blasted polycarbonate surface

	σ	m	σ / m
	μm	radian	μm
1	1.84	0.084	21.94
2	1.96	0.083	23.64
3	1.78	0.072	24.71
4	1.88	0.065	28.95
5	1.87	0.087	21.51
Avg	1.87	0.078	23.88

Table D.4: Roughness details for PC-SS-2 interface: Bead Blasted polycarbonate surface

	σ	m	σ / m
	μm	radian	μm
1	1.43	0.077	18.55
2	1.34	0.064	21.00
3	1.80	0.086	20.92
4	1.57	0.073	21.49
5	1.53	0.075	20.45
Avg	1.53	0.075	20.46

Table D.5: Roughness details for PC-PC-1 interface: Bead Blasted polycarbonate surface

	σ	m	σ / m
	μm	radian	μm
1	2.24	0.115	19.49
2	2.69	0.118	22.79
3	2.34	0.110	21.30
4	2.26	0.111	20.32
5	2.71	0.119	22.75
Avg	2.45	0.115	21.35

Table D.6: Roughness details for PC-PC-1 interface: Lapped polycarbonate surface

	σ	m	σ / m
	μm	radian	μm
1	0.43	0.065	6.62
2	0.40	0.062	6.39
3	0.43	0.068	6.31
4	0.36	0.056	6.48
5	0.35	0.058	6.00
Avg	0.39	0.062	6.36

Table D.7: Roughness details for PC-PC-2 interface: Bead Blasted polycarbonate surface

	σ	m	σ / m
	μm	radian	μm
1	1.63	0.083	19.61
2	1.83	0.085	21.56
3	1.55	0.072	21.47
4	1.89	0.082	23.04
5	2.00	0.096	20.80
Avg	1.78	0.084	21.28

Table D.8: Roughness details for PC-PC-2 interface: Lapped polycarbonate surface

	σ	m	σ / m
	μm	radian	μm
1	0.54	0.095	5.68
2	0.48	0.085	5.64
3	0.48	0.082	5.79
4	0.45	0.080	5.64
5	0.48	0.084	5.75
Avg	0.49	0.085	5.70

Appendix E

Microhardness Details

E.1 304 Stainless Steel

The average indentation diagonal, (d_V) for each of the microhardness measurements can be determined from the following:

$$d_V = \sqrt{\frac{1.854 \cdot \text{Load}}{H_V/9.81}} \quad (\mu m) \tag{E.1}$$

where *Load* is the applied load in grams and H_V is the Vickers microhardness measurement in GPa.

Table E.1: Vickers microhardness measurements, (H_V) and associated average indentation diagonal, (d_V) for 304 Stainless Steel under varying indenter load. Units of microhardness are GPa.

	$15g$	$25g$	$100g$	$200g$	$300g$	$500g$
1	3.2	2.95	2.94	2.58	2.22	1.9
2	3.51	3.01	2.73	2.32	2.37	1.95
3	3.29	3.18	2.42	2.4	2.07	2.04
4	3.28	2.84	2.63	2.38	2.31	1.91
5	3.65	3.12	2.66	2.4	2.3	1.92
Avg	3.38	3.02	2.68	2.42	2.25	1.95
d_V (μm)	8.98	12.27	26.05	38.77	49.24	68.29

E.2 Polymers

Table E.2: Vickers microhardness measurements, (H_V) and associated average indentation diagonal, (d_V) for Polycarbonate under varying indenter load. Loading time = 15 seconds. Units of microhardness are MPa.

	$5g$	$10g$	$20g$	$25g$	$50g$	$100g$	$200g$	$500g$
	122	127	131	132	132	130	131	131
	121	126	130	135	135	134	132	128
	123	121	129	133	134	135	131	131
	121	126	131	134	141	131	133	131
Avg	121	125	131	134	135	132	132	130
d_V (μm)	27.4	38.1	52.7	58.3	82.1	117.4	166.0	264.5

Table E.3: Vickers microhardness measurements, (H_V) and associated average indentation diagonal, (d_V) for Polycarbonate under varying indenter load. Loading time = 30 seconds. Units of microhardness are MPa.

	$5g$	$10g$	$20g$	$25g$	$50g$	$100g$	$500g$
1	118	125	129	127	128	124	125
2	118	121	128	127	130	124	124
3	115	123	129	128	133	125	127
4	120	123	128	126	125	124	127
Avg	117	123	128	127	129	124	126
d_V (μm)	27.9	38.5	53.3	59.8	84	121.1	268.7

Table E.4: Vickers microhardness measurements, (H_V) and associated average indentation diagonal, (d_V) for Polyvinyl Chloride (PVC) under varying indenter load. Loading time = 30 seconds. Units of microhardness are MPa.

	$5g$	$10g$	$20g$	$25g$	$50g$	$100g$	$500g$
1	143	146	149	150	148	146	145
2	145	148	146	150	150	145	144
3	144	149	149	153	150	145	143
4	142	151	151	149	151	145	142
Avg	144	149	149	150	150	145	144
d_V (μm)	25.1	34.9	49.4	55.1	77.9	112.0	251.3

Table E.5: Vickers microhardness measurements, (H_V) and associated average indentation diagonal, (d_V) for Acrylonitrile Butadiene Styrene (ABS) under varying indenter load. Loading time = 30 seconds. Units of microhardness are MPa.

	$2g$	$5g$	$10g$	$25g$	$50g$	$100g$	$500g$
1	92	90	92	95	92	91	89
2	89	93	93	95	92	90	89
3	93	92	93	92	91	91	88
4	90	92	91	96	92	87	87
Avg	91	92	92	95	92	90	89
d_V (μm)	20.0	31.4	44.5	69.2	99.4	142.2	319.7

Appendix F

Thermal Test Results

Table F.1: Test results of the stainless steel interface

P	T_m	ΔT_{total}	k_s	Q_1	Q_2	Q_{avg}	$R_{interface}$
kPa	$^\circ C$	$^\circ C$	$W/m \cdot K$	W	W	W	K/W
1180	128.0	24.5	16.5	10.1	9.1	9.6	2.55
1908	125.9	15.2	16.4	10.3	9.3	9.8	1.55
2753	123.5	11.4	16.4	10.2	9.3	9.8	1.17
3644	121.3	9.1	16.3	10.2	9.2	9.7	0.94
4529	119.4	7.6	16.3	10.2	9.1	9.6	0.78
5411	117.5	6.4	16.3	9.9	9.1	9.5	0.67
6296	116.0	5.5	16.2	9.8	9.0	9.4	0.58
7168	114.6	4.8	16.2	9.7	8.9	9.3	0.52
8017	112.9	4.3	16.1	9.6	8.8	9.2	0.46

Table F.2: Test results of PC-SS-1

P	T_m	ΔT_{total}	k_s	Q_1	Q_2	Q_{avg}	$R_{graphite}$	R_{bulk}	$R_{interface}$
kPa	$^\circ C$	$^\circ C$	$W/m \cdot K$	W	W	W	K/W	K/W	K/W
697	63.3	54.4	0.47	4.0	3.4	3.7	0.68	6.7	7.36
1220	61.6	44.5	0.47	4.3	3.7	4.0	0.38	6.7	4.10
2087	60.0	38.5	0.47	4.4	3.8	4.1	0.31	6.6	2.37
2965	59.1	36.2	0.47	4.5	3.9	4.2	0.29	6.6	1.75
3844	58.6	34.9	0.47	4.5	3.9	4.2	0.27	6.6	1.44
4715	58.0	33.8	0.47	4.5	3.9	4.2	0.27	6.6	1.19
5592	57.5	32.8	0.47	4.4	3.9	4.2	0.27	6.6	1.00
6457	57.0	32.1	0.47	4.4	3.9	4.1	0.25	6.6	0.89
7340	56.4	31.7	0.47	4.4	3.8	4.1	0.24	6.6	0.91

Table F.3: Test results of PC-SS-2

P	T_m	ΔT_{total}	k_s	Q_1	Q_2	Q_{avg}	$R_{graphite}$	R_{bulk}	$R_{interface}$
kPa	$^\circ C$	$^\circ C$	$W/m \cdot K$	W	W	W	K/W	K/W	K/W
525	61.1	54.2	0.47	3.8	3.2	3.5	0.68	6.7	8.32
1259	58.7	40.9	0.47	4.1	3.6	3.9	0.38	6.7	3.58
2124	57.2	36.0	0.47	4.2	3.7	4.0	0.31	6.6	2.14
2999	56.5	34.2	0.47	4.2	3.7	4.0	0.29	6.6	1.71
3871	56.3	33.1	0.47	4.3	3.7	4.0	0.27	6.6	1.39
4736	55.9	32.4	0.47	4.3	3.7	4.0	0.27	6.6	1.21
5605	55.6	31.9	0.47	4.2	3.7	4.0	0.27	6.6	1.12
6478	55.3	31.4	0.47	4.2	3.7	4.0	0.25	6.6	1.05
7343	54.8	30.8	0.47	4.2	3.7	3.9	0.24	6.6	0.99

Table F.4: Test results of PC-PC-1

P	T_m	ΔT_{total}	k_s	Q_1	Q_2	Q_{avg}	$R_{graphite}$	R_{bulk}	$R_{interface}$
kPa	$°C$	$°C$	$W/m \cdot K$	W	W	W	K/W	K/W	K/W
702	77.6	66.3	0.24	3.6	2.9	3.2	0.68	6.7	5.78
1215	76.7	59.3	0.24	3.7	3.2	3.4	0.38	6.7	3.15
2081	75.7	55.8	0.24	3.8	3.2	3.5	0.31	6.6	2.01
2952	74.7	53.8	0.24	3.8	3.2	3.5	0.29	6.6	1.52
3831	74.1	52.4	0.24	3.8	3.2	3.5	0.27	6.6	1.19
4712	73.5	51.7	0.24	3.7	3.2	3.5	0.27	6.6	1.06
5592	73.2	51.1	0.24	3.7	3.2	3.5	0.27	6.6	0.93
6468	72.8	50.4	0.24	3.7	3.2	3.5	0.25	6.6	0.78
7334	72.0	49.5	0.24	3.7	3.2	3.4	0.24	6.6	0.75
8157	70.7	48.2	0.24	3.6	3.1	3.3	0.22	6.6	0.75

Table F.5: Test results of PC-PC-2

P	T_m	ΔT_{total}	k_s	Q_1	Q_2	Q_{avg}	$R_{graphite}$	R_{bulk}	$R_{interface}$
kPa	$^\circ C$	$^\circ C$	$W/m \cdot K$	W	W	W	K/W	K/W	K/W
655	75.0	60.3	0.24	3.6	3	3.3	0.68	6.7	3.61
1238	74.3	55.5	0.24	3.7	3.2	3.4	0.38	6.7	2.13
2097	73.4	52.9	0.24	3.7	3.2	3.4	0.31	6.6	1.44
2974	72.7	51.4	0.24	3.7	3.2	3.4	0.29	6.6	1.11
3844	72.2	50.2	0.24	3.7	3.2	3.4	0.27	6.6	0.81
4735	72.0	49.8	0.24	3.7	3.2	3.4	0.27	6.6	0.70
5602	71.3	49.9	0.24	3.7	3.2	3.4	0.27	6.6	0.80

Appendix G

SY Elasto-Plastic Contact Model

H_{ep} Iteration

The calculation of H_{ep} for the SS-SS interface required the full iterative method described by Eqs. 2.39 to 2.45. An example of this process is shown in Table G.1 for the SS-SS interface at P = 1.180 MPa. The initial guess of H_{ep} for iteration 1 was calculated as $\sqrt{H_p \cdot H_e}$ where $H_p = 2.92\ GPa$ and $H_e = 6.70\ GPa$. At the completion of the fourth iteration the values of H_{ep} have converged to three decimal places.

Table G.1: An example of the SY elasto-plastic contact model iterative procedure to calculate H_{ep}.

		Iteration 1	Iteration 2	Iteration 3	Iteration 4
H_{ep}	GPa	4.42	3.502	3.452	3.449
S_f	GPa	2.13	1.49	1.46	1.46
ϵ_c^*		7.41	10.61	10.83	10.84
f_{ep}		0.54	0.59	0.59	0.59
λ	μm	3.29	3.25	3.25	3.25
a	μm	4.36	4.62	4.64	4.64
d_V	μm	10.94	11.58	11.62	11.63
H_{ep}	GPa	3.502	3.452	3.449	3.449
C_c		0.000663	0.000793	0.000802	0.000802

Appendix H

Comparison between Theory and Thermal Test Results

Table H.1: Experiment and theory results for the stainless steel interface

P	$R_{experiment}$	R_{CMY}	% Diff.	R_{Mikic}	% Diff.	$R_{SY\ E-P}$	% Diff.
kPa	K/W	K/W		K/W		K/W	
1180	2.55	2.71	-5.9	4.36	-41.4	2.48	-3.1
1908	1.55	1.71	-9.6	2.78	-44.4	1.58	2.3
2753	1.17	1.20	-2.9	1.98	-40.9	1.12	-4.3
3644	0.94	0.92	2.1	1.53	-38.3	0.86	-8.6
4529	0.78	0.75	4.9	1.25	-37.0	0.70	-10.8
5411	0.67	0.63	6.7	1.06	-36.3	0.59	-12.1
6296	0.58	0.55	6.7	0.92	-36.5	0.51	-12.0
7168	0.52	0.48	7.3	0.82	-36.4	0.45	-12.3
8017	0.46	0.43	6.5	0.74	-37.1	0.41	-12.2

Table H.2: Experiment and theory results for PC-SS-1

P	$R_{experiment}$	R_{CMY}	% Diff.	R_{Mikic}	% Diff.	$R_{SY\ E-P}$	% Diff.	R_{FM}	% Diff.
kPa	K/W	K/W		K/W		K/W		K/W	
697	7.36	9.78	-24.7	7.92	-7.1	6.39	15.2	4.38	68.1
1220	4.10	5.75	-28.7	4.68	-12.5	3.78	8.4	2.59	57.9
2087	2.37	3.45	-31.5	2.83	-16.3	2.28	3.7	1.57	50.7
2965	1.75	2.47	-29.1	2.03	-13.7	1.64	7.0	1.13	55.1
3844	1.44	1.93	-25.5	1.59	-9.5	1.28	12.1	0.89	62.3
4715	1.19	1.59	-25.2	1.31	-9.4	1.06	12.3	0.73	62.4
5592	1.00	1.35	-26.0	1.12	-10.5	0.90	10.9	0.62	60.3
6457	0.89	1.18	-24.5	0.98	-8.8	0.79	13.0	0.55	63.2
7340	0.91	1.04	-13.3	0.87	4.6	0.70	29.6	0.48	87.1

Table H.3: Experiment and theory results for PC-SS-2

P	$R_{experiment}$	R_{CMY}	% Diff.	R_{Mikic}	% Diff.	$R_{SY\ E-P}$	% Diff.	R_{FM}	% Diff.
kPa	K/W	K/W		K/W		K/W		K/W	
525	8.32	10.88	-23.5	8.57	-2.9	6.98	19.3	4.73	76.0
1259	3.58	4.74	-24.6	3.77	-5.0	3.07	16.6	2.09	71.3
2124	2.14	2.89	-25.9	2.30	-7.2	1.88	14.0	1.28	67.0
2999	1.71	2.08	-17.9	1.67	2.6	1.36	25.9	0.93	84.2
3871	1.39	1.63	-15.0	1.31	5.8	1.07	29.9	0.73	89.8
4736	1.21	1.35	-10.6	1.08	11.2	0.88	36.5	0.60	99.2
5605	1.12	1.15	-2.2	0.93	21.4	0.75	49.0	0.52	117.3
6478	1.05	1.00	5.3	0.81	30.5	0.66	60.2	0.45	133.5
7343	0.99	0.89	11.1	0.72	37.4	0.58	68.7	0.40	145.7

Table H.4: Experiment and theory results for PC-PC-1

P	$R_{experiment}$	R_{CMY}	% Diff.	R_{Mikic}	% Diff.	$R_{SY\ E-P}$	% Diff.
kPa	K/W	K/W		K/W		K/W	
702	5.78	17.82	-67.5	10.47	-44.8	9.29	-37.8
1215	3.15	10.58	-70.2	6.25	-49.6	5.55	-43.1
2081	2.01	6.34	-68.2	3.77	-46.6	3.34	-39.8
2952	1.52	4.55	-66.7	2.71	-44.1	2.41	-37.0
3831	1.19	3.55	-66.5	2.12	-44.0	1.88	-36.8
4712	1.06	2.92	-63.6	1.75	-39.3	1.55	-31.6
5592	0.93	2.48	-62.3	1.49	-37.2	1.32	-29.2
6468	0.78	2.16	-63.9	1.30	-39.9	1.15	-32.2
7334	0.75	1.92	-60.8	1.15	-34.9	1.02	-26.6
8157	0.75	1.73	-56.9	1.04	-28.4	0.93	-19.3

Table H.5: Experiment and theory results for PC-PC-2

P	$R_{experiment}$	R_{CMY}	% Diff.	R_{Mikic}	% Diff.	$R_{SY\ E-P} : f = 2.0$	% Diff.
kPa	K/W	K/W		K/W		K/W	
655	3.61	15.45	-76.6	8.35	-56.7	7.54	-52.1
1238	2.13	8.44	-74.7	4.59	-53.5	4.14	-48.5
2097	1.44	5.12	-71.9	2.80	-48.6	2.53	-43.1
2974	1.11	3.67	-69.9	2.01	-45.0	1.82	-39.2
3844	0.81	2.88	-71.9	1.58	-48.9	1.43	-43.4
4735	0.70	2.36	-70.4	1.30	-46.3	1.17	-40.5
5602	0.80	2.01	-60.3	1.11	-28.1	1.00	-20.4